2016

Mass Spectrometry-Based Protein Profiling And Investigations of TGF-ß1-Induced Epithelial-Mesenchymal Transition Signatures In Namru Murine Mammary Gland Epithelial Cells

Matsepo Ramaboli
University of South Carolina

MASS SPECTROMETRY-BASED PROTEIN PROFILING AND INVESTIGATIONS OF TGF-β1-INDUCED EPITHELIAL-MESENCHYMAL TRANSITION SIGNATURES IN NAMRU MURINE MAMMARY GLAND EPITHELIAL CELLS

by

Matsepo Ramaboli

Bachelor of Science
National University of Lesotho, 1997

Master of Science
University of Free State, 2002

Submitted in Partial Fulfillment of the Requirements

For the Degree of Doctor of Philosophy in

Chemistry

College of Arts and Sciences

University of South Carolina

2016

Accepted by:

Qian Wang, Major Professor

Caryn Outten, Committee Member

Guoan Wang, Committee Member

Stephen Morgan, Committee Member

Lacy Ford, Senior Vice Provost and Dean of Graduate Studies

DEDICATION

The work in this PhD thesis is dedicated to my late parents Mr. Shesha Booi Hlena and Mrs 'Masekete Hlena who taught me the value of good education. They spent most of their meager resources paying for quality education of their children in prestigious schools. They were known in our village community of Khanyane in the Leribe disctrict in Lesotho for their dedication in investing in their children's future. They themselves hardly completed high school but they made sure their children acquired college and graduate education.

Mom and dad, I would not be where I am if it were not for your commitment and the vision you had for our family.

May their souls rest in eternal peace!

ACKNOWLEDGEMENTS

I would like to express my sincere gratitude to my academic advisor Professor Qian Wang who accepted me as a graduate student in his lab. Without his scholarly guidance, supervision and persistent help, this dissertation would not have been possible.

I am deeply indebted to my committee members, Professor Stephen Morgan, Professor Caryn Outten and Professor Guoan Wang, for their mentorship and great contributions towards my candidacy and dissertation defense.

I thank all Wang lab members past and present for their support throughout this study. Among them, Dr. Gary Horvath, Dr. Yi Chen, Dr. Elizabeth Balizan, Dr. Xinrui Duan, Dr. Nikki Sitasuwan, Dr. Honglin Li, Dr. Jittima Luckanagul, Dr. Hong Guan, Enoch Adogla, and Napat Tandikul stand out as people from whom I learned various research and leadership skills.

My hearty regards go to the faculty and staff of the department of chemistry and biochemistry, staff of the international student services, and various on-, and off-campus organizations, and all my friends and family for their empowerment and support.

I am also indebted to various organizations for their financial support; the foreign Fulbright scholarship under the administration of the Institute of International Education; Graduate assistantship through a grant in Professor Wang's lab, and Graduate assistantship from Walker Institute of International Studies (African Studies program).

ABSTRACT

Breast cancer is the second-most common cancer and the second-leading cause of cancer-related deaths in women. Despite advances in cancer early detection, prevention and treatment, breast cancer is still a major health challenge due to low survival caused by breast cancer metastasis. This warrants critical attention and intervention. From the proteomic standpoint, a protein-based multiplex system that provides large array of informative signals for cancer identification and prognosis is still limited. In this dissertation work, we developed two mass spectrometry-based strategies involving chemical biology tools for rapid protein fingerprinting of breast cancer cell lines, and for probing the O-linked N-acetylglucosamine (O-GlcNAc) proteome in transforming growth factor-beta (TGF-β) induced epithelial-mesenchymal transition (EMT), a process that initiates metastasis. Investigation of O-GlcNAc EMT proteomics is critical in understanding how aberrant O-GlcNAc post-translational modification (PTM) promotes cancer invasion and metastasis, as well as in the identification of early stage therapeutic targets. Until now the role of O-GlcNAc PTM in TGF-β-induced EMT is unknown.

In Chapter 2, a novel 'one-step cell processing' method was developed as a prerequisite to rapid spectral profiling of mammalian cells using Matrix-Assisted Laser Desorption Ionization Time-of-Flight mass spectrometry (MALDI-TOF MS). Upon analysis of the mass spectral data of breast cancer cell lines with pattern recognition methods, discrimination between metastatic and non-metastatic cell lines was

accomplished, demonstrating the potential of MALDI-MS profiling in breast cancer diagnosis.

Chapter 3 reports a cleavable azide-reactive dibenzocyclooctyne-disulphide agarose-based beaded resin in Copper-free Click chemistry-based affinity enrichment of O-GlcNAc proteome from azido-GlcNAc labeled cellular extracts, that enabled the global O-GlcNAc proteomic profiling by shortgun proteomics with liquid chromatography-tandem mass spectrometry identification and label-free quantification. From TGF-β-induced EMT in MNuMG cells 196 proteins were identified. 125 of these were putative O-GlcNAc proteins, 75% of which have been previously identified among O-GlcNAc affinity enrichment samples. Downstream bioinformatics analyses of the O-GlcNAc proteome data were performed using Ingenuity Pathway Analysis (IPA) software. *In silico* protein-protein interactions revealed a regulatory network for metastasis, while the most significantly represented metabolic and signaling pathways included glycolysis and several TGF-β non-canonical pathways, respectively. A metastatic regulatory network that features core regulators β-catenin and cyclin-D1 both of which are regulated by O-GlcNAc transferase supports published study that shows that "O-GlcNAcylation Plays Essential Role in Breast Cancer Metastasis," has led us to hypothesize that TGF-β signaling cooperates with O-GlcNAc signaling in promoting EMT, invasion and metastasis, pending O-GlcNAc site-mapping and validation of the proteomic data.

TABLE OF CONTENTS

LIST OF TABLES

LIST OF FIGURES

List of Abbreviations

$AC_4GalNAz$ ..... Peracetylated N-azidoacetylgalactosamine

Acetyl CoA ..... Acetyl coenzyme A

ACN ..... Acetonitrile

ACTB ..... Beta-actin

ADP ..... Adenosine diphosphate

BRCA1 ..... Breast cancer 1, early onset

BSA ..... Bovine serum albumin

BTF3 ..... Basic transcription factor 3

CAV1 ..... Caveolin1

CCNN1 ..... Cyclin D1

CCT ..... Chaperonin-containing TCP1

CD44 ..... Cluster of differentiation 44

CTNNB1 ..... Beta-catenin

CuAAC ..... Copper-catalyzed Azide Alkyne Cycloaddition

DBCO ..... Dibenzocyclooctyne

DBCO-SS-NHS ..... Dibenzocyclooctyne disulphide-N-succinimide ester

dH_2O ..... Deionized water

DHAP ..... Dihydroxyacetophenone

DNA ..... Deoxyribonucleic acid

DTT ..... Dithiothreitol

EAH Sepharose 4B ..... Epoxy-activated Sepharose 4B resin

EEF2 ..... Eukaryotic Translation Elongation Factor 2

EGFR ..... Epidermal Growth Factor Receptor

eIF3 ..... Eukaryotic Translation Initiation Factor 3

EMT ..... Epithelial-mesenchymal transition

ER ..... Estrogen Receptor

ERBB2/HER2 ..... Human Epidermal Growth Factor Receptor 2

EZR ..... Ezrin

FITC ..... Fluorescein isothiocyanate

Fruc-6-P Fructose-6-phosphate

GalNAc ..... O-linked-N-acetyl-D-galactosamine

GalNAz ..... O-linked-N-azidoacetylgalactosamine

GAP Glyceraldehyde-6-phosphate

Glc ..... Glucose

Glc-6-P D-Glucose-6-phosphate

GlcN-6-P D-Glucosamine-6-phosphate

GlcNAc-1-P N-acetyl-D-glucosamine-1-phosphate

GlcNAc-6-P N-acetyl-D-glucosamine-6-phosphate

Gln ..... D-Glucosamine

GO ..... Gene ontology

HBP ..... Hexose Biosynthetic Pathway

HMGB1 ..... High Mobility Group Box 1

HNRNP ..... Heterogenous ribonucleoprotein

HSP ..... Heat Shock Protein

IgG ..... Immunoglobulin G

IPA ..... Ingenuity Pathway Analysis

K-Ras^{v12}-.....K-Ras glycine to valine mutant

KRT.....Keratin

LC-MS/MS .....Liquid chromatography tandem mass spectrometry

LTQ.....Linear trap quadrupole

MALDI-TOF MS.....

.....Matrix-assisted laser desorption/ionization-time of flight mass spectrometry

MMP-9.....Matrix metallopeptidase 9

MST1R.....Macrophage-stimulating 1 receptor

NADPH.....Reduced nicotinamide adenine dinucleotide phosphate

NMuMG.....Namru Murine Mammary Gland Epithelial

OGA.....O-linked-beta-N-acetyl-D-glucosaminidase

O-GlcNAc..... O-linked-N-acetyl-D-glucosamine

OGT ..... UDP-GlcNAc:protein-O-linked-beta-N-acetyl-D-glucosaminyl transferase

P120 .....Delta-catenin

PEP.....Phosphoenolpyruvate

PGR.....Progesterone receptor

PIK3CA.....Phosphatidylinositol-4,5-bisphosphate 3-kinase

PRKAA2.....5'-AMP-activated protein kinase catalytic subunit alpha 2

PSAP.....Prosaposin

RIPA .....Radioimmunoprecipitation assay

SDS .....Sodium dodecyl sulfate

SEER.....Surveillance, Epidemiology and End Results

Smad ..... Sma and Mad related protein

SPAAC..... Strain-promoted Azide Alkyne Cycloaddition

TβRI..... TGF-β Receptor Type I

TβRII..... TGF-β Receptor Type II

TBST..... Tris-buffered saline and Tween 20

TBTA .....Tris[(1-benzyl-1H-1,2,3-triazol-4-yl)mthyl]amine

TFA .....Trifluoroacetic acid

TGF-β .....Transforming Growth Factor Beta

UDP-GalNAc.....Uridine diphosphate N-acetyl-D-galactosamine

UDP-GlcNAc..... Uridine diphosphate N-acetyl-D-glucosamine

UPGMA ..... Unweighted pair group method with arithmetic mean

UTP .....Uridine triphosphate

UV-Vis..... Ultraviolet-visible

VIM..... Vimentin

YBX1/YB1 ..... Y box binding protein 1

CHAPTER 1

LITERATURE REVIEW

1.1 BACKGROUND

1.1.1 Significance and Rationale

Breast cancer is the second-most common cancer and the second leading cause of cancer-related deaths in women, with over 200,000 new cases and over 40,000 deaths estimated in USA in 2015[1]. The current USA SEER records show that survival from cancer has improved a great deal in the last 20 years due partly to advances in cancer prevention, early detection and treatment[1]. However, the 5-year relative survival during 2005-2011 was still remarkably low for metastatic (25%) breast tumors and high for localized (98%) and regional (84%) tumors[2]. This difference could be attributed to the fact that primary tumors can be controlled by early detection and adjuvant treatment while control of metastatic tumors, as accomplished by chemotherapy, is associated with complications[3]. These alarming records suggest that breast cancer is not only a public health problem, but that breast cancer metastasis is the prominent cause of breast cancer mortality and thus necessitates critical attention and intervention[4].

Breast cancer arises primarily from genetic alterations in the epithelium of the mammary gland ducts and lobules.[5] Breast cancer lesions in these glandular regions may start as benign and progress through *in situ* and invasive and ultimately become metastatic if not diagnosed accurately and treated efficiently[3, 6-7] (Figure 1.1). Breast cancer metastasis is a multi-step process[4]. It begins with switching of epithelial cells of

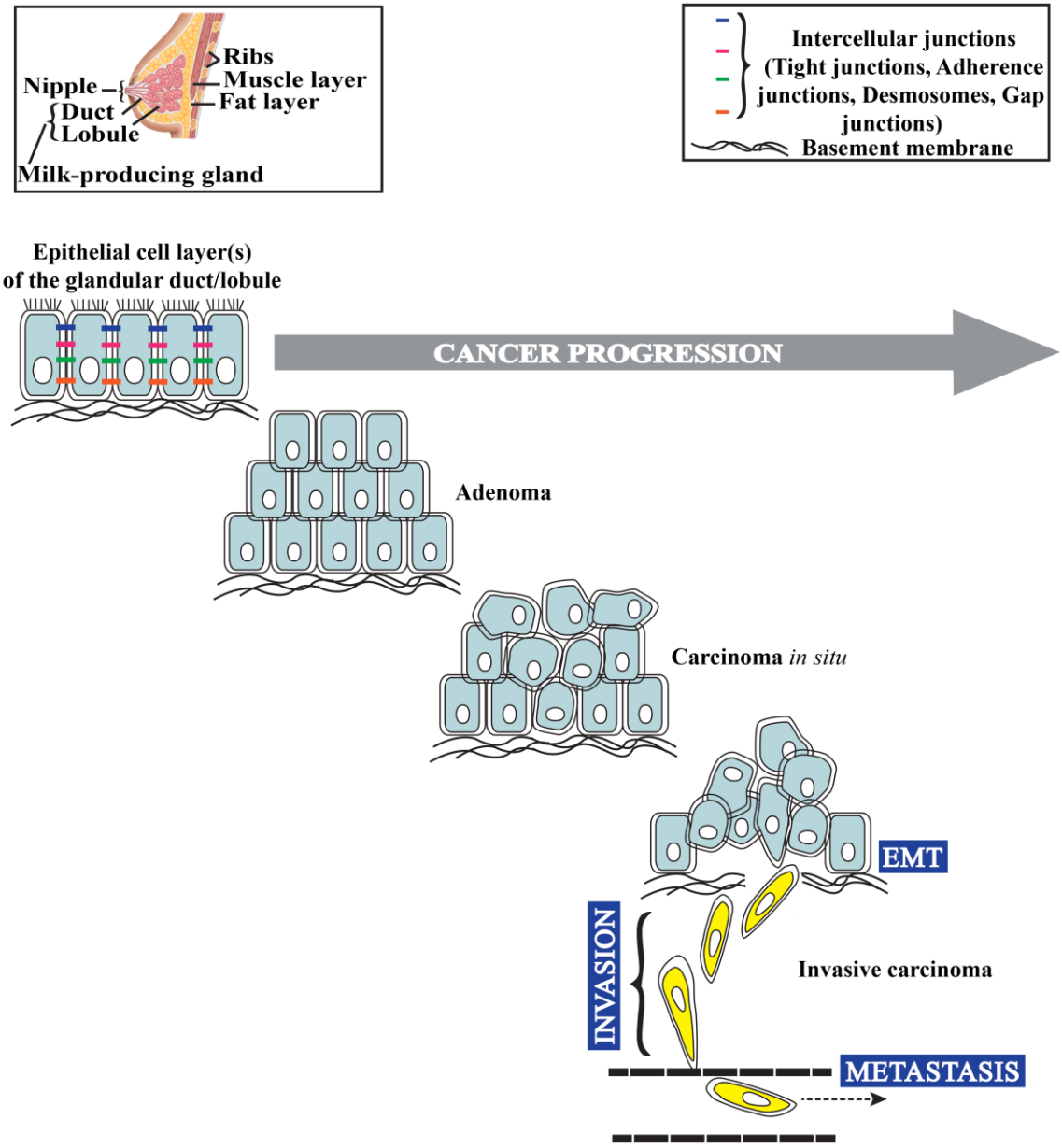

Figure 1.1 Illustration of different stages of progression of breast cancers of epithelial origin, showing that primary tumor cells acquire invasive behavior and become migratory through EMT. If cancer is not detected and treated effectively the migratory cells invade the surrounding stroma and gain access to the blood vessels by intravasation, and eventually get spread to secondary sites through metastasis. This schematic was adopted from a review of J. P. Thiery[6]. The breast anatomy was adopted from the webpage of C. Nordqvist[8].

the primary tumors to migratory and invasive forms that are able to invade the local tumor stroma and the lymphatic system. These motile cancer cells then enter the blood and get transported to distant sites where they switch back to epithelial and undergo survival and proliferation[6]. Gene expression profiling studies have shown that the metastatic potential of cancer is revealed very early at clonal stage, and that the expression signature for metastatic recurrence resembles that of epithelial-mesenchymal transition (EMT).[9] This suggests that early diagnosis is invaluable and that deciphering of EMT signatures could lead to discovery of efficient drug targets for breast cancer.

1.1.2 Breast Cancer and Molecular Profiling

Breast cancer is a collection of distinct neoplastic diseases that are complex and diverse in their pathological, clinical and molecular features[10]. The heterogeneous behavior of breast cancer has been characterized through molecular profiling using complementary DNA microarrays.[11] On the basis of patterns of gene expression and chromosomal aberrations, breast cancer has been classified into five molecularly and clinically distinct subtypes[12]. These are luminal A, luminal B, HER2-overexpressing, basal-like and normal breast tissue-like. Luminal A and B tumors are estrogen receptor-positive (ER+) and are associated with good prognosis. HER2-overexpressing and basal-like tumors have worst clinical outcome. HER2-overexpressing tumors are ER+ while basal-like ones are negative to ER, PR and HER2[13]. The gene expression pattern defining each subtype is the same for the *in situ* carcinoma and its concomitant invasive form while the aggressiveness due to chromosomal alterations changes with disease progression towards metastatic[14-15]. These insights about breast cancer have been unraveled through molecular profiling, an approach that has revolutionized the understanding of tumor biology[11].

Molecular profiling involves high-throughput analysis of gene expression and chromosomal aberrations on a global scale. It produces massive high dimensional data that requires further analysis by multivariate statistics and advanced computational methods[16]. Compared to the routine histological and immunological techniques that measure few variables known *apriori*, molecular profiling analyzes many previously unknown variables[17], thus it can reveal new information about breast cancer[18]. Through molecular profiling, combinations of gene alterations in the form of gene signatures with specificity regarding diagnosis, prognosis and prediction to therapeutic response have been deduced.[19] Some representative examples include MammaPrint© prognostic test (70-gene signature),[20-21] CINSARC prognostic signature for sarcomas (67-gene signature), Oncotype DX® prognostic kit (16-gene signature),[22] and Baylor College 92-gene signature predictive of response to Docetaxel in breast cancer. Among them, MammaPrint© and Oncotype DX® are the only ones that have been clinically validated.

Several benefits of the gene signatures that include the understanding of tumor biology and pathology, subtyping of cancer and development of clinical diagnostic, prognostic, and predictive tests have been recognized.[11] Of importance is the fact that while the propensity for metastasis and its recurrence could be predetermined and progressively acquired, respectively[23], as well as assessed using genetic tests, the therapeutic response is the result of interaction of cancer cells with the stroma and other underlying tissues, and would be best predicted using functional analyses[24-25]. Therefore, with the intent to develop molecular personalized treatments, proteins rather than DNA or RNA are the suitable targets for therapeutic response[17]. Proteomic profiling of breast cancer cells using high-throughput MS technologies is expected to reveal protein level

expression of different genes, from which proteomic signatures and disease biomarkers can be deduced. Specifically, proteomic profiling of EMT, a process that resembles metastatic recurrence by gene expression[9], could impact early diagnosis strategies and development of efficient therapeutic targets for metastatic breast cancer.

1.2 EMT AND CANCER

EMT is a developmental process in which epithelial cells are transformed biochemically and phenotypically to a migratory form that detaches from the basement membrane[26]. EMT plays a role in cellular changes occurring in embryogenesis, tissue fibrosis and tumorigenesis[27]. One the one hand EMT contributes to tissue development, wound healing and homeostasis[26], while on the under hand, under certain conditions it promotes malignancy[6]. In cancer, specifically, EMT is responsible for dissociation and migration of tumor cells from primary tumors, and invasion of surrounding tissues leading to metastasis[27]. EMT is highly regulated transcriptionally, post-transcriptionally, translationally, and post-translationally[28]. The transcriptional program that drives EMT involves activities of several transcription factors of different families[29]. Evidence of regulation by PTMs other than phosphorylation, such as O-GlcNAc that has bearing on physiological conditions of the cell, is still emerging[30]. During EMT, a distinct set of genes is upregulated or down-regulated and the corresponding gene products (RNA, Protein) may serve as EMT markers or be included in typical EMT signatures[31]. Investigation of potential cancer-related EMT protein markers and signatures are the focus of this thesis.

Several studies and reviews have described what happens to cells during EMT. Briefly, cells disassemble the epithelial intercellular junctions (Figure 1.1) and repress expression of junctional proteins. Concomitantly, cells upregulate expression of mesenchymal proteins and ECM metalloproteases, which promote cell invasion. Predominantly, loss of transmembrane adherence protein of epithelial cells, E-cadherin, that is often detected during cancer progression, is a characteristic feature of EMT[29]. This feature is also a marker for tumor cell invasion[6]. In addition, the genetic switch from epithelial to mesenchymal is accompanied by transformation in cellular morphology and reorganization of the actin cytoskeleton. Specifically, the actin protein changes structurally from cortical architecture to stress fibers associated with focal adhesion complex resulting in enhanced ability to migrate[32]. In some tumors, EMT provides cancer cells with the ability to dissociate, degrade the ECM, traverse the basal membrane and invade the surrounding stroma[33]. Clinically the EMT molecular hallmarks that include downregulation of E-cadherin, upregulation of mesenchymal genes and remodeling of extra-cellular matrix are thought to contribute to poor prognosis in many cancers including breast cancers[29].

A holistic view about EMT is that it involves a co-operation between changes in the cell shape, adherence and migration, resistance to apoptosis-inducing stimuli and metabolic pathways[34]. These processes are regulated via signaling pathways that might have common stimuli or characterized by crosstalk resulting in expression of characteristic sets of genes[31]. Thus, systems-based approaches are considered suitable in understanding molecular dynamics within EMT[29]. A typical genome-wide gene expression approach such as a proteomic study would identify and quantify proteins

associated with these changes[35]. It is envisaged that precise knowledge of such changes in cancer cells, as revealed by probing the proteome, may lead to characterization of new candidate biomarkers and therapeutic targets[34].

Various researchers have demonstrated that gene ontology and protein-protein interaction networks enable classification and visualization of distinct features of EMT from mass spectrometry-identified proteins[34, 36-37]. Biarc and coworkers observed protein level structural features of EMT in the form of differentially expressed functional groups of proteins, where each functional group was referred to as 'EMT signature' because of similarity of expression from two signals, mutant K-Ras^{v12}, and TGF-β both of which induced EMT in the same cell line[34]. The functional classes of proteins differentially expressed included ECM proteins, cell adhesion and intercellular junctional proteins, cytoskeletal proteins, degradation, translation and metabolic machineries. Similarly, Vergara and co-authors, obtained EMT-associated proteins from proteomic analyses of non-mesenchymal and mesenchymal breast cancer cellular models[37]. Protein-protein interaction networks revealed signaling pathways that regulate EMT including MAPK, STAT, Src, NF-κB and RhoA. Interestingly, several studies as reviewed elsewhere[4, 38], have shown that TGF-β can trigger many of these pathways that regulate EMT, hence our interest in investigating its possible cooperation with protein O-GlcNAc PTM as influenced by cellular metabolic changes.

1.3 EMT AND TGF-β

TGF-β signaling pathway that is triggered by TGF-β is recognized as the classical and key contributor to cancer progression[6, 39]. TGF-β is a prototype of a large family of

growth and differentiation cytokines, the TGF-β superfamily, whose members regulate a wide variety of cellular processes in different tissue and cell types[40-41]. TGF-β itself participates in major cellular processes such as proliferation, differentiation, migration and apoptosis[42]. As a potent inducer of EMT, TGF-β occurs in high levels in many kinds of tumors and its levels are often correlated to high invasion and onset of metastasis[43]. Of importance, also is the fact that TGF-β signaling has antagonistic effects between early and late tumor stages. Both effects have been demonstrated *in vitro* in mammary epithelial cellular models and many cancer cell lines[44], and confirmed through *in vivo* studies, involving TGF-β treatment. In early stages of cancer, TGF-β acts as a tumor suppressor by inhibiting cell proliferation and inducing apoptosis, whereas in later stages of cancer, it promotes tumorigenesis by stimulating EMT, angiogenesis, immune response escape, stemness, invasion and metastasis[45].

TGF-β/Smad signaling has been well studied and widely reviewed[43, 46-49]. Briefly, TGF-β initiates its signals of multifunctional effects by binding to type II serine-threonine kinase receptor (TβRII), thus causing a heteromeric complex formation of this receptor with type I kinase receptor (TβRI), resulting in trans-phosphorylation and activation of both receptors (Figure 1.2). From TβRI, different signaling cascades will be initiated depending on whether serine-threonine kinase or tyrosine kinase of the receptor is activated. In canonical TGF-β signaling, represented on Figure 1.2, the activated kinase activity of TβRI propagates the signal by phosphorylating serine-threonine residues of the Receptor-regulated Smads (R-Smads), Smad2 and Smad3. The activated R-Smads form heteromeric complex with Smad4 (Co-Smad), leading to translocation of the Smad

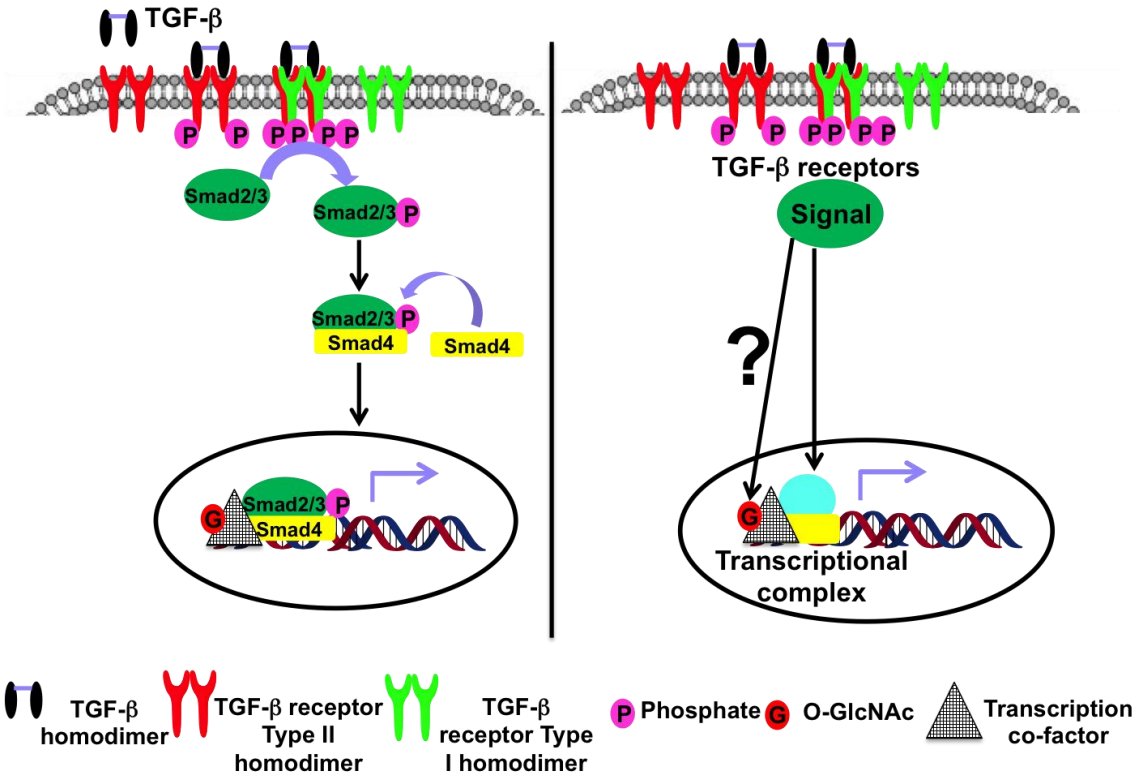

Figure 1.2 Schematic of the canonical TGF-β/Smad signaling showing that the effect of TGF-β, if any, on the O-GlcNAc modification is unknown. The illustration was adopted from a review of C. Heldin *et al*.[57]

complex into the nucleus where the Smad proteins modulate the transcription of TGF-β target genes, mainly those encoding Snail proteins and other EMT transcriptional regulators. In Smad signaling, these EMT regulators aid the heteromeric Smad complex in DNA promoter recognition and binding.

In non-canonical TGF-β signaling, TGF-β activates various non-Smad signaling effectors that produce responses that support EMT program[50]. These include Ras-Erk MAP kinase pathway, that mediates growth stimulation; p38 MAP kinase pathway, that promotes apoptosis; JNK MAP kinase pathway, that modulates phosphorylation of Smad3 thus enhancing Smad signaling[50]; mTOR kinase pathway that promotes increase in cell size and protein synthesis thus supporting cell motility and invasion[51]; PI3K/Akt pathway that sequesters Smad3 thus inhibiting antiproliferative effect of Smad3[52]; RhoA pathway that mediates disassembly of tight junctions[53]; Integrin-Paxillin, that promotes focal adhesion formation as adherence junctions disassemble[54]. In addition, TGF-β signaling can activate other signaling pathways such as Ras and Notch signaling pathways[55]. Notch cooperates with hypoxia to regulate Snail transcription factors and support tumorigenic EMT[56].

Mechanistically, TGF-β activates complex transcriptional networks to establish EMT[57]. The components of the heteromeric Smad complex have low affinity for DNA and therefore, require interaction with and co-activation by transcriptional co-factors[58], some of which are regulated by O-GlcNAcylation, the PTM under investigation in this thesis work. The sequential co-activation of the heteromeric co-Smad complex and its transcriptional effects has been extensively reviewed. However, hardly any reviews show

the detailed regulation of this co-activation by PTMs such as O-GlcNAcylation in the EMT literature. Park *et al.* have demonstrated how the O-GlcNAc modification of Snail1 regulates its transcriptional activities and its phosphorylation[59]. Certainly, though Snail1 is one of the major regulators of EMT, it is not the only O-GlcNAc regulated transcriptional co-factor of the heteromeric co-Smad complex. The extent of O-GlcNAcylation of the heteromeric co-Smad complex transcriptional co-factors and various TGF-β signaling molecules, as well as interplay between the O-GlcNAc and phosphorylation modifications in this context, have to be explored in order to understand how aberrant metabolic changes influence EMT, and possibly to demonstrate if inhibition of such metabolic changes can inhibit EMT, invasion and metastatic spread[34].

1.4 N-ACETYLGLUCOSAMINE POSTTRANSLATIONAL MODIFICATION (PTM)

Research on O-GlcNAcylation in breast cancer has gained interest since the discovery about five years ago that global GlcNAcylation levels are associated with breast cancer formation and metastasis[60]. Unlike the classical N-linked and O-linked glycosylation, O-GlcNAcylation is a PTM in which a monosaccharide N-acetylglucosamine (GlcNAc) is attached in β-O-linkage to Serine and Threonine hydroxyl groups of nucleocytoplasmic proteins[61-62]. It has no consensus motif and it is abundant and reversible and occurs in multicellular eukaryotes[63]. It is similar to phosphorylation but different from the traditional N-, and O-linked glycosylation[64-65]. Both phosphorylation and O-GlcNAcylation are dynamic in their response to biological stimulus and widespread among regulatory and signaling proteins[66]. Different functional classes of proteins including transcriptional and translational machinery, degradation proteins, cytoskeletal and signaling proteins are modified and regulated by phosphorylation and O-

GlcNAcylation[67-69]. Both PTMs modify same proteins and compete for the same Serine and Threonine sites of proteins, where their effect is reciprocal and is characterized by a 'yin-yang' relationship[70-71]. Each PTM has two recycling enzymes, one that attaches the modification (i.e. kinase and OGT), and the other that removes the modification (i.e. phosphatase and O-GlcNAcase)[72-73]. These enzymes and their target proteins are in close proximity since they are colocalized thus allowing for dynamic effect to take place[63]. However, the enzymes responsible for N-, and O-linked glycosylation are located in different cellular compartments (Golgi and ER versus lumen of exocytic and endocytic organelles), thus making dynamic response unlikely[63].

Despite its resemblance of phosphorylation, O-GlcNAcylation is distinct in that it is directly associated with the nutritional and energy status of the cell[74]. It is considered a nutrient sensor because of its responsiveness to the nutrient state of the cell that is coupled with modulation of function of target proteins making them respond appropriately to extracellular stimuli[75]. From the external sources including glucose and glucosamine, O-GlcNAc is made available for post-translational modification through the hexosamine biosynthetic pathway (HBP)[76] (Figure 1.3). This pathway is linked to glycolysis during the rate-limiting step in which Fructose-6-phosphate is converted in the presence of glutamine to Glucosamine-6-phosphate by GFAT[77]. HBP ultimately produces UDP-GlcNAc, the substrate for modification of serine and threonine residues of proteins by OGT enzyme. Aside from glycolysis, several other metabolic pathways are linked to HBP, hence UDP-GlcNAc is synthesized from several metabolites including glutamine, acetyl-coenzyme A, uridine and ATP[78-79].

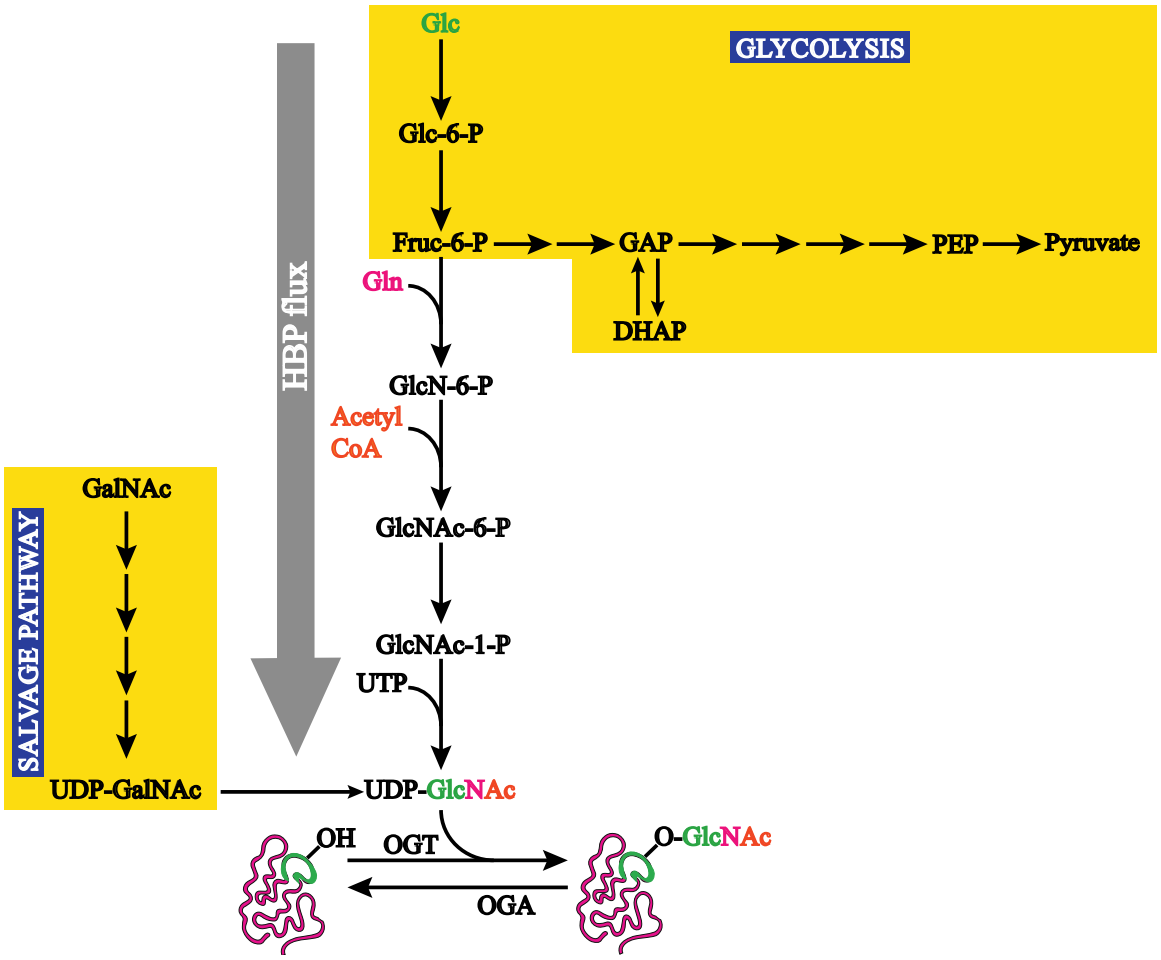

Figure 1.3 Schematic illustration of the hexosamine biosynthetic pathway showing flow of metabolites from other pathways especially glycolysis and the salvage pathways. The scheme was adopted from the review of L. Wells and G. W. Hart [76], and C. Slawson *et al.*[82]

There are many ways in which glucose uptake and flux through glycolysis are altered to modulate HBP[80]. Several signals including those induced by cellular stress, insulin and many cytokines increase glucose uptake through upregulation of glucose transporters[81]. These signals tend to be disease-specific and some are triggered in response to environmental glucose concentration. In hyperglycaemic conditions, for instance, high extracellular glucose levels alter cellular function through upregulation of the HBP leading to elevated levels of UDP-GlcNAc that promote insulin resistance, a hallmark of type II diabetes[77]. In cancer, increased glucose flux through HBP is influenced by abnormal regulation of glycolysis, owing to high energy demands of cancer cells, regardless of hyperglycaemic conditions[82]. With regards to TGF-β signaling, high glucose was found to induce endogenous TGF-β1 production mediated by HBP in murine mesangial cells[83]. The autocrine TGF-β stimulation resulted in upregulation of ECM proteins and reduced proliferation. These observations imply that glycolysis-influenced glucose flux characteristic to cancer might enhance TGF-β-induced EMT. However, the influence of TGF-β on glycolysis and HBP to modulate O-GlcNAcylation is not known.

1.5 O-GLCNACYLATION AND METABOLISM IN BREAST CANCER

1.5.1 "Warburg Effect"

Metabolic dysfunction in cancer was first described by O. Warburg in 1956[84]. Now known as "Warburg effect", this metabolic shift involves increase in glycolysis under conditions of high oxygen tension, resulting in enhanced lactate production, as well as increase in glucose uptake and use of the elevated amounts of glucose as a carbon source for biosynthesis[85-86]. It is known that 2-5% of glucose entering the cell is used to produce

UDP-GlcNAc through Hexose Biosynthetic Pathway[87]. Elevated levels of UDP-GlcNAc increase the activity of OGT since it is tightly dependent on the concentration of the substrate UDP-GlcNAc in the cell[88]. Thus, enhanced glucose uptake and metabolism result in elevated intracellular (global) O-GlcNAcylation and subsequent modulation of target proteins to the advantage and support of the cancer phenotypes[89]. O-GlcNAc levels are increased in many tumor types[89].

O-GlcNAcylation has a role in many biological processes under normal and diseased states, where in the latter, its effects may be due to faulty metabolic regulation that contributes to disease pathology[60]. For instance, in cancer, several tumor-associated proteins, mostly transcription factors, have been identified as O-GlcNAcylated proteins[59, 69, 90]. The effects of O-GlcNAcylation on the function of only a few of these proteins, as well as the roles of their O-GlcNAcylation in cancer progression, have been investigated[59]. Snail1, a mediator of TGF-β signaling and EMT transcriptional inducer, is one such protein. The co-regulation of Snail1 through O-GlcNAcylation and TGF-β signaling during cancer progression has not been made clear.

1.5.2 O-GlcNAcylation and Invasion and Metastasis

TGF-β- induced EMT is crucial in breast cancer metastasis since many of the breast carcinomas are of epithelial origin[91]. It has been established that since loss of E-cadherin is associated with poor clinical outcome[92], the molecule that causes this loss becomes a marker of malignancy, and a good target for anti-invasive cancer therapy[93]. Therefore, it is important to establish E-cadherin repressors during tumor progression. To this end, the mechanism by which O-GlcNAcylation leads to cancer invasion and metastasis is still not

clearly understood[60], as illustrated in Fig. 1.4. Suppression of E-cadherin was found to be one way in which the effects of O-GlcNAcylation in breast cancer are mediated[60]. Coincidentally, down-regulation of E-cadherin is known to be the key mechanism and hallmark of EMT, a process that initiates invasion and metastasis[6]. Therefore, it is surprising that in investigating the mechanism of how O-GlcNAcylation contributes to cancer invasion, an upstream process such as EMT nor the signal transduction pathways associated with it, have not been considered[60]. Nonetheless, down-regulation of E-cadherin due to O-GlcNAcylation suggests a crosstalk between O-GlcNAcylation and signaling pathways leading to EMT, invasion and metastasis, in which, proteins that regulate and mediate EMT, invasion and metastasis are, in turn regulated by O-GlcNAcylation. In the context of TGF-β-induced EMT in breast cancer, Snail1 is the only regulatory O-GlcNAcylated protein that has been characterized[59]. The O-GlcNAcylation of E-cadherin binding partners, p120 and β-catenin in breast cancer suggests that there might be other proteins relevant to breast cancer whose regulation by O-GlcNAcylation is still unknown. Similar to Snail1, these proteins could be targets for therapeutic interventions during TGF-β-mediated EMT, invasion and metastasis. Detailed knowledge of the critical roles played by O-GlcNAcylation and other modifications on the function of such proteins is therefore essential.

1.5.3 O-GlcNAcylation and TGF-β Signaling

O-GlcNAcylation is known as a link between nutrient sensing and signaling[94]. Although this fact is well established in insulin signaling[77], few studies provide evidence for the linking role of O-GlcNAcylation in TGF-β signaling. Figure 1.4 illustrates the roles that

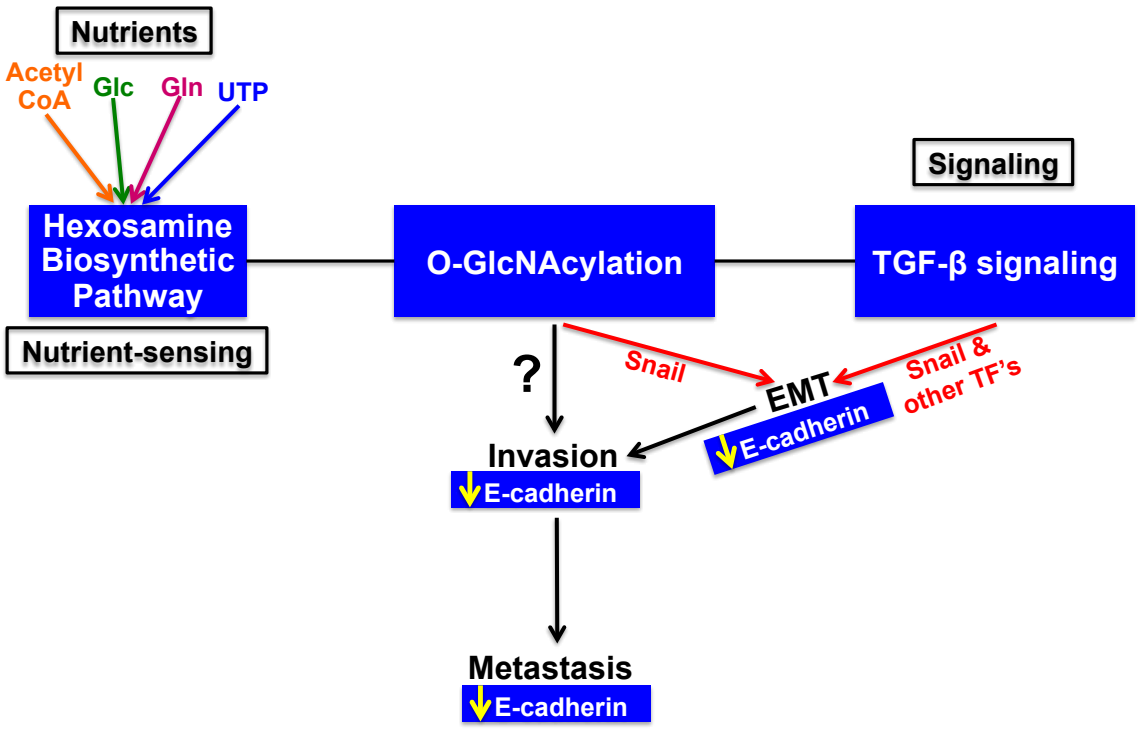

Figure 1.4 Illustration of the relationship between O-GlcNAcylation and TGF-β signaling, constructed from connections made from findings and reviews of Y. Gu *et al.*[60], S. Y. Park *et al.*[59], and S. Hardiville and G. W. Hart[94].

glucose and its metabolic sensor (HBP) play in TGF-β signaling. On the one hand, glucose induces phosphorylation of Smad3, and activates Akt-TOR signaling thus causing increase in protein synthesis and cellular hypertrophy[95]. Previously, glucose had been shown to stimulate autocrine activation of TGF-β in murine mesangial cells, which in turn induces collagen gene expression and protein synthesis[83, 96]. On the other hand, upregulation of Snail1 by O-GlcNAcylation due to high glucose flux through HBP leads to tumorigenic EMT, invasion and metastasis[59]. Although O-GlcNAcylation is not implicated in the phosphorylation of Smad3, both effects contribute to cancer malignancy.

Taken together, the previous studies show that TGF-β signaling is a well-studied signal transduction pathway whose role in cancer progression is known but whose contribution to metabolic dysfunction with regards to Warburg effect of carcinogenesis is not clear. Therefore study of dynamic regulation of cellular metabolic pathways by TGF-β is critical. Neither the investigation of O-GlcNAcylation of E-cadherin and its binding partners, p120 and Catenin, nor O-GlcNAcylation of Snail1 alone is sufficient to demonstrate how TGF-β causes metabolic shift and promotes malignancy. Perhaps a combination of quantitative proteomics and metabolic analysis as reported in Shaw *et al*. is a suitable approach[97]. In this thesis, we intend to use mass spectrometry to explore the O-GlcNAc proteome during TGF-β-induced EMT, as this proteome can reveal the relationship between O-GlcNAcylation and TGF-β signaling.

1.6 MS-BASED PROTEOMICS

1.6.1 Background

The field of proteomics is a collection of various technical disciplines that deal with large-scale determination of gene and cellular functions directly at the protein level[98]. A proteomic approach may take any one of these two routes: 1) MS-based identification of proteins isolated from cells or tissues, and 2) activity-based biochemical and genomic analyses that may involve cell imaging, array and chip experiments, and genetic readouts[98-99]. In the post-genomic era, rapid identification of proteins using mass spectrometry is a common proteomic practice[100]. However, in the traditional sense, this approach is inadequate for functional proteomics investigations and requires improvements to be suitable for site-specific mapping of post-translational modifications and protein-protein interactions[25]. Recent advancements in MS-based techniques for protein identification and PTM site-mapping have accelerated functional proteomics and methodologies are evolving to address inherent challenges posed by the nature of the biological sample[101].

Due to a large dynamic range of proteins in complex biological samples, there is a bias toward detecting high abundance proteins[63]. As a result, proteins with low copy number, many of which are regulatory and post-translationally modified have low sequence coverage and are unlikely to be detectable[102]. In addition to being low abundance proteins, the low stoichiometry of the PTMs and their lability during collision-induced dissociation (CID) make it more challenging to analyze PTMs[103]. Hence the traditional analytical proteomic approach involving separation of proteins using 2D-

PAGE prior to LC-MS/MS is replaced or augmented by affinity enrichment approaches that selectively isolate sub-population of peptides and proteins bearing the O-GlcNAc PTM, prior to LC-MS/MS[63]. By complementing sample pre-fractionation, these approaches not only effectively reduce sample complexity but also increase proteome coverage and may be amenable to PTM site mapping.

1.6.2 Affinity Enrichment Approaches for O-GlcNAc PTM

Affinity tags coupled to solid supports such as agarose constitute popular affinity enrichment strategies for O-GlcNAc-modified peptides and proteins[63, 104]. Since the discovery of O-GlcNAc PTM about 30 years ago[61], different methodologies involving covalent and non-covalent attachment to affinity probes have been employed and widely reviewed[105]. These include the non-covalent anti-O-GlcNAc antibody-, and lectin-based strategies, as well as the highly specific chemoenzymatic-, and click-chemistry-based methodologies. The chemoenzymatic-based method originally involved labeling GlcNAc sites of proteins with [^{3}H]galactose from UDP-[^{3}H]galactose, with the catalytic action of β-1,4-galactosyltransferase[61-62], and subsequent detection of the radiolabeled amino acid using Edman sequencing[106]. Khidekel *et al*. eliminated the use of radiolabeling and modified this method to incorporate keto-galactose using a suitable recombinant β-1,4-galactosyltransferase, followed by biotinylation at its keto moiety, avidin affinity chromatography and subsequent protein identification by LC-MS/MS[107]. Wang *et al*. improved the strategy by using a novel photocleavable biotin probe that improved the analytical capability of chemoenzymatic labeling[103]. This strategy was even further improved by using Click chemistry-based photocleavable biotin probe as described in Alfaro *et al*[108].

Prior to the method modification championed by Khidekel and co-workers, O-GlcNAc sites on only 80 mammalian proteins had been reported[109]. Using chemoenzymatic labeling and Orbitrap LC-MS/MS Khidekel *et al*. then contributed additional 30 proteins[110]. Although their strategy revolutionized the affinity enrichment of O-GlcNAc proteins, the analytical performance had low throughput. Due to this limitation, the improved methodology applied in Alfaro *et al*.[108] is the one considered instead among the highly promising strategies for O-GlcNAc affinity enrichment[111]. Alfaro and coworkers performed chemoenzymatic labeling of the O-GlcNAc proteome from brain tissue using GalNAz, followed by biotinylation using PC-PEG-biotin-alkyne, and enrichment using avidin affinity chromatograpy. In that study the largest number of O-GlcNAc sites, 458 from 195 proteins was reported. On the non-covalent front, lectin weak affinity chromatography strategy as developed by Vosseller *et al*.[112], and applied later in Trinidad *et al*.[113] and Myers *et al*.[114] is also "high-throughput" proteome-wide, since the latter yielded 142 O-GlcNAc sites from 62 proteins[111]. Nonetheless, use of Click chemistry-based strategies involving cleavable reagent as demonstrated in Alfaro *et al*. and Wang Z. *et al*. have opened a door to diversity of countless possibilities for exploiting the CuAAC and SPAAC for affinity enrichment of O-GlcNAc proteins. Although the CuAAC-based approaches are common, the reagents of the CuAAC reaction are viewed as toxic and destructive to peptides and to components of the biotin-avidin system[115]. Therefore development of SPAAC approaches that exclude biotin-avidin system is necessary.

In the past few years there has been a growing interest in the application of Click chemistry involving [3 + 2] azide-alkyne cycloaddition for probing chemically modified

proteins bearing bioorthogonal chemical tags. More than a decade ago Bertozzi and co-workers established that incorporation of unnatural metabolite provides opportunities for protein modification and selective labeling of proteins[116]. In particular these authors showed that labeling glycoproteins with a unique chemical tag permits their selective modification from complex mixtures. Such chemical tags eventually facilitate identification of glycoproteins by proteomic strategies. Various strategies previously employed in tagging O-GlcNAc modified proteins to form a handle for Click chemistry-based affinity enrichment are shown in Table 1.2. In general, the enrichment route begins by attaching the chemical handle to O-GlcNAc proteins through chemoenzymatic or metabolic labeling, followed by conjugation of the functionalized proteins to the enrichment probe that may be biotin-, or non-biotin-based. Subsequently the affinity-enriched proteins are released from the probe and analyzed by LC-MS/MS.

The common practice in click chemistry-based strategies involving metabolic labeling has been described in the studies of Bertozzi and coworkers[117]. Treatment of cells with either N-azidoacetylglucosamine, N-azidogalactosamine or N-alkynylglucosamine results in the metabolic incorporation of the azido sugar into nuclear and cytoplasmic proteins in place of O-GlcNAc. Briefly, the exogenously added AC_4GlcNAz, AC_4GalNAz or AC_4GlcNAlk will diffuse into the cells and be deacetylated by action of intracellular esterases. The deacetylated Azido sugar will then enter the salvage pathway of the hexosamine biosynthesis where UDP-GlcNAz, a donor substrate for O-GlcNAcylation of nucleocytoplasmic proteins, is produced. The azido-tagged post-

Table 1.2 Click chemistry-based O-GlcNAc affinity enrichment strategies

O-GlcNAc Labeling	Conjugation to Probe	Biotin or none	Affinity Enrichment	Downstream Analysis	Results	References
Chemoenzymatic	CuAAC	Biotin-based	GalNAz labeling + Biotin-PEG-PC-Alkyne + Biotin/Avidin	LC-CID/HCD/ETD-MS/MS	458 O-GlcNAc sites on 195 proteins	Alfaro *et al.* 2012[108]
			GalNAz labeling + Biotin-alkyne + Biotin/Avidin	LC-CID-MS/MS	213 Putative (67 previously reported)	Clark *et al.* 2008[118]
		No biotin	GalNaz labeling + Phospho-alkyne + Phospho/TiO_2	LC-HCD/ETD-MS/MS	42 O-GlcNAc peptides (7 novel O-GlcNAc sites)	Parker *et al.* 2011[119]
Metabolic	Staudinger ligation	Biotin-based	GlcNAz labeling +Biotin-phosphine + Biotin/Avidin	LC-CID-MS/MS	10 O-GlcNAc + 41 Putative	Sprung *et al.* 2005[120]

Table 1.1 (Contd.)

				199 Putative (23 validated)	Nandi *et al*. 2006[121]
	CuAAC	Biotin-based	GlcNAz labeling +Biotin-alkyne + Biotin/Avidin	LC-CID-MS/MS	32 Putative (14 previously unreported)	Gurcel *et al*. 2008[122]
			GlcNAlk labeling + Azido-azo-biotin + Biotin/Avidin	LC-CID-MS/MS	374 Putative (279 previously unreported)	Zaro *et al*. 2011[123]
					431 Putative (115 previously unreported)	Gurel and Zaro *et al*. 2014[124]
		No biotin	GlcNAz labeling + resin-alkyne	BEMAD + LC-CID/HCD-MS/MS	1500 O-GlcNAc proteins + 185 O-GlcNAc sites on 80 proteins	Hahne *et al*. 2013[111]

translationally modified O-GlcNAc proteins can be covalently derivatized with biochemical probes that may be biotin-based, in which case the resin should also be derivatized with the corresponding affinity material, avidin; or alkyne. These affinity probes are suitable for peptides only, proteins only or both. Below is a synopsis of selected downstream MS analytical strategies that will be used for proteomic profiling of breast tumor cells and mammary epithelial tumor model cells.

1.7 MS INSTRUMENTATION FOR PROTEOMIC PROFILING

1.7.1 Background

Mass spectrometry (MS) has become a suitable tool for rapid analysis of proteins sourced from complex biological mixtures[99]. As a discipline within the multifaceted field of proteomics, MS-based proteomics is the current indispensable technology for giving information about the primary structure of a protein, its post-translational modifications and its interactions with other proteins[125]. Most importantly, MS-based proteomics is capable of solving biological and clinical questions as it can allow: generation of protein-protein interaction maps; gene ontology annotations based on the protein identification technology; and analysis of protein expression profiles as a function of cellular state thus making inference of cellular function possible[126]. The key role of MS-based proteomics in cancer research is characterization of proteins through identification, quantification, and functional assignment, thus, contributing to the understanding of molecular events involved in cancer progression[25]. It has been recognized that the proteomic information will improve cancer diagnosis, prognosis, prevention and treatment through development of cancer biomarkers and targeted therapies[127]. In this thesis work MS-based proteomics

technology will be applied in protein profiling of breast cancer cell lines as well EMT breast tumor model cells to test the efficiency of novel sample preparation strategies in revealing distinguishing features that reflect breast cancer biomarkers and O-GlcNAc EMT signatures as well as unknown protein functions. Two approaches of protein profiling, namely; intact cell MALDI-TOF-MS profiling and O-GlcNAc proteomic profiling will be undertaken. To understand these proteomic approaches, the capabilities of the two MS instruments of interest, namely; MALDI-TOF-MS and LC-MS/MS (LTQ orbitrap) have been briefly reviewed.

A mass spectrometer is an instrument that determines the mass of molecules by measuring their mass-to-charge ratio (m/z) and generates a mass spectrum[128]. It consists of three main parts, namely; 1) ion source, where analyte molecules are ionized in gaseous form, 2) mass analyzer, that measures the mass-to-charge (m/z) ratio of the ions, and 3) a detector, that records the number of ions at m/z and gives out a signal[98]. Although a mass spectrometer was invented in the 19th century, analysis of biomolecules was only made possible following the discovery of "soft" ionization techniques, MALDI and ESI, in the late 20th century[129-130]. These ionization techniques result in minimal fragmentation of the analyte. MALDI sublimates, in a vacuum, the mixture of matrix and sample and uses laser pulses to ionize the analyte out of this dry, crystalline mixture of matrix and sample[131]. ESI ionizes the analyte coming out of sample solution and is therefore usually coupled to liquid chromatography[132].

Mass measurement of analyte ions generated using either of these two processes would not be possible if it were not for the powerful mass analyzers coupled therewith that possess superior qualities required for good analytical performance. Such analytical

performance parameters include sensitivity, resolution, mass accuracy and ability to generate information-rich MS/MS spectra from peptide fragments[133]. The four basic types of mass analyzers with stellar qualities for MS measurements are TOF, ion trap, quadrupole and Fourier-Transform cyclotron[98]. MALDI is usually coupled to TOF analyzer that measures the mass of intact peptides while ESI is often coupled to ion trap and triple quadrupole mass spectrometers in which fragment ion spectra of selected precursor ions are generated[134]. Modern mass spectrometers come with advanced technology that brings outstanding analytical performance owing to the contribution of parts that make up their hybrid mass analyzers[135-138]. Such improvement accounts for higher mass accuracy, higher detection capability and shorter cycling times that enable increased throughput and more reliable data[139]. A typical example of such instruments is the Linear Trap Quadrupole-Orbitrap ion trap velos mass spectrometer[140] (Thermo Fisher Scientific, Germany) that has been employed in the proteomics studies in this thesis.

1.7.2 The LTQ Orbitrap Mass Spectrometer

In principle, LTQ Orbitrap mass spectrometer has five basic components, namely; an API ion source, in which the analyte is ionized under atmospheric pressure; LTQ mass analyzer, in which the masses of ions are analyzed using MS and MS^n scan modes; a C-trap, that allows accumulation and external storage of ions before they are pulsed into the Orbitrap. The components are shown on Figure 1.5. It is in the orbitrap that the ions assume circular trajectories around the center electrode and their axial oscillations along this electrode are detected. The Orbitrap uses the Fourier Transform function to detect ions hence it shares a similar feature with the high resolution FTICR mass spectrometer[138]. Invented by Makarov before commercialization in 2005, the Orbitrap is

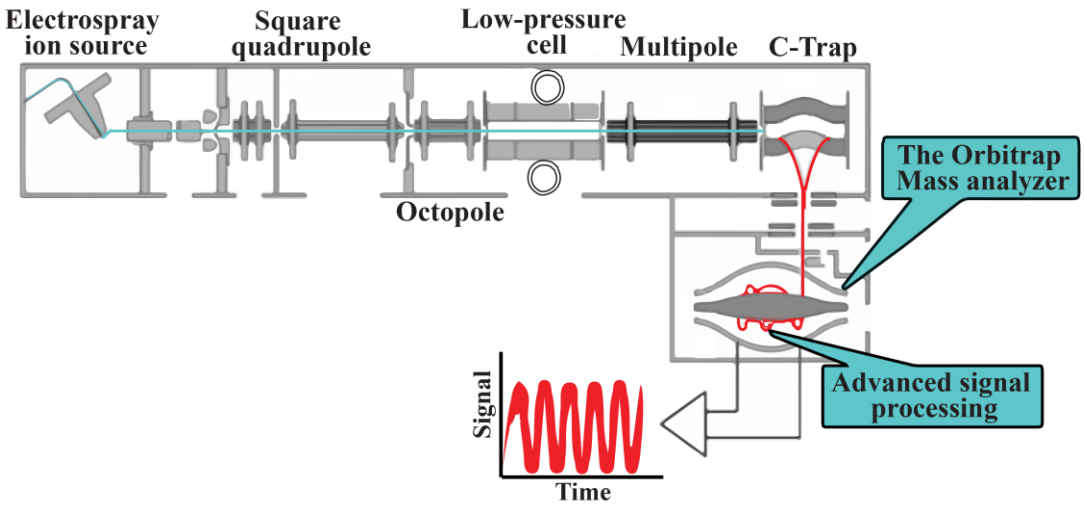

Figure 1.5 Diagram showing the route of ions and signal in the LTQ Orbitrap MS, adopted from S. Eliuk and A. Marakarov[102]. The horizontal turquoise line represents the flow of ions. The converging red edges coming from the C-Trap represent the ion packet (pulse) injected into the orbitrap mass analyzer where advanced signal processing by Fourier Transform function takes place.

one of the newest mass analyzers with outstanding analytical features that include high mass resolution (up to 150 000), large space charge capacity, and high mass accuracy (2-5 ppm)[141-142]. Collectively, the combination of the patented Orbitrap technology and the powerful Finnigan LTQ linear ion trap in an LTQ Orbitrap mass spectrometer provides faster, more sensitive and more reliable detection and identification platform for MS-based proteomics[102, 137].

Moreover, Orbitrap mass spectrometer is an instrument of choice for functional proteomics[102]. It allows fragmentation of peptides by different modes, collision-induced dissociation, electron transfer dissociation and high-energy C-trap dissociation[102]. The commonly used CID for conventional peptide sequence analysis causes neutral loss of GlcNAc as an oxonium ion prior to fragmentation of the peptide backbone. As a result, the peptide bearing the GlcNAc cannot be located[143]. Conversely, ETD causes fragmentation of the backbone with GlcNAc modification intact therefore it allows identification of that peptide and GlcNAc site mapping[144-145]. HCD also leaves the modified peptide intact[146]. Hence, as shown in Table 1.2, affinity enrichment strategies such as those of Alfaro *et al.*[108] and Hahne *et al.*[111] that were followed by MS analysis involving combinations of fragmentations resulted in reports of high number of O-GlcNAc sites and proteins with valid O-GlcNAc. Derivatization of peptides using BEMAD improves site identification using CID[125]. For more confident O-GlcNAc site mapping a combination of ETD and HCD is recommended[147].

1.7.3 The MALDI-TOF Mass Spectrometer

MALDI-TOF mass spectrometer, in particular, is widely used for protein profiling and discovery of disease biomarkers from different biological samples[148]. As illustrated in Figure 1.6, it uses pulsed laser irradiation of a co-crystal of a UV-absorbing compound (a matrix) and the analyte to desorb and ionize the analyte molecules in a gaseous phase[131]. A spectrum is then recorded directly following the drift of ions in the flight-tube and their subsequent detection. Each mass spectrum is a graph of protein intensity against m/z and consists of a series of protein peaks. MALDI-TOF-MS has proven to be a suitable instrument for rapid profiling of different biological samples including intact cells[151-156]. It has been applied previously for rapid profiling of bacteria, fungi, and human clinical specimen such as serum and biopsies[153, 157-159]. It has been employed in this thesis for profiling of breast cancer cells involving novel sample preparation.

1.8 SPECIFIC AIMS AND RESEARCH QUESTIONS

In chapter 2 of this thesis we asked whether breast cancer cell lines could be rapidly profiled and distinguished based on their protein mass spectral differences. The specific aims were to 1) develop a novel sample preparation methodology for rapid MALDI MS profiling of mammalian cells; and 2) apply the established methodology to distinguish breast cancer cell lines of different metastatic potential. The novel sample preparation strategy involved “one-tube” pretreatment of cell pellet with a mixture of unique composition containing some known MALDI solvents and matrices, followed by instrumental analysis of the samples to generate their mass spectral profiles, as well as application of computational methods to reveal and visualize the differences.

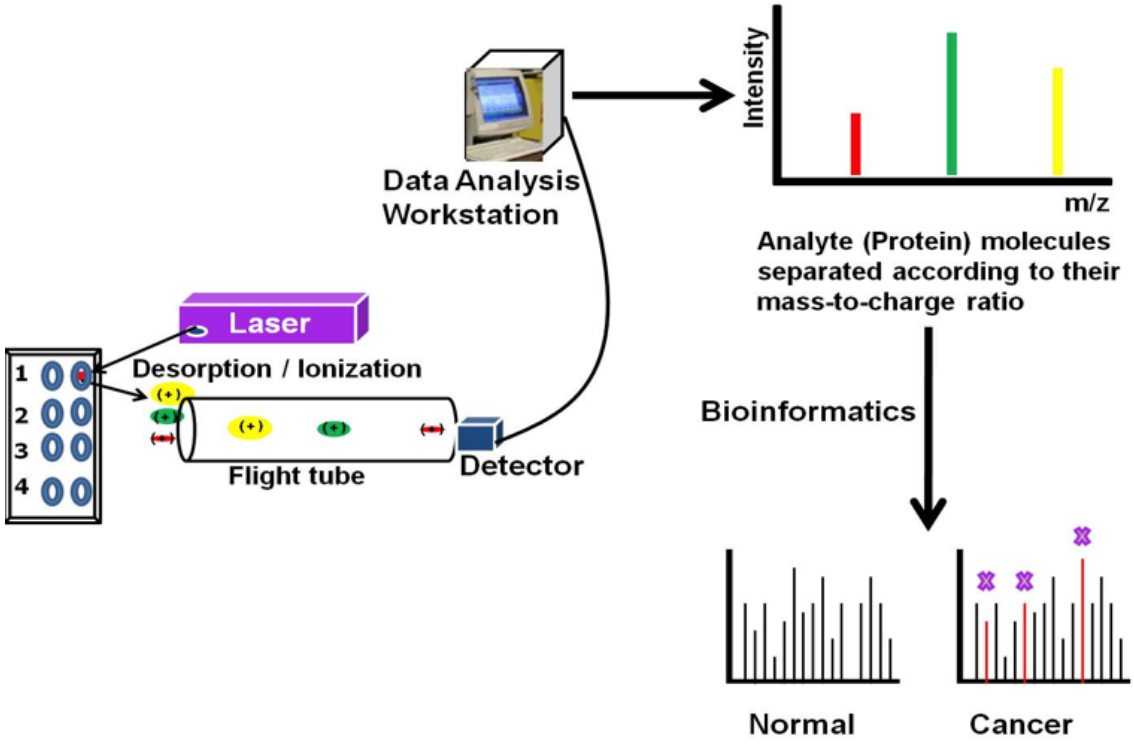

Figure 1.6 Schematic of the MALDI-TOF-MS analysis starting from desorption/ionization of the protein molecules through display of a spectrum and discrimination between normal and cancer samples using bioinformatics methods. This illustration was adopted from reports of C. Laronga and R. Drake[149], as well as Y. Yasui *et al*.[150]

In Chapter 3, we sought to develop a SPAAC-based affinity enrichment strategy and use it to obtain insights on O-GlcNAc proteome of TGF-β induced EMT. We asked whether TGF-β, in inducing EMT, modulates O-GlcNAc modification of nucleocytoplasmic proteins. Could there be a crosstalk between TGF-β and O-GlcNAc signaling pathways during EMT? The specific aims were to 1) characterize the affinity enrichment dibenzocyclooctyne-disulphide-beaded resin probe; 2) metabolically label cellular proteins with GalNAz and enrich the labeled proteome through SPAAC using the resin; and 3) employ shotgun proteomics to identify and quantify the azido-labeled O-GlcNAc-proteome of NMuMG cells undergoing EMT. The biochemical probe employed in this thesis is a unique "Click-able and cleavable" dibenzocyclooctyne-modified resin that serves as an affinity enrichment tool for the purpose of facilitating mass spectrometric identification of azido-labeled O-GlcNAc-modified proteins from TGF-β-induced EMT.

REFERENCES

1. R. L. Siegel, K. D. Miller, A. Jemal, Cancer statistics, 2015. *CA Cancer J. Clin.,* **2015,** 65, 5-29.

2. B. A. Kohler, R. L. Sherman, N. Howlader, A. Jemal, A. B. Ryerson, K. A. Henry, *et al.,* Annual Report to the Nation on the Status of Cancer, 1975-2011, Featuring Incidence of Breast Cancer Subtypes by Race/Ethnicity, Poverty, and State. *J. Natl. Cancer Inst.,* **2015,** 107, djv048.

3. A. Journet, M. Ferro, The potentials of MS-based subproteomic approaches in medical science: the case of lysosomes and breast cancer. *Mass Spectrom. Rev.,* **2004,** 23, 393-442.

4. E. Foubert, B. De Craene, G. Berx, Key signalling nodes in mammary gland development and cancer. The Snail1-Twist1 conspiracy in malignant breast cancer progression. *Breast Cancer Res.,* **2010,** 12.

5. W. Clarke, Z. Zhang, D. W. Chan, The application of clinical proteomics to cancer and other diseases. *Clin. Chem. Lab. Med.,* **2003,** 41, 1562-1570.

6. J. P. Thiery, Epithelial-mesenchymal transitions in tumour progression. *Nat. Rev. Cancer,* **2002,** 2, 442-454.

7. P. O'Connell, V. Pekkel, S. A. Fuqua, C. K. Osborne, G. M. Clark, D. C. Allred, Analysis of loss of heterozygosity in 399 premalignant breast lesions at 15 genetic loci. *J. Natl. Cancer Inst.,* **1998,** 90, 697-703.

8. C. Nordqvist Breast Cancer: Causes, Symptoms and Treatments. http://www.medicalnewstoday.com/articles/37136.php (accessed October 01, 2015).

9. S. Ramaswamy, K. N. Ross, E. S. Lander, T. R. Golub, A molecular signature of metastasis in primary solid tumors. *Nat. Genet.,* **2003,** 33, 49-54.

10. P. T. Simpson, J. S. Reis-Filho, T. Gale, S. R. Lakhani, Molecular evolution of breast cancer. *J. Pathol.,* **2005,** 205, 248-254.

11. C. M. Perou, T. Sorlie, M. B. Eisen, M. van de Rijn, S. S. Jeffrey, C. A. Rees, *et al.,* Molecular portraits of human breast tumours. *Nature,* **2000,** 406, 747-752.

12. T. Sorlie, C. M. Perou, R. Tibshirani, T. Aas, S. Geisler, H. Johnsen, *et al.*, Gene expression patterns of breast carcinomas distinguish tumor subclasses with clinical implications. *Proc. Natl. Acad. Sci. U. S. A.,* **2001,** 98, 10869-10874.

13. T. Sorlie, R. Tibshirani, J. Parker, T. Hastie, J. S. Marron, A. Nobel, *et al.*, Repeated observation of breast tumor subtypes in independent gene expression data sets. *Proc. Natl. Acad. Sci. U. S. A.,* **2003,** 100, 8418-8423.

14. J. S. Reis-Filho, S. R. Lakhani, The diagnosis and management of pre-invasive breast disease: genetic alterations in pre-invasive lesions. *Breast Cancer Res.,* **2003,** 5, 313-319.

15. M. Aubele, A. Mattis, H. Zitzelsberger, A. Walch, M. Kremer, G. Welzl, *et al.*, Extensive ductal carcinoma In situ with small foci of invasive ductal carcinoma: evidence of genetic resemblance by CGH. *Int. J. Cancer,* **2000,** 85, 82-86.

16. S. R. Morris, L. A. Carey, Molecular profiling in breast cancer. *Rev. Endocr. Metab. Disord.,* **2007,** 8, 185-198.

17. F. Bertucci, D. Birnbaum, A. Goncalves, Proteomics of breast cancer - Principles and potential clinical applications. *Mol. Cell. Proteomics,* **2006,** 5, 1772-1786.

18. A. Goncalves, F. Bertucci, Clinical application of proteomics in breast cancer: state of the art and perspectives. *Med. Princ. Pract.,* **2011,** 20, 4-18.

19. F. Chibon, Cancer gene expression signatures - the rise and fall? *Eur. J. Cancer,* **2013,** 49, 2000-2009.

20. L. J. van 't Veer, H. Dai, M. J. van de Vijver, Y. D. He, A. A. Hart, M. Mao, *et al.*, Gene expression profiling predicts clinical outcome of breast cancer. *Nature,* **2002,** 415, 530-536.

21. M. J. van de Vijver, Y. D. He, L. J. van't Veer, H. Dai, A. A. Hart, D. W. Voskuil, *et al.*, A gene-expression signature as a predictor of survival in breast cancer. *N. Engl. J. Med.,* **2002,** 347, 1999-2009.

22. S. Paik, S. Shak, G. Tang, C. Kim, J. Baker, M. Cronin, *et al.*, A multigene assay to predict recurrence of tamoxifen-treated, node-negative breast cancer. *N. Engl. J. Med.,* **2004,** 351, 2817-2826.

23. R. Bernards, R. A. Weinberg, A progression puzzle. *Nature,* **2002,** 418, 823.

24. S. Cleator, A. Ashworth, Molecular profiling of breast cancer: clinical implications. *Br. J. Cancer,* **2004,** 90, 1120-1124.

25. J. D. Wulfkuhle, K. C. McLean, C. P. Paweletz, D. C. Sgroi, B. J. Trock, P. S. Steeg, *et al.*, New approaches to proteomic analysis of breast cancer. *Proteomics,* **2001,** 1, 1205-1215.

26. R. Kalluri, R. A. Weinberg, The basics of epithelial-mesenchymal transition. *J. Clin. Invest.,* **2009,** 119, 1420-1428.

27. J. P. Thiery, J. P. Sleeman, Complex networks orchestrate epithelial-mesenchymal transitions. *Nat. Rev. Mol. Cell Biol.,* **2006,** 7, 131-142.

28. B. De Craene, G. Berx, Regulatory networks defining EMT during cancer initiation and progression. *Nat. Rev. Cancer,* **2013,** 13, 97-110.

29. H. Peinado, D. Olmeda, A. Cano, Snail, Zeb and bHLH factors in tumour progression: an alliance against the epithelial phenotype? *Nat. Rev. Cancer,* **2007,** 7, 415-428.

30. H. B. Ruan, Y. Nie, X. Yang, Regulation of protein degradation by O-GlcNAcylation: crosstalk with ubiquitination. *Mol. Cell. Proteomics,* **2013,** 12, 3489-3497.

31. K. Lee, C. M. Nelson, New insights into the regulation of epithelial-mesenchymal transition and tissue fibrosis. *Int. Rev. Cell Mol. Biol.,* **2012,** 294, 171-221.

32. S. B. Jakowlew, Transforming growth factor-beta in cancer and metastasis. *Cancer Metastasis Rev.,* **2006,** 25, 435-457.

33. G. Moreno-Bueno, H. Peinado, P. Molina, D. Olmeda, E. Cubillo, V. Santos, *et al.*, The morphological and molecular features of the epithelial-to-mesenchymal transition. *Nat. Protoc.,* **2009,** 4, 1591-1613.

34. J. Biarc, P. Gonzalo, I. Mikaelian, L. Fattet, M. Deygas, G. Gillet, *et al.*, Combination of a discovery LC-MS/MS analysis and a label-free quantification for the

characterization of an epithelial-mesenchymal transition signature. *J. Proteomics,* **2014,** 110, 183-194.

35. A. Gamez-Pozo, J. Berges-Soria, J. M. Arevalillo, P. Nanni, R. Lopez-Vacas, H. Navarro, *et al.*, Combined Label-Free Quantitative Proteomics and microRNA Expression Analysis of Breast Cancer Unravel Molecular Differences with Clinical Implications. *Cancer Res.*, **2015,** 75, 2243-2253.

36. S. Cha, M. B. Imielinski, T. Rejtar, E. A. Richardson, D. Thakur, D. C. Sgroi, *et al.*, In situ proteomic analysis of human breast cancer epithelial cells using laser capture microdissection: annotation by protein set enrichment analysis and gene ontology. *Mol. Cell. Proteomics,* **2010,** 9, 2529-2544.

37. D. Vergara, P. Simeone, P. del Boccio, C. Toto, D. Pieragostino, A. Tinelli, *et al.*, Comparative proteome profiling of breast tumor cell lines by gel electrophoresis and mass spectrometry reveals an epithelial mesenchymal transition associated protein signature. *Mol. Biosyst.*, **2013,** 9, 1127-1138.

38. J. Zavadil, E. P. Bottinger, TGF-beta and epithelial-to-mesenchymal transitions. *Oncogene,* **2005,** 24, 5764-5774.

39. J. P. Thiery, H. Acloque, R. Y. Huang, M. A. Nieto, Epithelial-mesenchymal transitions in development and disease. *Cell,* **2009,** 139, 871-890.

40. J. Massague, A. Hata, F. Liu, TGF-beta signalling through the Smad pathway. *Trends Cell Biol.*, **1997,** 7, 187-192.

41. C. H. Heldin, K. Miyazono, P. ten Dijke, TGF-beta signalling from cell membrane to nucleus through SMAD proteins. *Nature,* **1997,** 390, 465-471.

42. X. Guo, X. F. Wang, Signaling cross-talk between TGF-beta/BMP and other pathways. *Cell Res.*, **2009,** 19, 71-88.

43. A. Moustakas, C. H. Heldin, Induction of epithelial-mesenchymal transition by transforming growth factor beta. *Semin. Cancer Biol.*, **2012,** 22, 446-454.

44. E. Piek, A. Moustakas, A. Kurisaki, C. H. Heldin, P. ten Dijke, TGF-(beta) type I receptor/ALK-5 and Smad proteins mediate epithelial to mesenchymal

transdifferentiation in NMuMG breast epithelial cells. *J. Cell Sci.,* **1999,** 112 (Pt 24), 4557-4568.

45. G. J. Inman, Switching TGFbeta from a tumor suppressor to a tumor promoter. *Curr. Opin. Genet. Dev.,* **2011,** 21, 93-99.

46. C. D. Morrison, J. G. Parvani, W. P. Schiemann, The relevance of the TGF-beta Paradox to EMT-MET programs. *Cancer Lett.,* **2013,** 341, 30-40.

47. J. Xu, S. Lamouille, R. Derynck, TGF-beta-induced epithelial to mesenchymal transition. *Cell Res.,* **2009,** 19, 156-172.

48. J. Massague, TGF-beta signal transduction. *Annu. Rev. Biochem.,* **1998,** 67, 753-791.

49. J. Massague, TGFbeta in Cancer. *Cell,* **2008,** 134, 215-230.

50. P. M. Siegel, J. Massague, Cytostatic and apoptotic actions of TGF-beta in homeostasis and cancer. *Nat. Rev. Cancer,* **2003,** 3, 807-821.

51. S. Lamouille, R. Derynck, Cell size and invasion in TGF-beta-induced epithelial to mesenchymal transition is regulated by activation of the mTOR pathway. *J. Cell Biol.,* **2007,** 178, 437-451.

52. H. J. Cho, K. E. Baek, S. Saika, M. J. Jeong, J. Yoo, Snail is required for transforming growth factor-beta-induced epithelial-mesenchymal transition by activating PI3 kinase/Akt signal pathway. *Biochem. Biophys. Res. Commun.,* **2007,** 353, 337-343.

53. N. A. Bhowmick, M. Ghiassi, A. Bakin, M. Aakre, C. A. Lundquist, M. E. Engel, *et al.,* Transforming growth factor-beta1 mediates epithelial to mesenchymal transdifferentiation through a RhoA-dependent mechanism. *Mol. Biol. Cell,* **2001,** 12, 27-36.

54. X. Han, J. E. Stewart, Jr., S. L. Bellis, E. N. Benveniste, Q. Ding, K. Tachibana, *et al.,* TGF-beta1 up-regulates paxillin protein expression in malignant astrocytoma cells: requirement for a fibronectin substrate. *Oncogene,* **2001,** 20, 7976-7986.

55. E. Janda, K. Lehmann, I. Killisch, M. Jechlinger, M. Herzig, J. Downward, *et al.*, Ras and TGF[beta] cooperatively regulate epithelial cell plasticity and metastasis: dissection of Ras signaling pathways. *J. Cell Biol.,* **2002,** 156, 299-313.

56. N. Tiwari, A. Gheldof, M. Tatari, G. Christofori, EMT as the ultimate survival mechanism of cancer cells. *Semin. Cancer Biol.,* **2012,** 22, 194-207.

57. C. H. Heldin, M. Landstrom, A. Moustakas, Mechanism of TGF-beta signaling to growth arrest, apoptosis, and epithelial-mesenchymal transition. *Curr. Opin. Cell Biol.,* **2009,** 21, 166-176.

58. J. Massague, How cells read TGF-beta signals. *Nat Rev Mol Cell Bio,* **2000,** 1, 169-178.

59. S. Y. Park, H. S. Kim, N. H. Kim, S. Ji, S. Y. Cha, J. G. Kang, *et al.*, Snail1 is stabilized by O-GlcNAc modification in hyperglycaemic condition. *EMBO J.,* **2010,** 29, 3787-3796.

60. Y. Gu, W. Mi, Y. Ge, H. Liu, Q. Fan, C. Han, *et al.*, GlcNAcylation plays an essential role in breast cancer metastasis. *Cancer Res.,* **2010,** 70, 6344-6351.

61. C. R. Torres, G. W. Hart, Topography and polypeptide distribution of terminal N-acetylglucosamine residues on the surfaces of intact lymphocytes. Evidence for O-linked GlcNAc. *J. Biol. Chem.,* **1984,** 259, 3308-3317.

62. G. D. Holt, G. W. Hart, The subcellular distribution of terminal N-acetylglucosamine moieties. Localization of a novel protein-saccharide linkage, O-linked GlcNAc. *J. Biol. Chem.,* **1986,** 261, 8049-8057.

63. K. Vosseller, L. Wells, G. W. Hart, Nucleocytoplasmic O-glycosylation: O-GlcNAc and functional proteomics. *Biochimie,* **2001,** 83, 575-581.

64. L. Wells, K. Vosseller, G. W. Hart, Glycosylation of nucleocytoplasmic proteins: signal transduction and O-GlcNAc. *Science,* **2001,** 291, 2376-2378.

65. F. I. Comer, G. W. Hart, O-glycosylation of nuclear and cytosolic proteins - Dynamic interplay between O-GlcNAc and O-phosphate. *J. Biol. Chem.,* **2000,** 275, 29179-29182.

66. K. Vosseller, K. Sakabe, L. Wells, G. W. Hart, Diverse regulation of protein function by O-GlcNAc: a nuclear and cytoplasmic carbohydrate post-translational modification. *Curr. Opin. Chem. Biol.,* **2002,** 6, 851-857.

67. R. Dentin, S. Hedrick, J. Xie, J. Yates, 3rd, M. Montminy, Hepatic glucose sensing via the CREB coactivator CRTC2. *Science,* **2008,** 319, 1402-1405.

68. X. Yang, P. P. Ongusaha, P. D. Miles, J. C. Havstad, F. Zhang, W. V. So, *et al.*, Phosphoinositide signalling links O-GlcNAc transferase to insulin resistance. *Nature,* **2008,** 451, 964-969.

69. C. Slawson, G. W. Hart, O-GlcNAc signalling: implications for cancer cell biology. *Nat. Rev. Cancer,* **2011,** 11, 678-684.

70. P. Hu, S. Shimoji, G. W. Hart, Site-specific interplay between O-GlcNAcylation and phosphorylation in cellular regulation. *FEBS Lett.,* **2010,** 584, 2526-2538.

71. L. S. Griffith, B. Schmitz, O-linked N-acetylglucosamine levels in cerebellar neurons respond reciprocally to pertubations of phosphorylation. *Eur. J. Biochem.,* **1999,** 262, 824-831.

72. R. S. Haltiwanger, G. D. Holt, G. W. Hart, Enzymatic addition of O-GlcNAc to nuclear and cytoplasmic proteins. Identification of a uridine diphospho-N-acetylglucosamine:peptide beta-N-acetylglucosaminyltransferase. *J. Biol. Chem.,* **1990,** 265, 2563-2568.

73. D. L. Dong, G. W. Hart, Purification and characterization of an O-GlcNAc selective N-acetyl-beta-D-glucosaminidase from rat spleen cytosol. *J. Biol. Chem.,* **1994,** 269, 19321-19330.

74. K. R. Harwood, J. A. Hanover, Nutrient-driven O-GlcNAc cycling - think globally but act locally. *J. Cell Sci.,* **2014,** 127, 1857-1867.

75. G. W. Hart, M. P. Housley, C. Slawson, Cycling of O-linked beta-N-acetylglucosamine on nucleocytoplasmic proteins. *Nature,* **2007,** 446, 1017-1022.

76. L. Wells, G. W. Hart, O-GlcNAc turns twenty: functional implications for post-translational modification of nuclear and cytosolic proteins with a sugar. *FEBS Lett.,* **2003,** 546, 154-158.

77. D. A. McClain, Hexosamines as mediators of nutrient sensing and regulation in diabetes. *J. Diabetes Complications,* **2002,** 16, 72-80.

78. K. E. Wellen, C. Lu, A. Mancuso, J. M. Lemons, M. Ryczko, J. W. Dennis, *et al.*, The hexosamine biosynthetic pathway couples growth factor-induced glutamine uptake to glucose metabolism. *Genes Dev.,* **2010,** 24, 2784-2799.

79. H. N. Moseley, A. N. Lane, A. C. Belshoff, R. M. Higashi, T. W. Fan, A novel deconvolution method for modeling UDP-N-acetyl-D-glucosamine biosynthetic pathways based on (13)C mass isotopologue profiles under non-steady-state conditions. *BMC Biol.,* **2011,** 9, 37.

80. W. Yi, P. M. Clark, D. E. Mason, M. C. Keenan, C. Hill, W. A. Goddard, 3rd, *et al.*, Phosphofructokinase 1 glycosylation regulates cell growth and metabolism. *Science,* **2012,** 337, 975-980.

81. N. E. Zachara, G. W. Hart, Cell signaling, the essential role of O-GlcNAc! *Biochim. Biophys. Acta,* **2006,** 1761, 599-617.

82. C. Slawson, R. J. Copeland, G. W. Hart, O-GlcNAc signaling: a metabolic link between diabetes and cancer? *Trends Biochem. Sci.,* **2010,** 35, 547-555.

83. F. N. Ziyadeh, K. Sharma, M. Ericksen, G. Wolf, Stimulation of Collagen Gene-Expression and Protein-Synthesis in Murine Mesangial Cells by High Glucose Is Mediated by Autocrine Activation of Transforming Growth-Factor-Beta. *J. Clin. Invest.,* **1994,** 93, 536-542.

84. O. Warburg, Origin of Cancer Cells. *Science,* **1956,** 123, 309-314.

85. C. V. Dang, G. L. Semenza, Oncogenic alterations of metabolism. *Trends Biochem. Sci.,* **1999,** 24, 68-72.

86. G. Kroemer, J. Pouyssegur, Tumor cell metabolism: cancer's Achilles' heel. *Cancer Cell,* **2008,** 13, 472-482.

87. S. Marshall, V. Bacote, R. R. Traxinger, Discovery of a Metabolic Pathway Mediating Glucose-Induced Desensitization of the Glucose-Transport System - Role of Hexosamine Biosynthesis in the Induction of Insulin Resistance. *J. Biol. Chem.,* **1991,** 266, 4706-4712.

88. J. E. Rexach, P. M. Clark, D. E. Mason, R. L. Neve, E. C. Peters, L. C. Hsieh-Wilson, Dynamic O-GlcNAc modification regulates CREB-mediated gene expression and memory formation. *Nat. Chem. Biol.*, **2012,** 8, 253-261.

89. S. A. Caldwell, S. R. Jackson, K. S. Shahriari, T. P. Lynch, G. Sethi, S. Walker, *et al.*, Nutrient sensor O-GlcNAc transferase regulates breast cancer tumorigenesis through targeting of the oncogenic transcription factor FoxM1. *Oncogene*, **2010,** 29, 2831-2842.

90. K. Kamemura, B. K. Hayes, F. I. Comer, G. W. Hart, Dynamic interplay between O-glycosylation and O-phosphorylation of nucleocytoplasmic proteins: alternative glycosylation/phosphorylation of THR-58, a known mutational hot spot of c-Myc in lymphomas, is regulated by mitogens. *J. Biol. Chem.*, **2002,** 277, 19229-19235.

91. A. E. Lenferink, J. Magoon, C. Cantin, M. D. O'Connor-McCourt, Investigation of three new mouse mammary tumor cell lines as models for transforming growth factor (TGF)-beta and Neu pathway signaling studies: identification of a novel model for TGF-beta-induced epithelial-to-mesenchymal transition. *Breast Cancer Res.*, **2004,** 6, R514-530.

92. A. K. Perl, P. Wilgenbus, U. Dahl, H. Semb, G. Christofori, A causal role for E-cadherin in the transition from adenoma to carcinoma. *Nature*, **1998,** 392, 190-193.

93. A. Barrallo-Gimeno, M. A. Nieto, The Snail genes as inducers of cell movement and survival: implications in development and cancer. *Development*, **2005,** 132, 3151-3161.

94. S. Hardiville, G. W. Hart, Nutrient regulation of signaling, transcription, and cell physiology by O-GlcNAcylation. *Cell Metab.*, **2014,** 20, 208-213.

95. L. Wu, R. Derynck, Essential role of TGF-beta signaling in glucose-induced cell hypertrophy. *Dev. Cell*, **2009,** 17, 35-48.

96. B. L. Riser, P. Cortes, J. Yee, A. K. Sharba, K. Asano, A. Rodriguez-Barbero, *et al.*, Mechanical strain- and high glucose-induced alterations in mesangial cell collagen metabolism: role of TGF-beta. *J. Am. Soc. Nephrol.*, **1998,** 9, 827-836.

97. P. G. Shaw, R. Chaerkady, T. Wang, S. Vasilatos, Y. Huang, B. Van Houten, *et al.*, Integrated proteomic and metabolic analysis of breast cancer progression. *PLoS One*, **2013,** 8, e76220.

98. R. Aebersold, M. Mann, Mass spectrometry-based proteomics. *Nature,* **2003,** 422, 198-207.

99. B. F. Cravatt, G. M. Simon, J. R. Yates, 3rd, The biological impact of mass-spectrometry-based proteomics. *Nature,* **2007,** 450, 991-1000.

100. P. A. Haynes, S. P. Gygi, D. Figeys, R. Aebersold, Proteome analysis: Biological assay or data archive? *Electrophoresis,* **1998,** 19, 1862-1871.

101. Q. Zhang, V. Faca, S. Hanash, Mining the plasma proteome for disease applications across seven logs of protein abundance. *J. Proteome Res.,* **2011,** 10, 46-50.

102. S. Eliuk, A. Makarov, Evolution of Orbitrap Mass Spectrometry Instrumentation. *Annu. Rev. Anal. Chem. (Palo Alto Calif.),* **2015,** 8, 61-80.

103. Z. Wang, N. D. Udeshi, M. O'Malley, J. Shabanowitz, D. F. Hunt, G. W. Hart, Enrichment and site mapping of O-linked N-acetylglucosamine by a combination of chemical/enzymatic tagging, photochemical cleavage, and electron transfer dissociation mass spectrometry. *Mol. Cell. Proteomics,* **2010,** 9, 153-160.

104. H. T. Tan, Y. H. Lee, M. C. Chung, Cancer proteomics. *Mass Spectrom. Rev.,* **2012,** 31, 583-605.

105. J. Ma, G. W. Hart, O-GlcNAc profiling: from proteins to proteomes. *Clin. Proteomics,* **2014,** 11, 8.

106. A. J. Reason, H. R. Morris, M. Panico, R. Marais, R. H. Treisman, R. S. Haltiwanger, *et al.*, Localization of O-GlcNAc modification on the serum response transcription factor. *J. Biol. Chem.,* **1992,** 267, 16911-16921.

107. N. Khidekel, S. Arndt, N. Lamarre-Vincent, A. Lippert, K. G. Poulin-Kerstien, B. Ramakrishnan, *et al.*, A chemoenzymatic approach toward the rapid and sensitive detection of O-GlcNAc posttranslational modifications. *J. Am. Chem. Soc.,* **2003,** 125, 16162-16163.

108. J. F. Alfaro, C. X. Gong, M. E. Monroe, J. T. Aldrich, T. R. Clauss, S. O. Purvine, *et al.*, Tandem mass spectrometry identifies many mouse brain O-GlcNAcylated proteins including EGF domain-specific O-GlcNAc transferase targets. *Proc. Natl. Acad. Sci. U. S. A.,* **2012,** 109, 7280-7285.

109. N. Khidekel, S. B. Ficarro, E. C. Peters, L. C. Hsieh-Wilson, Exploring the O-GlcNAc proteome: direct identification of O-GlcNAc-modified proteins from the brain. *Proc. Natl. Acad. Sci. U. S. A.*, **2004,** 101, 13132-13137.

110. N. Khidekel, S. B. Ficarro, P. M. Clark, M. C. Bryan, D. L. Swaney, J. E. Rexach, *et al.*, Probing the dynamics of O-GlcNAc glycosylation in the brain using quantitative proteomics. *Nat. Chem. Biol.*, **2007,** 3, 339-348.

111. H. Hahne, N. Sobotzki, T. Nyberg, D. Helm, V. S. Borodkin, D. M. van Aalten, *et al.*, Proteome wide purification and identification of O-GlcNAc-modified proteins using click chemistry and mass spectrometry. *J. Proteome Res.*, **2013,** 12, 927-936.

112. K. Vosseller, J. C. Trinidad, R. J. Chalkley, C. G. Specht, A. Thalhammer, A. J. Lynn, *et al.*, O-linked N-acetylglucosamine proteomics of postsynaptic density preparations using lectin weak affinity chromatography and mass spectrometry. *Mol. Cell. Proteomics*, **2006,** 5, 923-934.

113. J. C. Trinidad, D. T. Barkan, B. F. Gulledge, A. Thalhammer, A. Sali, R. Schoepfer, *et al.*, Global identification and characterization of both O-GlcNAcylation and phosphorylation at the murine synapse. *Mol. Cell. Proteomics*, **2012,** 11, 215-229.

114. S. A. Myers, B. Panning, A. L. Burlingame, Polycomb repressive complex 2 is necessary for the normal site-specific O-GlcNAc distribution in mouse embryonic stem cells. *Proc. Natl. Acad. Sci. U. S. A.*, **2011,** 108, 9490-9495.

115. M. A. Nessen, G. Kramer, J. Back, J. M. Baskin, L. E. J. Smeenk, L. J. de Koning, *et al.*, Selective Enrichment of Azide-Containing Peptides from Complex Mixtures. *J. Proteome Res.*, **2009,** 8, 3702-3711.

116. D. J. Vocadlo, H. C. Hang, E. J. Kim, J. A. Hanover, C. R. Bertozzi, A chemical approach for identifying O-GlcNAc-modified proteins in cells. *Proc. Natl. Acad. Sci. U. S. A.*, **2003,** 100, 9116-9121.

117. S. T. Laughlin, C. R. Bertozzi, Metabolic labeling of glycans with azido sugars and subsequent glycan-profiling and visualization via Staudinger ligation. *Nat. Protoc.*, **2007,** 2, 2930-2944.

118. P. M. Clark, J. F. Dweck, D. E. Mason, C. R. Hart, S. B. Buck, E. C. Peters, *et al.*, Direct in-gel fluorescence detection and cellular imaging of O-GlcNAc-modified proteins. *J. Am. Chem. Soc.*, **2008,** 130, 11576-11577.

119. B. L. Parker, P. Gupta, S. J. Cordwell, M. R. Larsen, G. Palmisano, Purification and identification of O-GlcNAc-modified peptides using phosphate-based alkyne CLICK chemistry in combination with titanium dioxide chromatography and mass spectrometry. *J. Proteome Res.,* **2011,** 10, 1449-1458.

120. R. Sprung, A. Nandi, Y. Chen, S. C. Kim, D. Barma, J. R. Falck, *et al.,* Tagging-via-substrate strategy for probing O-GlcNAc modified proteins. *J. Proteome Res.,* **2005,** 4, 950-957.

121. A. Nandi, R. Sprung, D. K. Barma, Y. Zhao, S. C. Kim, J. R. Falck, *et al.,* Global identification of O-GlcNAc-modified proteins. *Anal. Chem.,* **2006,** 78, 452-458.

122. C. Gurcel, A. S. Vercoutter-Edouart, C. Fonbonne, M. Mortuaire, A. Salvador, J. C. Michalski, *et al.,* Identification of new O-GlcNAc modified proteins using a click-chemistry-based tagging. *Anal. Bioanal. Chem.,* **2008,** 390, 2089-2097.

123. B. W. Zaro, Y. Y. Yang, H. C. Hang, M. R. Pratt, Chemical reporters for fluorescent detection and identification of O-GlcNAc-modified proteins reveal glycosylation of the ubiquitin ligase NEDD4-1. *Proc. Natl. Acad. Sci. U. S. A.,* **2011,** 108, 8146-8151.

124. Z. Gurel, B. W. Zaro, M. R. Pratt, N. Sheibani, Identification of O-GlcNAc modification targets in mouse retinal pericytes: implication of p53 in pathogenesis of diabetic retinopathy. *PLoS One,* **2014,** 9, e95561.

125. L. Wells, K. Vosseller, R. N. Cole, J. M. Cronshaw, M. J. Matunis, G. W. Hart, Mapping sites of O-GlcNAc modification using affinity tags for serine and threonine post-translational modifications. *Mol. Cell. Proteomics,* **2002,** 1, 791-804.

126. R. I. Somiari, S. Somiari, S. Russell, C. D. Shriver, Proteomics of breast carcinoma. *J Chromatogr B,* **2005,** 815, 215-225.

127. G. Chambers, L. Lawrie, P. Cash, G. I. Murray, Proteomics: a new approach to the study of disease. *J. Pathol.,* **2000,** 192, 280-288.

128. J. Micallef, M. Dharsee, J. Chen, S. Ackloo, K. Evans, L. Qiu, *et al.,* Applying mass spectrometry based proteomic technology to advance the understanding of multiple myeloma. *J. Hematol. Oncol.,* **2010,** 3, 13.

129. M. Karas, F. Hillenkamp, Laser desorption ionization of proteins with molecular masses exceeding 10,000 daltons. *Anal. Chem.*, **1988,** 60, 2299-2301.

130. J. B. Fenn, M. Mann, C. K. Meng, S. F. Wong, C. M. Whitehouse, Electrospray ionization for mass spectrometry of large biomolecules. *Science*, **1989,** 246, 64-71.

131. F. Hillenkamp, M. Karas, The MALDI Process and Method. In *MALDI MS. A Practical Guide to Instrumentation Methods and Applications*, Hillenkamp, F.; Peter-Karalinc, J., Eds. Wiley-VCH Verlag GmbH & Co. KGaA: Weinheim, 2007.

132. J. R. Yates, C. I. Ruse, A. Nakorchevsky, Proteomics by mass spectrometry: approaches, advances, and applications. *Annu. Rev. Biomed. Eng.*, **2009,** 11, 49-79.

133. W. G. Fisher, K. P. Rosenblatt, D. A. Fishman, G. R. Whiteley, A. Mikulskis, S. A. Kuzdzal, *et al.*, A robust biomarker discovery pipeline for high-performance mass spectrometry data. *J. Bioinform. Comput. Biol.*, **2007,** 5, 1023-1045.

134. M. Wilm, A. Shevchenko, T. Houthaeve, S. Breit, L. Schweigerer, T. Fotsis, *et al.*, Femtomole sequencing of proteins from polyacrylamide gels by nano-electrospray mass spectrometry. *Nature*, **1996,** 379, 466-469.

135. H. R. Morris, T. Paxton, A. Dell, J. Langhorne, M. Berg, R. S. Bordoli, *et al.*, High sensitivity collisionally-activated decomposition tandem mass spectrometry on a novel quadrupole/orthogonal-acceleration time-of-flight mass spectrometer. *Rapid Commun. Mass Spectrom.*, **1996,** 10, 889-896.

136. M. Sharon, C. V. Robinson, The role of mass spectrometry in structure elucidation of dynamic protein complexes. *Annu. Rev. Biochem.*, **2007,** 76, 167-193.

137. J. C. Schwartz, M. W. Senko, J. E. Syka, A two-dimensional quadrupole ion trap mass spectrometer. *J. Am. Soc. Mass Spectrom.*, **2002,** 13, 659-669.

138. E. Denisov, E. Damoc, O. Lange, A. Makarov, Orbitrap mass spectrometry with resolving powers above 1,000,000. *Int J Mass Spectrom*, **2012,** 325, 80-85.

139. B. Domon, R. Aebersold, Mass spectrometry and protein analysis. *Science*, **2006,** 312, 212-217.

140. J. V. Olsen, J. C. Schwartz, J. Griep-Raming, M. L. Nielsen, E. Damoc, E. Denisov, *et al.*, A dual pressure linear ion trap Orbitrap instrument with very high sequencing speed. *Mol. Cell. Proteomics,* **2009,** 8, 2759-2769.

141. Q. Hu, R. J. Noll, H. Li, A. Makarov, M. Hardman, R. Graham Cooks, The Orbitrap: a new mass spectrometer. *J. Mass Spectrom.,* **2005,** 40, 430-443.

142. A. Makarov, E. Denisov, A. Kholomeev, W. Balschun, O. Lange, K. Strupat, *et al.*, Performance evaluation of a hybrid linear ion trap/orbitrap mass spectrometer. *Anal. Chem.,* **2006,** 78, 2113-2120.

143. R. J. Chalkley, A. L. Burlingame, Identification of GlcNAcylation sites of peptides and alpha-crystallin using Q-TOF mass spectrometry. *J. Am. Soc. Mass Spectrom.,* **2001,** 12, 1106-1113.

144. L. M. Mikesh, B. Ueberheide, A. Chi, J. J. Coon, J. E. Syka, J. Shabanowitz, *et al.*, The utility of ETD mass spectrometry in proteomic analysis. *Biochim. Biophys. Acta,* **2006,** 1764, 1811-1822.

145. J. E. Syka, J. J. Coon, M. J. Schroeder, J. Shabanowitz, D. F. Hunt, Peptide and protein sequence analysis by electron transfer dissociation mass spectrometry. *Proc. Natl. Acad. Sci. U. S. A.,* **2004,** 101, 9528-9533.

146. J. V. Olsen, B. Macek, O. Lange, A. Makarov, S. Horning, M. Mann, Higher-energy C-trap dissociation for peptide modification analysis. *Nat. Methods,* **2007,** 4, 709-712.

147. P. Zhao, R. Viner, C. F. Teo, G. J. Boons, D. Horn, L. Wells, Combining high-energy C-trap dissociation and electron transfer dissociation for protein O-GlcNAc modification site assignment. *J. Proteome Res.,* **2011,** 10, 4088-4104.

148. X. Zhang, S. M. Leung, C. R. Morris, M. K. Shigenaga, Evaluation of a novel, integrated approach using functionalized magnetic beads, bench-top MALDI-TOF-MS with prestructured sample supports, and pattern recognition software for profiling potential biomarkers in human plasma. *Journal of biomolecular techniques : JBT,* **2004,** 15, 167-175.

149. C. Laronga, R. R. Drake, Proteomic approach to breast cancer. *Cancer Control,* **2007,** 14, 360-368.

150. Y. Yasui, M. Pepe, M. L. Thompson, B. L. Adam, G. L. Wright, Jr., Y. Qu, *et al.*, A data-analytic strategy for protein biomarker discovery: profiling of high-dimensional proteomic data for cancer detection. *Biostatistics,* **2003,** 4, 449-463.

151. H. Dong, W. Shen, M. T. Cheung, Y. Liang, H. Y. Cheung, G. Allmaier, *et al.*, Rapid detection of apoptosis in mammalian cells by using intact cell MALDI mass spectrometry. *Analyst,* **2011,** 136, 5181-5189.

152. A. J. Madonna, F. Basile, I. Ferrer, M. A. Meetani, J. C. Rees, K. J. Voorhees, On-probe sample pretreatment for detection of proteins above 15 KDa from whole cell bacteria by matrix-assisted laser desorption/ionization time-of-flight mass spectrometry. *Rapid Commun. Mass Spectrom.,* **2000,** 14, 2220-2229.

153. J. M. Hettick, M. L. Kashon, J. E. Slaven, Y. Ma, J. P. Simpson, P. D. Siegel, *et al.*, Discrimination of intact mycobacteria at the strain level: a combined MALDI-TOF MS and biostatistical analysis. *Proteomics,* **2006,** 6, 6416-6425.

154. T. C. Cain, D. M. Lubman, W. J. Weber, Differentiation of Bacteria Using Protein Profiles from Matrix-Assisted Laser-Desorption Ionization Time-of-Flight Mass-Spectrometry. *Rapid Commun. Mass Spectrom.*, **1994,** 8, 1026-1030.

155. S. Vaidyanathan, C. L. Winder, S. C. Wade, D. B. Kell, R. Goodacre, Sample preparation in matrix-assisted laser desorption/ionization mass spectrometry of whole bacterial cells and the detection of high mass (>20 kDa) proteins. *Rapid Commun. Mass Spectrom.,* **2002,** 16, 1276-1286.

156. T. L. Williams, D. Andrzejewski, J. O. Lay, S. M. Musser, Experimental factors affecting the quality and reproducibility of MALDI TOF mass spectra obtained from whole bacteria cells. *J. Am. Soc. Mass Spectrom.,* **2003,** 14, 342-351.

157. B. L. Adam, Y. Qu, J. W. Davis, M. D. Ward, M. A. Clements, L. H. Cazares, *et al.*, Serum protein fingerprinting coupled with a pattern-matching algorithm distinguishes prostate cancer from benign prostate hyperplasia and healthy men. *Cancer Res.*, **2002,** 62, 3609-3614.

158. E. T. Fung, V. Thulasiraman, S. R. Weinberger, E. A. Dalmasso, Protein Biochips for Differential Profiling. *Curr. Opin. Biotechnol.,* **2001,** 12, 65-69.

159. L. A. Liotta, E. F. Petricoin, Serum peptidome for cancer detection: spinning biologic trash into diagnostic gold. *J. Clin. Invest.*, **2006,** 116, 26-30.

CHAPTER 2

A Comprehensive and Informative Methodology for MALDI-TOF MS Profiling and Discrimination of Breast Cancer cells

2.1 ABSTRACT

Matrix-assisted Laser Desorption/Ionization time-of-flight mass spectrometry (MALDI-TOF MS), the state-of-the-art high-throughput technology, has been employed in profiling of breast cancer cell lines leading to their discrimination based on mass spectral fingerprints. The reported novel sample preparation strategy for profiling of mammalian cells involves a one-step processing of whole cells to produce the sample from which protein mass spectra are generated. Spectra were acquired in the m/z range 3000-20000 and consisted of the largest array of peaks ever to be reported in this range. Among the cell lines profiled, NIH3T3 (murine) cells were used for method development while the human breast cancer cell lines were used for method application. Analysis of the mass spectral data by pattern recognition and learning classification methods has enabled us to discriminate between the cancerous and non-cancerous cells lines, and between metastatic and non-metastatic cell lines. Specifically, results of unsupervised clustering show that the established MALDI-TOF MS strategy has the potential to discriminate breast cancer cell lines, and therefore could be an alternative to Surface Enhanced Laser Desorption Ionization (SELDI) TOF MS with ProteinChip. However, similar to SELDI approach, the discrimination by the MALDI fingerprints requires further fine-tuning using supervised classification. The reported results portray the one-step cell processing

method as an informative and simple way of profiling and classifying cells in a highly cost-effective and reproducible manner. The comprehensive methodology has a potential to expand the role of MALDI-TOF MS in several fields related to cell and tissue profiling for disease diagnosis and therapy.

2.2 INTRODUCTION

Breast cancer is the second leading cause of cancer-related mortality in women[1-2]. Although significant advances in early detection and treatment of breast cancer have been made, a protein-based multiplex system that provides large array of informative signals for cancer identification and prognosis is still limited[3]. As a step towards advancing the future tools in cancer diagnostics, we focused our multivariate analytical tool for human cell lines derived from breast cancers. These breast cancer cell lines represent some of the key molecular tumor subtypes and serve as representative models for studying breast cancers[4-6]. Profiling of such cells by the state-of-the-art high-throughput technologies such as MALDI-TOF MS can lead to the discovery of potential diagnostic and prognostic biomarkers of breast cancers[7].

MALDI-MS is an analytical technique that uses laser irradiation of a matrix-sample co-crystal to vaporize molecules for injection into a mass spectrometer to obtain information on molecular weight[8]. The distinctive advantages over other ionization techniques, such as electrospray ionization and atmospheric pressure chemical ionization, lie in the soft ionization nature by which singly-charged ions are produced without fragmentation of the fragile biomolecules (i.e. peptides, proteins, nucleic acids)[9]. In addition, MALDI is usually coupled with a time-of-flight (TOF) analyzer to provide, in theory, a potentially unlimited measurement of masses of macromolecules[10]. These

features, among others, have made MALDI-MS a popular analytical tool for the rapid, sensitive and efficient detection of various analytes relevant to protein chemistry, biotechnology, and cell and molecular biology[9, 11-12].

MALDI-TOF MS protein profiling with or without protein identification has been employed in the field of proteomics in the identification of bacteria and fungi and in the discrimination of disease states of various cancers[13-15]. Although this mass spectrometric approach for dissecting organisms and diseases does not reveal the entire proteome, the mass spectra reflect a small but sufficient portion that can be used to characterize organisms and diseases[9, 16]. The spectral patterns generated provide large arrays of valuable information that permit classification at taxonomic and biological levels[17]. Such a remarkable revelation of biological information requires, prior to analysis, appropriate preparation of the sample[18], a part of the MALDI-MS analytical technique that is often challenging due to the complexity of biological samples, such as cells[19-20].

There are thousands of different proteins in the cell co-existing with lipids, carbohydrates and nucleic acids, and the total amount of protein varies significantly with each cell type[9]. Moreover, some abundant proteins produce very strong ionization signals that suppress signals from less abundant proteins, hiding the signals that carry biologically important information[21]. Preparative methods, such as cell-sample pretreatment, matrix selection , matrix solution conditions and spotting technique, also affect the quality of the mass spectra[18]. Consequently, while in theory the MALDI-TOF MS based approach is appealing, in practice, the sample preparation and the complexity of the sample make the entire process quite arduous for obtaining informative and reproducible mass spectral patterns[22].

Since Cain *et al*. began profiling bacteria by MALDI-TOF MS and demonstrated the potential of MS-based profiling in 1994, several investigations on bacterial cell sample preparation, experimental factors involved and detection of high molecular weight proteins for the improvement of MALDI-MS profiles have been documented[23]. Vaidyanathan *et al*. investigated different sample preparation approaches to increase the detection range of proteins from whole bacterial cells using MALDI-MS[24]; Williams *et al*. explored the influence of experimental factors on mass spectra from whole-cell bacteria by MALDI-MS[17]; and Madonna *et al*. published a methodology to enhance the signal-to-base-line ratio of high molecular weight protein signals from bacteria by MALDI-MS[25]. In contrast to the bacterial cells, mammalian cells exhibit an even greater structural complexity, thereby making their analysis by mass spectrometry a more challenging effort[9]. The cell culture methods and heterogenous cell populations complicate the MALDI-MS profiling of mammalian cells, hence very few reports on MALDI-MS profiling of mammalian cells have been published[9, 26-30].

Herein, we report a comprehensive and informative methodology for the direct and rapid protein profiling of whole mammalian cells. Our protocol, depicted on Figure 2.1, involves a simple and reproducible one-step sample processing for analyzing whole mammalian cells by MALDI-TOF MS to produce mass spectral fingerprints of each cell type, and a down-stream computational data analytic step for the discrimination of cell types. The key step in our sample preparation is carried out by just a one-step operation, rinsing of cells with a novel DHB- and Isopropanol-containing MALDI matrix solution A (Figure 2.1) to simultaneously lyse cells and extract proteins. No additional purification and fractionation of the cell sample are involved. Fewer sample preparation steps in

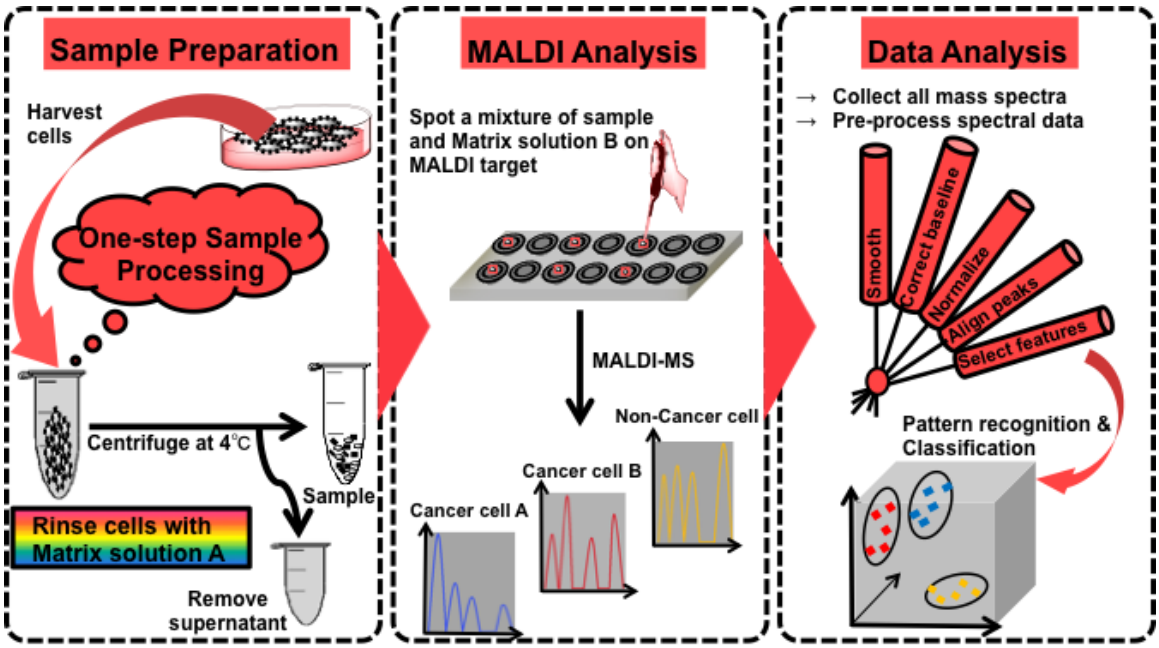

Figure 2.1 A Schematic workflow in MALDI-MS profiling and discrimination of cancer cells, featuring the novel one-step cell sample processing in sample preparation.

comparison with previously published methods minimize the risk of poor reproducibility thereby make the profiling methodology rapid and reliable[9, 29-30]. We firstly applied an in-house data analytic pipeline, based on the preprocessing algorithms of the Bioinformatics Toolbox (Mathworks, Natick, MA), pattern recognition and learning classification algorithms, to analyze the complex mass spectral data. Secondly, we employed a commercial software to further explore patterns in the data. The results show that MALDI-TOF MS profiling can be employed in the discrimination of breast cancer cells in a rapid, high-throughput and reproducible manner. This comprehensive and informative methodology might be useful for the identification and analysis of cancerous, stem, and differentiating cells.

2.3 EXPERIMENTAL SECTION

2.3.1 Materials

2,5-Dihydroxybenzoic acid (gentisic acid, DHB), 3,5-dimethoxy-4-hydroxycinnamic acid (Sinapinic acid, SA), α-cyano-4-hydroxycinnamic acid (CHCA) and ammonium hydrogencitrate (AHC) were purchased from Sigma-Aldrich, St. Louis, USA. 2'6'-Dihydroxyacetophenone (DHAP) was purchased from Acros Organics, New Jersey, USA. Dulbecco's modified phosphate-buffered saline (DPBS) and all cell culture reagents were purchased from Thermo Scientific Hyclone Laboratories, Inc., Utah, USA. Deionized water (dH_2O) was produced from a Millipore Purification System (18 MΩ·cm at 25 ºC). MALDI matrix solution A (5 mg/mL DHB in [V_{C3H8O}:V_{ACN}:V_{dH2O} = 2:1:1]) was prepared by mixing equal volumes of isopropanol with that of 10 mg DHB/mL of acetonitrile and dH_2O (1:1). MALDI matrix solution B is a DHAP matrix solution described by Wenzel *et al.*[31]. It was prepared by suspending 50 µmol DHAP in 375 µL

ethanol and 125 µL of 10 µmol ammonium hydrogencitrate (stock solution: 27 mg in 1.5 mL dH_2O), and vortexing for at least a minute to dissolve the DHAP. The composition of the SA matrix solution was 10 mg/mL SA in (V_{ACN}:V_{dH2O}:V_{TFA} = 10:10:1), while that of CHCA matrix solution was 10 mg/mL CHCA in (V_{ACN}:V_{dH2O}:V_{TFA} = 30:70:1). NIH-3T3 cells were provided by Dr. Kim E. Creek (Center for Colon Cancer Research, University of South Carolina). MCF-7 and MCF-10A cells were kind gifts from Dr. Hexin Chen (Center for Colon Cancer Research, University of South Carolina). MDA-MB231 cellculture was obtained from the American Type Culture Collection (ATCC number HTB26, ATCC, Manassas, VA, USA).

2.3.2 Cell Culture and Harvesting

The two human breast cancer cell lines, MCF-7 and MDA-MB231, and the mouse embryonic fibroblast cell line, NIH-3T3 were maintained in high glucose Dulbecco's Modified Eagle's Medium (DMEM) containing 4 mM L-glutamine, 1 mM sodium pyruvate, and supplemented with penicillin (100 U/mL), streptomycin (100 µg/mL), and 10% foetal bovine serum (FBS) or 10% neonatal calf serum (NCS), respectively. The human breast immortalized normal cell line MCF-10A was cultured in DMEM:F12 (50/50) medium containing similar supplements as the DMEM above in addition to 10 µg/mL insulin, 20 ng/mL epidermal growth factor, 100 ng/mL cholera toxin and 0.5 µg/mL hydrocortisone. All cell cultures were maintained at 37 ºC and 5% CO_2 in air in a humidified incubator. Cells were cultured in triplicates in T75 flasks for 2 days. At about 80% confluence, cells in one of the flasks were trypsinized and passaged in a split ratio of 1:3. Cells from the other two flasks were also trypsinized, transferred to 15 mL Falcon tubes and harvested by 5 min centrifugation in a Beckman Coulter Benchtop centrifuge at

100 × *g* at room temperature. After discarding the supernatant the harvested cells were resuspended in DPBS and transferred into pre-weighed sterile 1.5 mLeppendorf tubes, rinsed twice with DPBS and spinned in Eppendorf centrifuge at 500 × *g* for 5 min to pellet out the cells.

2.3.3 Sample Preparation Featuring the 'One-step Cell Processing'

A cell pellet of approximately (2-5) x 10^6 cells in an eppendorf tube were pre-treated in 'one-step cell processing' by mixing with 200 µL of MALDI matrix solution A. The mixture was stirred for 20~30 seconds using a tipped pipette and placed on ice for transfer to a cold centrifuge. Centrifugation was done in a Beckman Coulter Microfuge at 14000 rpm at 4 ºC for 3 minutes. The supernatant was carefully removed and discarded and the wet cell pellet was weighed. For consistency, the pellet weight was employed, based on Equation 2.1 below, in the determination of the volume of dH_2O required for resuspension of the pellet. The processed cell suspension sample was thoroughly stirred to ensure homogeneity and was maintained on ice for stability. After sample dilution with dH_2O to 24 mg/µLfor NIH3T3 (and 190 mg/µL for breast cell lines), equal amounts of the sample, 2%TFA and MALDI matrix solution B were mixed together. Two 0.5 µL aliquots of this mixture were spotted onto a MALDI-MS target plate (AnchorChipTM , Bruker Daltonics) using dried droplet method, and dried at room temperature before analysis.

$$\textbf{Volume (µL)} = \frac{\textbf{Weight of Pellet (mg)}}{\textbf{18.8 mg}} \times \textbf{50 µL}$$

Equation 2.1

2.3.4 MALDI-TOF MS Analysis

Mass spectra were generated with a MALDI-TOF mass spectrometer (Ultraflex I TOF/TOF, Bruker Daltonics) operated in linear delayed extraction positive ion mode. Nitrogen laser (λ = 337 nm) at a frequency of 20 Hz was employed for desorption/ ionization and a mass range from 3000 Da to 35000 Da was selected. Spectra were calibrated using Protein Calibration Standard I (Bruker Daltonics), based on the average values of $[M+H^+]^+$ of insulin, ubiquitin I, cytochrome C, myoglobin, at 'mass/charge', (*m/z*) 5734.56, 8565.89, 12361.09, and 16952.55, respectively. The mass accuracy was on the order of 0.05%. A total of 2000 shots was taken from two spots of the same sample.

2.3.5 Data Analysis

2.3.5.1 Preliminary Analysis

In the establishment of the sample preparation strategy, minimal data analysis was carried out. Spectra were overlaid and visually examined for presence of peaks, which was evidence that proteins were detected; differences and similarities in peak location and intensities, reflecting on different proteins and their relative abundances; and observable drift in baseline, an indicator of the quality of the spectrum. Spectra with minimal or no observable drift in baseline were considered for evaluations of the sample preparation strategy.

2.3.5.2 Using Data Analytic Pipeline of Morgan *et al.*[32]

In the application of the established sample preparation strategy, for protein profiling of breast cancer cell lines, two data analytic routines were utilized, one that was developed and used by Morgan *et al.*[32] and the other, a commercial software, BioNumerics version 7.3.1 (Austin, Texas; www.applied-maths.com), following the instructions provided. The

Morgan data analytic pipeline consists of preprocessing, pattern recognition, and classification utilities written in MatLab (The Mathworks, Natick, MA). The dataset consisting of 73 spectra/samples of the breast cancer cell lines, shown on Figure 2.9, was generated following the optimized sample preparation method. The raw spectra were exported as ASCII files and converted to CSV files before being uploaded into Matlab. Prior to statistical analyses spectra were preprocessed using routines from the Matlab bioinformatics toolbox. Each of these spectra initially had total features of about 130,600 different ion masses from m/z 3000 to 30000. Given the lack of discriminating information at feature values higher than m/z 25000, only about 100,600 feature values below m/z 25,000 were used for further analysis.

Upon preprocessing the resampling algorithm in the Matlab bioinformatics toolbox was then employed to reduce the data to 8,000 mass features per spectrum. This algorithm was designed for complex mass spectrometric data to preserve significant peaks heights while eliminating features representing noise. The data was then broken into three data sets containing three combinations: (1) normal versus non-metastatic (47 samples), (2) normal versus metastatic (36 samples), and (3) non-metastatic versus metastatic (63 samples). For each of these comparisons, further feature selection was performed using single-feature two-group t-tests to select m/z values of high discriminating power. Features were retained for further analysis if they were associated with a calculated Student's *t*-statistic larger than the critical value of *t* (Bonferroni-corrected error rate of 0.05). This strategy produced number of features ranging from 230 to 301, which were then used for principal component analysis.

2.3.5.3 Using the Commercial BioNumerics Data Analytic Procedure

Alternatively, the data files of the 73 spectra were imported into the BioNumerics software interface and preprocessed using the given methods. Upon peak detection, peak matching was done to create peak classes that represent detected proteins. In BioNumerics a peak is defined on the basis of the spectrum during preprocessing while a peak class is defined on a basis of a group of spectra and peak classes are generated during peak matching. Many peaks may have been detected at a signal-to-noise ratio of 5 during spectral preprocessing, but 109 peak classes, corresponding to expressed proteins, were created during the subsequent peak matching. On the basis of these 109 proteins, relationships among the samples were determined by cluster analyses.

2.3.5.3.1 Cluster Analysis

Cluster analysis is a multivariate procedure of pattern recognition that detects natural groupings in data and examines similarities and dissimilarities between observations[33]. BioNumerics software was used according to the UPGMA algorithm to obtain hierarchical agglomerative clustering of the data. This algorithm constructs a rooted tree (dendogram) that reflects the structure of a similarity matrix in a pairwise comparison where the distance between two clusters is the distance between the average over the elements of each cluster. The distances were measured with Pearson Correlation, as a similarity metric.

2.3.5.3.2 Principal Component Analysis (PCA)

Similar to the hierarchical clustering, PCA is also a clustering method that operates without any prior knowledge of grouping[34]. However, PCA is a mathematical procedure for reducing dimensionality of data. It extracts variance in the data and simultaneously transforms possibly correlated variables into a smaller number of uncorrelated variables,

the principal components, which are linear combinations of the original variables. The first principal component accounts for as much of the variance in the data as possible while the other components account for the remaining maximum proportion of the variance. PCA computation, involving covariance matrix and standardized principal component scores, was performed using BioNumerics and the in-house pipeline of Morgan *et al*.[32]

2.4 RESULTS AND DISCUSSION

In this study we used NIH-3T3 cell line as a model for developing the MALDI-MS cell profiling method since it can be easily cultured and represents a stable, and fast growing cell line[35]. Despite the complexity of the sample and limited details on MS profiling of mammalian cells, we focused our work to two areas. The first goal was to develop an optimum sample preparation method for MALDI-TOF MS characterization of different mammalian cell types in a fast and reproducible manner. Such a method should permit protein fingerprinting of mammalian cells in the range of 3000-30000 so as to facilitate the differentiation of cells. If such a method could generate a large number of peaks, especially above m/z 15000, an upper limit obtained by Zhang *et al*.,[30] it would increase the chance of generating unique spectral profiles[25] that contain more information about the differences and similarities among mammalian cell types.

The second goal was to use the established method to obtain distinctive spectra of the breast cancer cell lines and to classify the cell lines based to their spectral fingerprints. For the purpose of establishing the desired methodology, we investigated several matrixes that include DHB[30], SA[20, 28], CHCA[27], and DHAP[31, 36]; organic solvents such as chloroform, acetone, ethanol[25], methanol[23], isopropanol[19], acetonitrile, and

trifluoroacetic acid; and matrix additives such as di-ammonium hydrogen citrate[31], that have previously been used in MALDI analyses[37]. The purpose of matrix solvents and additives is to enable the release of proteins from the cells while the matrix aids in the ionization of proteins and thus influences the mass range of the proteins detected[36].

2.4.1 MALDI-TOF MS Profiling: Method Development using NIH3T3 Cell Line

2.4.1.1 Establishment of the Sample Preparation Protocol

Since it is well appreciated that the optimization of key parameters in sample preparation is empirical and that the discovery of a desirable method is a matter of trial-and-error experimentation[38], we sought to find out if spectra with protein peaks spanning a wide mass range i.e. 3000-20000, would be obtained from MALDI-MS analysis of whole-cell NIH3T3 pellet rinsed with ACN solution (V_{ACN}:V_{dH2O}:V_{TFA} = 10:10:1), DHB matrix solution (10 mg/mL DHB in V_{ACN}:V_{dH2O}:V_{TFA} = 10:10:1) or just water. Rinsing cells with DHB matrix solution was a strategy used by Zhang *et al*. who first reported MALDI spectral profiles of mammalian cells in the m/z range 4000-16000[30]. Our hypothesis was that changing the composition of the DHB rinsing solution in a similar manner as those who attempted to generate high-mass spectral profiles for bacteria (i.e. varying matrixes, their solvents and additives), might result in observation of peaks with m/z > 16000. For spotting samples on the target plate, we initially applied the matrixes, DHB, DHB mixed with CHCA (V_{DHB}:V_{CHCA} = 1:1), and a mixture of DHB, CHCA and SA (V_{DHB}:V_{CHCA}:V_{SA} = 1:1:1), since DHB is a suitable matrix for proteins in complex biological mixtures[30]. All samples were spotted onto a prestructured (AnchorChip 600) target plate by the common dried droplet method[24]. From these attempts, we obtained spectra with few or no peaks at all. The useful spectra consisted of about 20 peaks in the

mass range 4000-16000 and were obtained, as shown on Figure 2.2, from cells rinsed with DHB in water (NIH3T3 [spectrum A]) or acetonitrile solution (BHK [spectrum B] and HeLa [spectrum C]), and spotted with a co-matrix of DHB and CHCA. Although these spectra could be reproduced, they lacked peaks above m/z 16000.

We then diversified both our rinsing solution and spotting matrix by involving different organic solvents and matrixes. Sonication and rinsing of samples with aqueous chloroform solution (V_{CHCl3}:V_{dH2O} = 1:1) to delipidate the cells resulted in spectra with number of peaks in the range 50-80, having slightly higher intensities compared to the former spectra consisting of about 20 peaks . However, hardly any peaks with m/z >16000 were obtained from the chloroform-treated sonicated samples irrespective of the spotting matrix (Figure 2.3). The number of peaks was further elevated to ≥100 when the DHB-rinsed instead of chloroform-rinsed samples were homogenized with with a 26-G needle fixed to a 1 mL syringe and spotted with DHAP matrix (Figure 2.4). Action of needle and syringe increases the surface area for proteins within the rubble of the complex cell material to be effectively mixed and co-crystallized with the matrix, and may have positive effect on the MALDI process. However, sonication of syringe-processed samples resulted in low-quality spectra with fewer peaks and lower intensities (Figure 2.4 – spectrum E), making it unsuitable for mammalian cell sample preparation. Varying sample processing conditions without changing the DHAP spotting matrix influenced our choice of DHAP as a suitable spotting matrix for mammalian cells, especially since peaks with m/z around 20000 were observed.

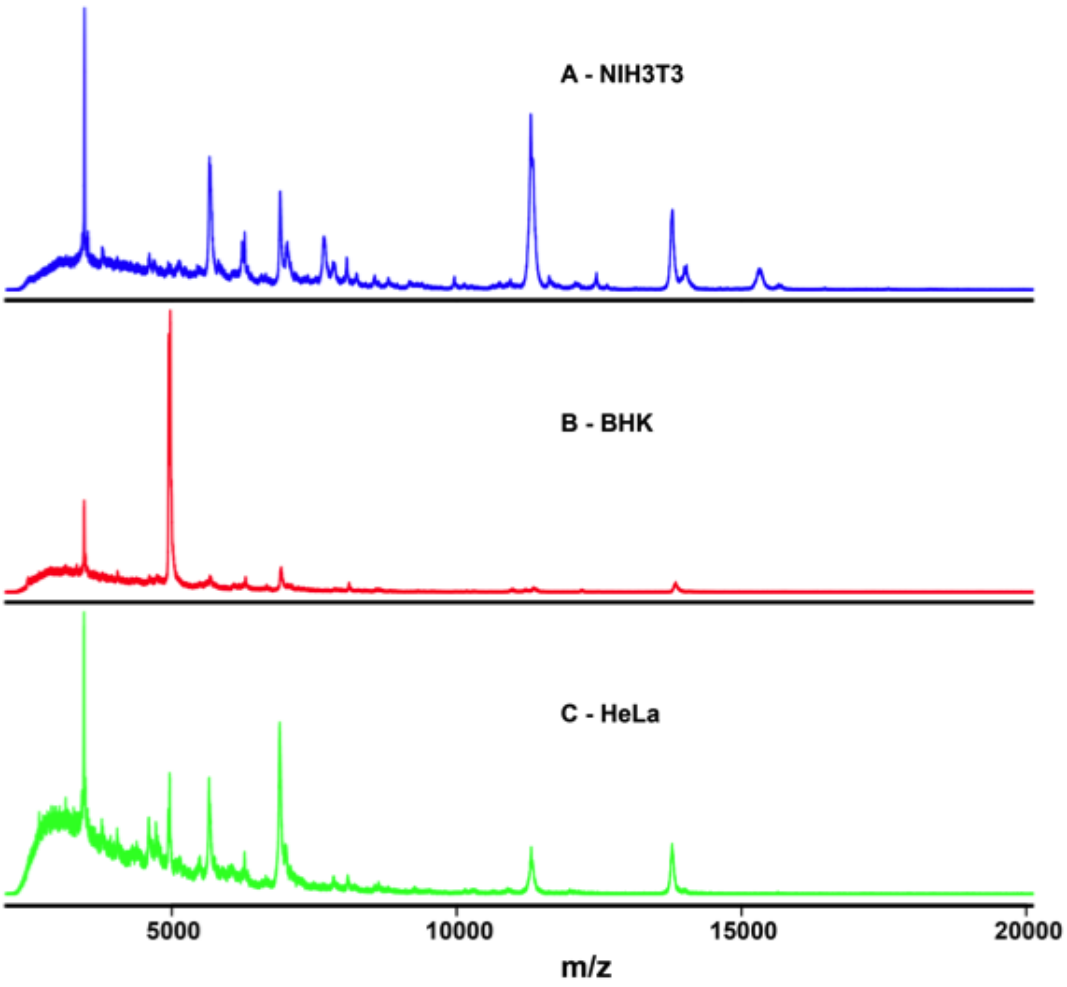

Figure 2.2 The intial MALDI TOF spectra of the cell lines NIH3T3 (blue), BHK (red) and HeLa (green).

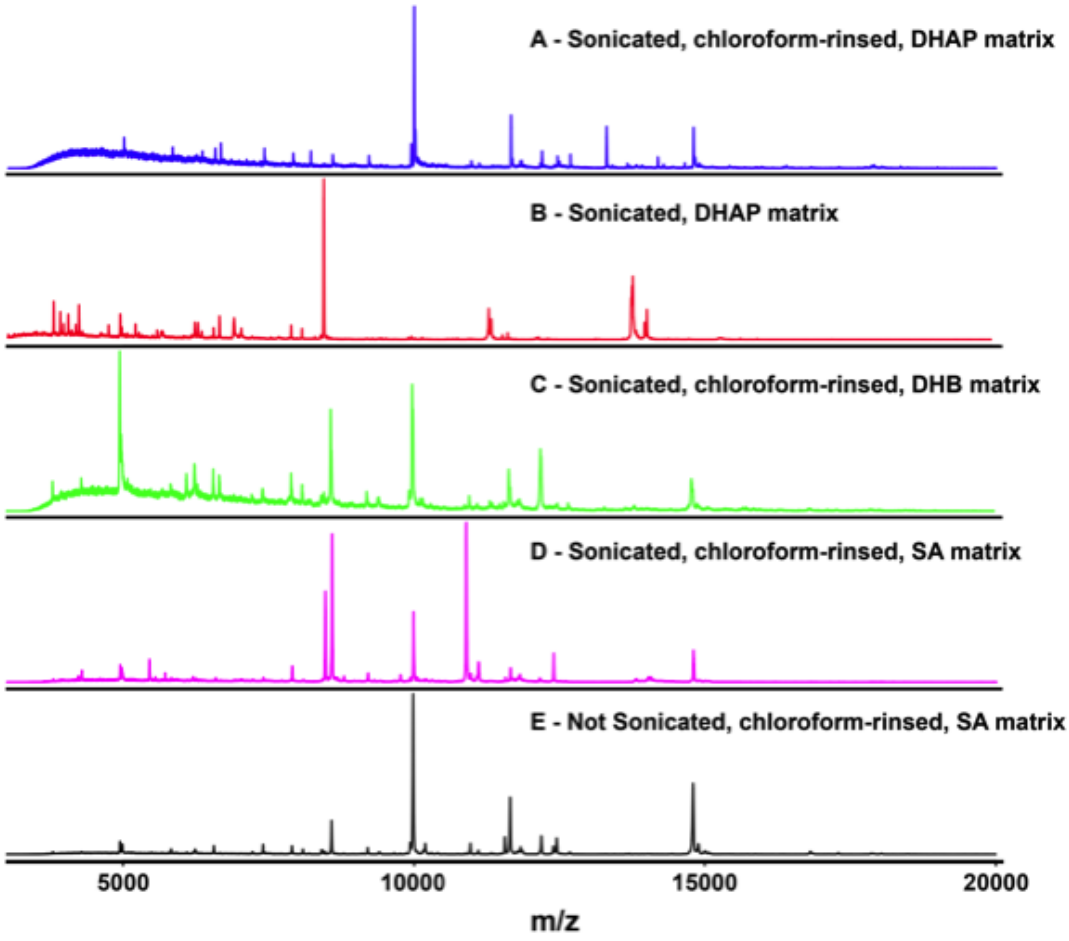

Figure 2.3 Spectra of NIH3T3 cells generated after rinsing cells with a mixture of chloroform and water (1:1, v/v), in the presence or absence of sonication or homogenization by syringe and needle, and after spotting samples with different MALDI matrix compounds. Hardly any peaks with m/z >16000 were obtained. Blue-, red-, green- and magenta-colored spectra – samples were sonicated or homogenized before rinising and spotted with DHAP, DHAP mixed with AHC, DHB and SA matrixes, respectively. The black-colored spectrum was recorded from MALDI analysis of the sample that was not sonicated.

With further modifications of the rinsing solution, the number of peaks were increasing. Figure 2.5 shows effect on the cell spectra of the five different cell rinsing solutions: DHB/isopropanol, DHB, DHB/methanol, SA, and DHAP, respectively. Of these five, DHB/isopropanol resulted in peaks at m/z 16000 and overall higher intesities for many peaks. Hence, the DHB/isopropanol rinsing solution was optimized to find the DHB and isopropanol proportions that could lead to spectra with high number of peaks. Use of the optimized novel rinsing matrix solution of the composition 5 mg/mL DHB in (V_{C3H8O}:V_{ACN}:V_{dH2O}= 2:1:1) and the established DHAP spotting matrix solution[31] resulted in spectra with more than 200 peaks. More specifically, spectra of about 200 peaks were obtained in the m/z range 3000-20000 when using these two optimized matrix solutions, one for rinsing the cells, called "matrix solution A", and the other for spotting the cell sample, referred to as "matrix solution B". The whole analysis was completed in 30-45 min, the shortest time ever for MALDI profiling of cells.

In spite of the novelty of our sample preparation, there are other sample preparation strategies for MALDI profiling of mammalian cells that have been published (Table 2.1). These strategies differ with respect to the MALDI reagents and methodologies used. While spectral profiles with unique peaks were obtained using these strategies, certain features make them less suitable for robust profiling with the ultimate goal of application in disease diagnostics. For example, sample pre-treatment involving fractionation and sample clean-up as was respectively done by van Adrichem *et al.*[9] and Lokhov *et al.*[29] makes the profiling seem tedious and costly. Also, spectra generated by Marvin-Guy *et al.*[20] and Dong *et al.*[27] from minimally processed cell samples, without rinsing and extraction steps, did not have any peaks above m/z 16000. Our method was

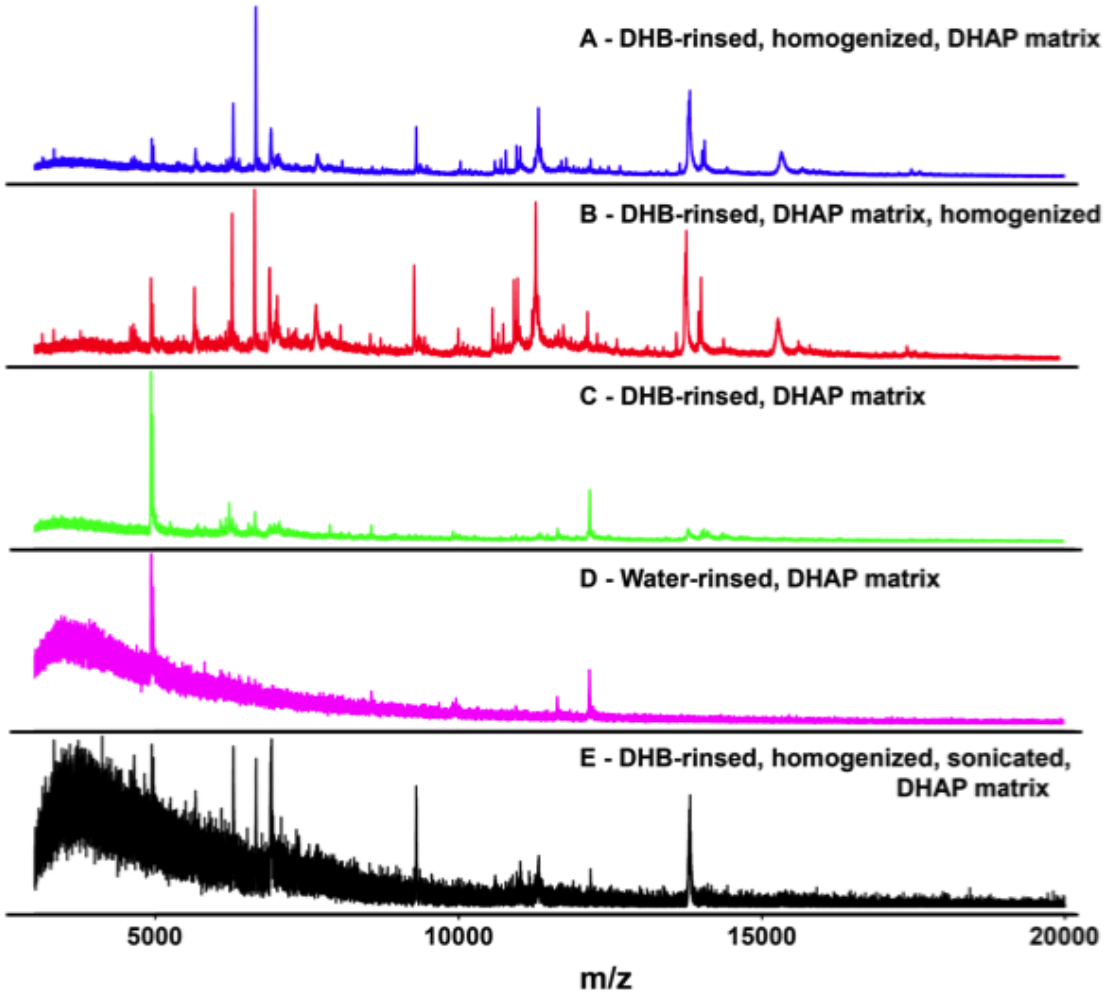

Figure 2.4 Spectra of needle- and syringe-homogenized, DHB-rinsed and DHAP-spotted NIH3T3 samples showing peaks above m/z 16000. Blue –cell pellet rinsed before homogenization, red – cell pellet homogenized after addition of DHAP spotting matrix, green – cell suspension in DHB not pelleted, magenta – cell pellet rinsed with water instead of DHB, and black – the homogenized cell pellet had been sonicated before spotting.

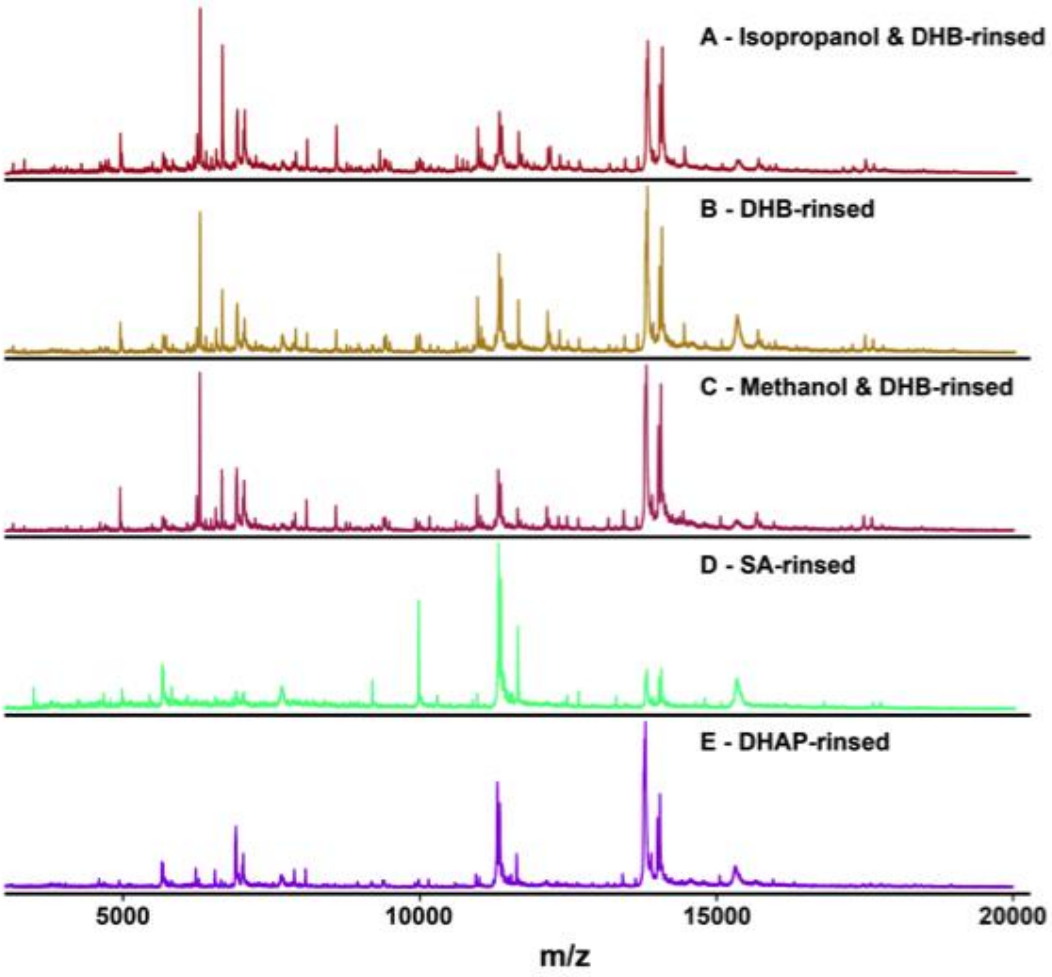

Figure 2.5 Effect on the cell spectra of the five different cell-rinsing matrix solutions, DHB/Isopropanol (A), DHB only (B), DHB/methanol (C), SA only (D), and DHAP only (E). Spectra A, B and C, obtained from DHB-rinsed cells have peaks above m/z 16000. Of these DHB/Isopropanol resulted overall in higher-intensity peaks.

adopted from Zhang *et al.*[30] who simultaneously processed cells by rinsing, lysis, and extraction, and possibly desalted them, using DHB solution. One solution was used to perform four tasks in one step, a strategy that makes sample preparation time-, and cost-effective. However, unlike in Zhang *et al.*[30] where only DHB solution in water was used to lyse cells and extract proteins directly from cells without any sample clean-up, we useda solution of DHB, isopropanol and acetonitrile for rinsing cells, cell lysis and protein extraction.

While Zhang *et al.*[30] reported spectra in the m/z range 4000-16000, we obtained typical spectra with m/z range 3000-20000. We believe that addition of a mixture of organic solvents (i.e. acetonitrile – efficient extraction solvent; and isopropanol – a lipophilic solvent with good extraction properties) and a mild acid to the cells followed by vigorous mixing resulted in simultaneous lysis of the cells, extraction and solubilization of some lipids from the cell membrane, and extraction and precipitation of both the hydrophilic and hydrophobic proteins directly from the cells. Since cell membrane proteins co-exist with lipids, extraction of lipids exposes proteins and makes them more accessible than would do mild acid treatment alone. When the sample-rinsing matrix solution mixture was spinned down at 4 ^{o}C, the extracted proteins were retained in the pellet while the lipids were removed with the supernatant. Subsequent spotting of the dH_2O-diluted and 2% TFA-acidified cell pellet onto a prestructured MALDI target with DHAP matrix solution resulted in the generation of peaks up to m/z 20000. Since we modified the composition of both the rinsing matrix solution and the spotting matrix solution in sample preparation to extend the m/z range of peaks from 4-16k to 3-20k, further modifications of these two solutions could lead to acquisition of spectra in higher.

Table 2.1 Previously used and currently proposed MALDI-TOF MS profiling strategies for mammalian cells[9, 20, 29-30]

	Different MALDI-TOF MS Profiling Strategies				
	van Adrichem et al., 1998	Zhang et al., 2006	Marvin-Guy et al., 2008	Lokhov et al., 2009	The One-step Cell Processing
Key Steps in Sample Preparation					
Washing of Cells	PBS	PBS	-	0.9% NaCl	PBS
Rinsing of Cells	-	DBH/water	-	Cold trypsin in 0.9% NaCl	DBH/water/ACN/ Isopropanol
Cell Lysis	Lysis buffer	DBH/water	-	-	DBH/water/ACN/ Isopropanol
Extraction	-	DBH/water	-	-	DBH/water/ACN/ Isopropanol
MS Sample Pre-treatment	Detergent for removal of lipids	-	-	ZipTipC18 for desalting	DBH/water/ACN/ Isopropanol
Sample Dilution	-	DBH/water	0.1% TFA	-	2% TFA
Spotting Matrix	Ferulic acid	CHCA; SA	SA	DHB	DHAP/AHC

Type of Sample	Cell lysate	Mixture of cells and lysate	Cell suspension	Protein fragments	Mixture of cells and lysate
Test Cells	CHO cell line	K562 cell line	T84 cell line	Primary fibroblasts	NIH3T3 cell line

mass range (i.e. >20k) that could precede generation of more unique MALDI fingerprints for cells and greater potential for discovery of unique biomarkers. Such changes would still require optimization of key steps to ensure reproducibility and reliability of MALDI profiles[39]

2.4.1.2 Determination of the suitable Cell Concentration

Successful comparison of spectral patterns has been reported to be dependent on the reproducibility of mass spectra[16, 40]. Poor reproducibility, as shown by inconsistent appearance of peaks, can lead to gross errors[41]. Cell concentration is one of the experimental factors with strong effect on the observed mass spectra[17], and hence their reproducibility. Previous studies on bacterial profiling have shown that less satisfactory spectra with fewer peaks could be resulted from samples with either too high or too low cell concentrations[42-43]. In this study a cell concentration higher than 380 mg/μL and lower than 12 mg/μL yielded mass spectra that could not be reproduced and had raised base line, respectively (data not shown). This implies that there is an optimal concentration range that could give good quality spectra, and this is in agreement with above-mentioned published reports.

The effect of cell concentration on the number of peaks was investigated by profiling varying concentrations of the processed NIH3T3 cell pellet. After the one-step processing, the cell pellet weighing 18.8 mg was dispersed in cold 50 μL dH_2O to make sample A. Next, this sample was serially diluted in a 1:1 ratio resulting in 9 different samples with the concentrations 380, 190, 95, 47, 24, 12, 6, 3, and 1 mg/μL, respectively. The experiment was performed in triplicates. The spectra of the first six samples from one of the triplicate experiments are shown in Fig 2.6. The corresponding number of

peaks in these samples were 143, 215, 225, 272, 285, and 261, respectively. It was observed that as the cell concentration decreased, the number of peaks in a spectrum increased for the first five concentrations but decreased with further sample dilution. The 24 mg/μL cell concentration not only yielded the largest average number of peaks but it also resulted in repeatable spectra characterized by lowest variability or smallest standard deviation of the average number of peaks (Figure 2.6). From these results we conclude that the optimum cell concentration for MALDI profiling of NIH-3T3 cell line is around 24 mg/μL. Using the same strategy the optimum concentration for MALDI profiling of the breast cancer cell lines was around 190 mg/μL (Section 2.4.2 below).

2.4.1.3 Short-term Stability of the Cell Sample

Apart from the cell concentration, other experimental factors such as time and temperature of sample preparation and storage are important for whole cell analysis since they influence stability of the proteins. The stability of protein samples during preparation could be improved through inhibition of activity of endogenous proteases by maintenance of samples on ice or addition of a protease inhibitor. This short-term stability was investigated in two ways: 1) processing two parallel samples, one with and one without protease inhibitor (2 mM phenylmethylsulfonyl fluoride, AMRESCO, Solon, OH, USA); and 2) varying the time between the one-step sample processing and application of matrix while keeping samples on ice at 0 ºC.

Figure 2.7 shows mass spectra of samples processed in the absence and the presence of protease inhibitor, respectively. No differences were observed between these two spectra. This implies that during time of processing of about 20-30 min at 0 ºC protease activity, if any, is minimized and the integrity of the sample is maintained.

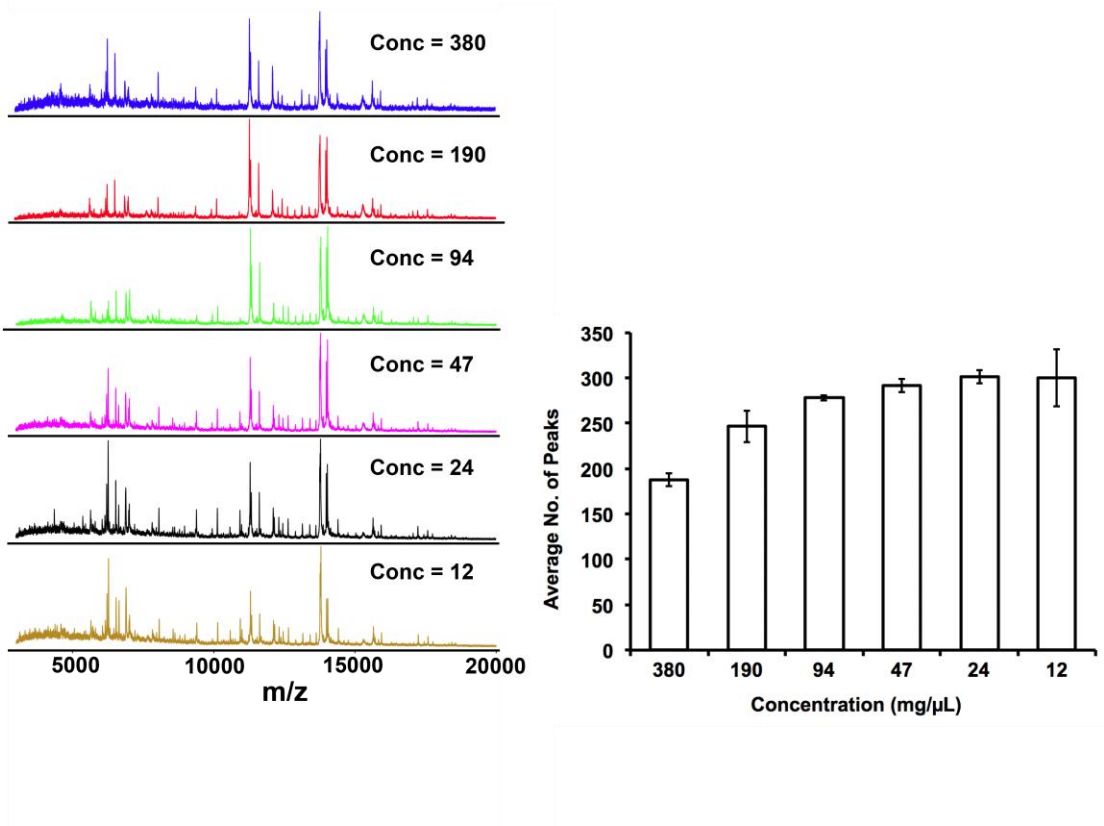

Figure 2.6 *Right* panel: The bar graph of the average peak numbers and standard deviations of spectra generated from triplicate samples of NIH3T3 cells sequentially diluted into six concentrations 380, 190, 95, 47, 24 and 12 mg wet cell pellet weight/µL water. 24 mg/µL was found to be the optimum concentration because it resulted in a combination of large number of peaks and a small standard deviation. The error bars represent ± standard deviation. *Left* panel: Representative spectra from each of the six dilutions. Although the spectra are similar the average number of peaks increase with decreasing concentrations and plateaus at 47 mg/µL onwards.

Therefore protease inhibitor is not needed. In addition, sample stability was tested by incubation of multiple samples on ice at different time durations, i.e. 0 h, 3 h, 5 h and 19 h, before application of the spotting matrix. The aim was to see if the spectra would be the same if the samples are left on ice prior to MALDI MS. In this experiment, sample preparation (i.e. one-step processing) and parameters for instrumental analysis were kept the same for all samples while duration prior to MALDI analysis was varied. Mass spectra of the 0 h, 1h, 3 h and 5 h cell samples expressed nearly all same peaks while differences such as at m/z 3457 and 15848 were observed between these four samples and the 19h sample (Figure 2.8). Stability of the samples is not affected by long incubation on ice prior to MALDI analysis, but repeatability might be compromised. Nonetheless, short or no incubation is essential to ensure the rapidness of the analytical methodology.

2.4.2 Application of the Established Methodology in Discrimination of Breast Cancer Cells

Traditional approaches to analysis of biochemical systems associated with human disease involve study of biochemical transformations and identification of target molecules. Typically such studies vary only a few experimental factors thought apriori to be relevant with the result that they reduce complexity of research hypothesis but may preclude important information that would better characterize the complexity and diffusivity of the same biochemical systems. With the growth of the "omics" technologies it has been possible to characterize these biochemical systems on the basis of fingerprints displayed by their cellular proteins of previously unknown identities. The key is to record, in a single analysis, in the form of a profile, the relative abundances and masses of several hundreds or thousands of proteins measured. MALDI-TOF MS provides this information in a high-throughput, simple and rapid manner[44]. The spectral fingerprints generated by

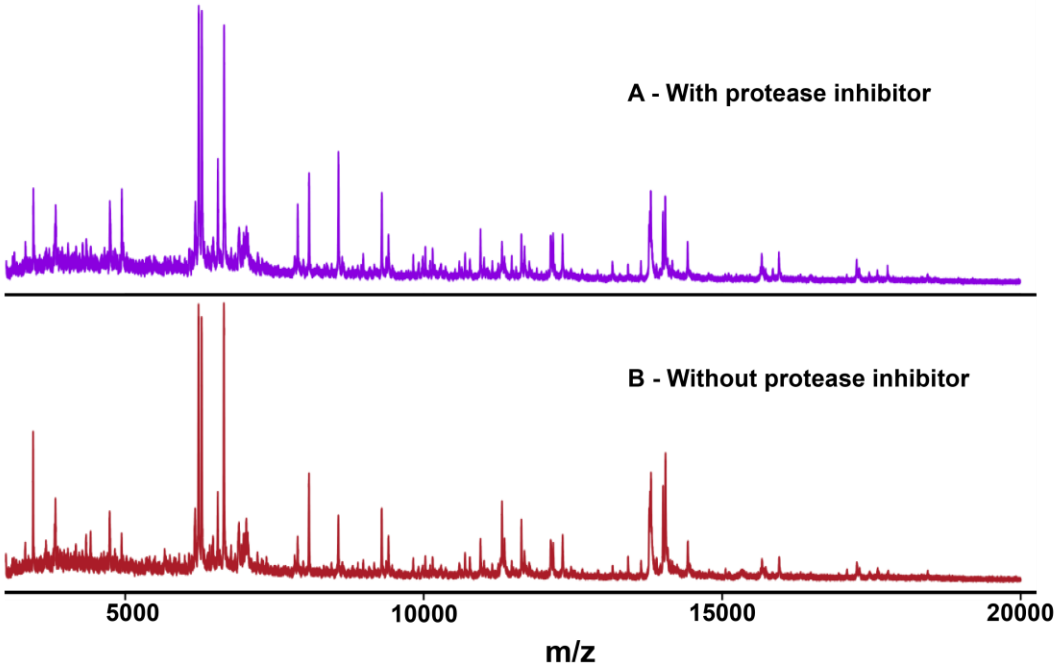

Figure 2.7 Mass spectra showing no effect from treatment of NIH3T3 with PMSF protease inhibitor. Blueviolet – spectrum from inhibitor-treated cells and firebrick – spectrum from control.

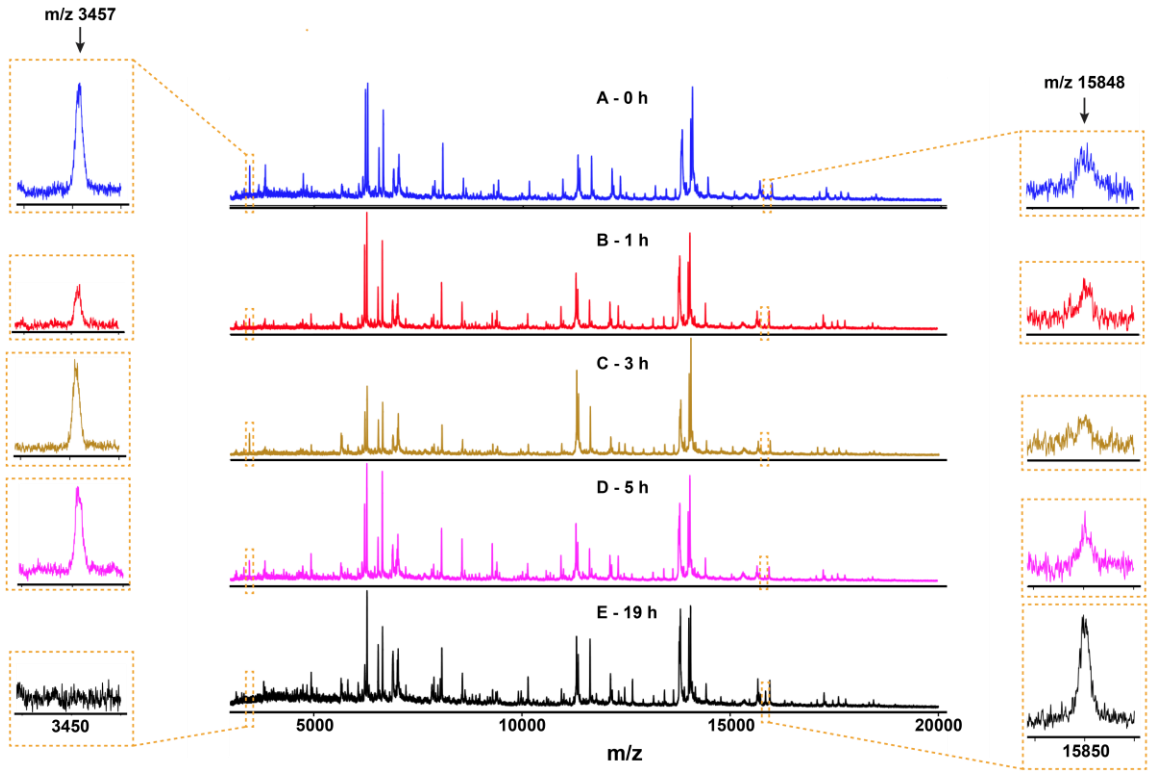

Figure 2.8 Spectra showing effect of short-term stability when incubated on ice prior to MALDI analysis. The middle column has the actual spectra while the two side columns are zoom-in views of the peaks at m/z 3457 and 15848. The spectra from 0 h, 1 h, 3 h and 5 h samples had nearly all same peaks while differences such as at m/z 3457 and 15848 were observed between these four samples and the 19 h sample. To ensure repeatability, samples should not be kept too long on ice prior to MALDI analysis.

the MALDI-TOF MS are highly dimensional data that require application of bioinformatics and multivariate statistical methods for pattern recognition and revelation of distinguishing features. In the case of cancer, for instance, different biological samples such as body fluids, biopsies and intact tissues have been profiled using MALDI MS to establish and rapidly screen for disease biomarkers. However, regarding breast cancer, few attempts have been made to profile the breast cancer cell lines, the very essential and widely used systems in studying the complex breast cancer pathobiology and in screening of newly developed therapeutics.

2.4.2.1 Subtypes and profiling of breast cancer

Breast cancers are molecularly heterogeneous manifestations of one disease[45]. They have been grouped into five subtypes that are not only biologically distinct but also have specific clinical course and response to treatment[46]. The five molecular subtypes are luminal A, luminal B, ERBB2-overexpressing, basal-like and normal-like[47]. Luminal A and B tumors express markers of the luminal epithelial cells lining the normal breast ducts and are ER-positive. The basal-like tumors express markers of the basal epithelial cells lining the normal breast ducts and are ER-negative. The ERBB2-overexpressing tumors express genes co-amplified with ERBB2 that encodes HER2 and are HER2-positive. Normal-like tumors share expression patterns of the normal breast tissue. Of these, the basal-like breast cancer has poor prognosis and hardly any treatment[48].

To improve the understanding of the breast cancer phenotypes, the merits of integrated genomic and proteomic profiling of the breast cancer cell lines have been appreciated[49]. A comprehensive comparison of the molecular and biological features of a collection of 51 breast cancer cell lines with those of primary tumors performed by Neve

et al. revealed that the breast cancer cell lines resemble primary tumors with respect to genomic and transcriptional abnormalities as well as response to pathway-targeted therapeutic agents[6]. Similarly Kao *et al*. profiled gene expression and DNA copy number alterations of 52 widely used breast cancer cell lines and made same observations[50]. Based on the resemblance of cell lines to primary tumors, the breast cancer cell lines have been categorized into 3 subtypes: luminal, basal A and basal B. Luminal cell lines are ER-positive. Basal A cell lines are associated with BRCA1 expression. Basal B cell lines display mesenchymal and stem cell properties and have upregulated EMT[51]. Both basal A and basal B cell lines share same expression patterns of the basal-like tumors while luminal cell lines resemble either luminal A or luminal B tumors.

It is evident from the works of Neve and Kao and their co-workers that genomic and proteomic analyses of breast cancer cell lines can accurately reflect how genes contribute to breast cancer pathophysiology. Proteomic profiling of breast cancer cell lines has been previously undertaken using surface-enhanced laser desorption/ionization (SELDI) ProteinChip™ arrays[52]. The cell lines were successfully sub-classified into similar groups as with corresponding earlier gene expression and immunohistochemistry studies. A diagnostic protein signature was developed and new biomarkers identified. The study demonstrated that MS-based methods can be reliably employed in profiling of breast cancer cell lines. While the SELDI MS profiling involved a lengthy sample preparation procedure due to prior incubation of protein sample with the chip and subsequent purification, our MALDI-TOF MS profiling strategy involves just a one-step cell sample processing, the procedure of which is simple and rapid. Our goal was to use this established MALDI-TOF MS-based method as an alternative to rapidly profile breast

cancer cell lines and to demonstrate their discrimination based on the biological differences captured in the spectral fingerprints, a feature that is invaluable for development of diagnostic tool and biomarker discovery. In this study, the cell lines profiled were MCF-7, MCF-10A, MDA-MB231, MDA-MB468, SKBR-3 and T47-D, and their characteristics are shown in Table 2.2.

Six but one of these cell lines are human breast cancer cell lines widely used as *in vitro* tumor models. MCF-10A is an immortalized normal breast cell line derived from fibrocystic disease and commonly used as a non-cancerous control in breast cancer studies[53]. Previous studies on gene expression microarray and immunohistochemical analyses, as well as SELDI MS profiling have shown that MCF-7, SKBR-3 and T47-D share characteristics of the luminal-like tumors while MCF-10A and MDA-MB231 share same characteristics as the basal-like tumors[54]. MDA-MB468 was not included in that study. Since SELDI MS, a MALDI MS-related analysis could reveal distinct groups as with other biochemical approaches, we hypothesized that MALDI-TOF mass spectral fingerprinting following pre-treatment of breast cancer cell lines using the one-step cell sampling processing should result not only in similar groupings but also in observation of some known and possibly new disease biomarkers. To test this hypothesis, an inhouse bioinformatics pipeline and a commercial software were applied in analyses of mass spectral data of six breast cell lines. The specific aim was to distinguish the metastatic cell lines, MDA-MB231 and MDA-MB468 from the non-metastatic cell lines, MCF-7, SKBR-3 and T47-D, and in turn, from the normal cell line, MCF-10A.

Table 2.2. The clinicopathological features[6, 50, 54] and the number of spectral profiles of the 6 breast cancer cell lines

Cell line	Subtype	ER *	PR *	HER2 *	Source	Tumor type	No. of spectra
MCF-7	Luminal A	+	+	-	PE	Met AC	15
MCF-10A	Basal B	-	-	-	RM	F	10
MDA-MB231	Basal B	-	-	-	PE	Met AC	16
MDA-MB468	Basal A	-	-	-	PE	Met AC	10
SKBR-3	HER2	-	-	+	PE	AC	12
T47-D	Luminal	+	+	-	PE	IDC	10
							Total: 73

2.4.2.2 Repeatability and Consistency of Cell Morphology

Initially cell morphologies of the cell lines in several consecutive passages were tested for similarity. To do that, MCF-7 and MDA-MB231 were cultured and passaged following designated protocols. Each passage was cultured in two T75 flasks resulting in two replicate samples. In order to ensure reproducible MALDI-MS profiles, efforts were made to get similar cell morphologies throughout different passages. Three images (Figure 2.7) were obtained from three different passages of MCF7 and MDA-MB231 cells to show that, prior to harvesting, the cells had similar morphology and confluency.

2.4.2.3 Selection of the Suitable Time for One-step Processing of Breast Cancer Cells

In addition to ensuring consistent cell morphology, an attempt was made to find a suitable length of time at which the harvested cells could be mixed with the extraction/lysis matrix solution A prior to pelleting. This time is critical because if it is too short, the extraction and removal of lipids will not be sufficient to release the proteins and make them available for ionization during MALDI; conversely, if this time is too long, release of endogenous proteases may lead to degradation of the protein analyte and reduction of MALDI-MS signal. To find the suitable length of time for sample processing, cells were resuspendend in 4 mL PBS after harvesting, and then sub-divided into 1 mL aliquots. After washing in PBS, the four samples were treated with the extraction/lysis matrix solution A for 5, 20, 100, and 200 sec, respectively. The cell pellet of each sample was dispersed in water and diluted to concentrations of 0.19 and 0.094 mg/µL, respectively. The MALDI-MS spectra of all the samples were generated the peaks above noise level of about 200 a.u. were manually counted and used to evaluate the effect of the duration of extraction/lysis on the MALDI-MS spectra of the cells. The

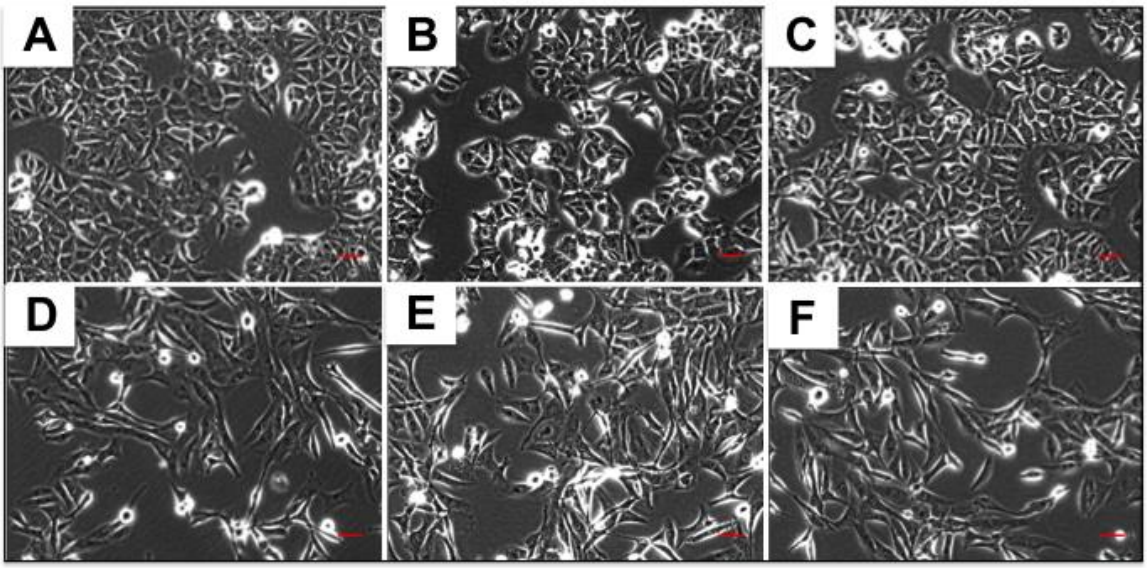

Figure 2.9 Light microscope images of MCF-7 (A, B and C) and MDA-MB231 (D, E and F) cells from three consecutive passages. Scale bar = 100 μm. The cell morphology was similar throughout successive passages.

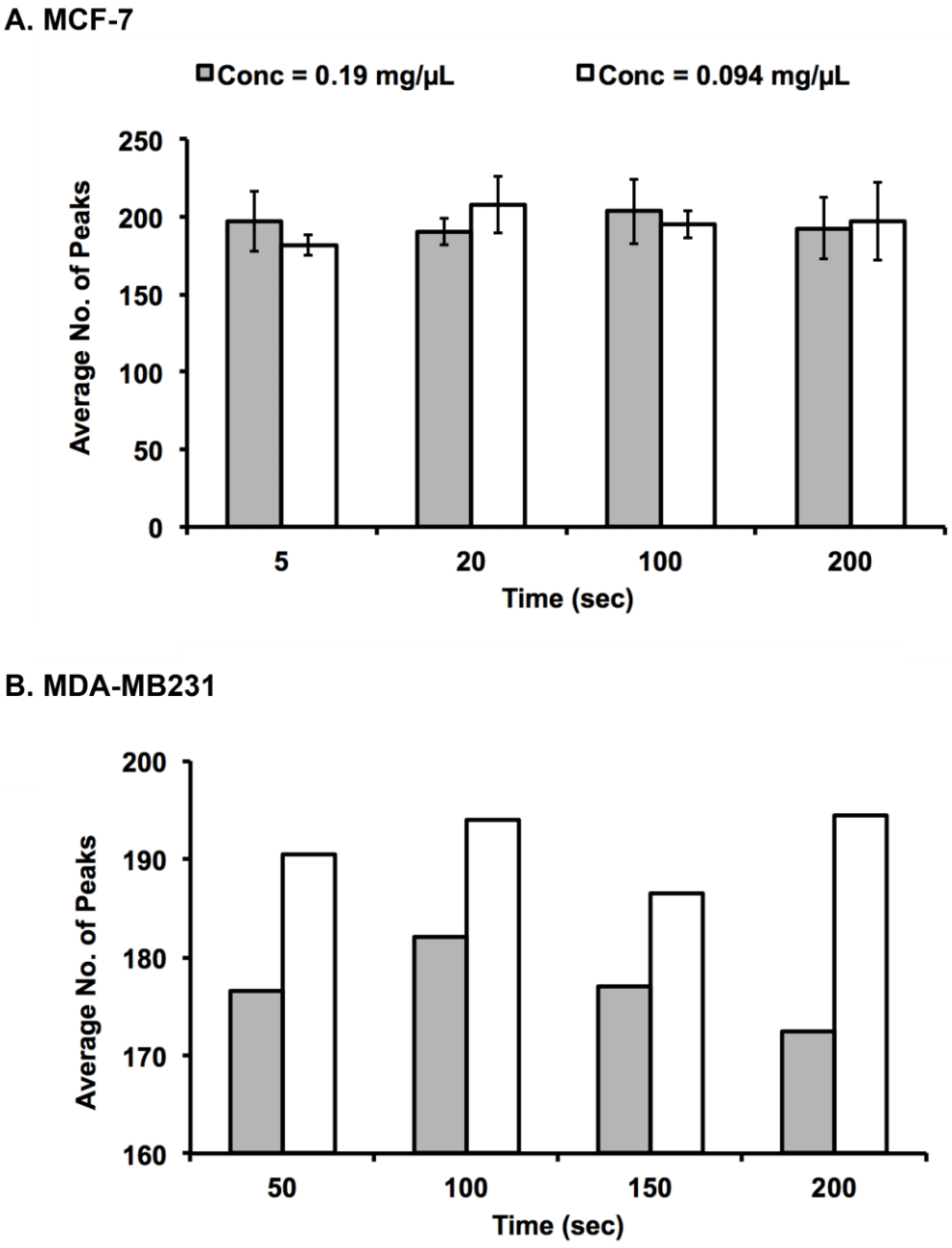

Figure 2.10 Effect of the time of rinsing cells with extraction/lysis matrix solution on the spectra of MCF-7 and MDA-MB231. 100 sec was most suitable because of large average number of peaks and small standard deviation at cell concentration of 0.094 mg/µL.

experiment was performed in triplicates for the MCF-7 and in duplicates for MDA-MB231 cells.

The duration of extraction/lysis was found to have little or no effect on the number of spectral peaks as shown on Figure 2.8. For MCF-7, although the mass spectra of about the same number of peaks (200) were obtained at each concentration after treatment with extraction/lysis solution for 5, 20, 100 and 200 sec, spectra from 100 sec treatment had relatively higher intensities than all other treatments, indicating high signal-to-noise ratio. For MDA-MB231, a trend was observed only at higher concentration (0.19 mg/µL) at which the highest average number of peaks was obtained from 100 sec treatment. Based on these results the time 100 sec and the 0.19 µg/µL cell concentration were used for profiling of the human breast cancer cell lines.

2.4.2.4 PCA Analysis using the In-house Data Analytic Pipeline

Prior to PCA analysis, selection of discriminatory features by the multiple t-tests was performed resulting in data matrix sizes of 47 samples by 301 features for normal versus non-metastatic, 36 samples by 230 features for normal versus metastatic, and 63 samples by 280 features for metastatic versus non-metastatic. For these 3 comparisons, projections of the data into the space of the first two principal components were found to be adequate to achieve 100% leave-one-out cross-validated classification accuracy, based on Mahalanobis distances to cluster group centroids. Group membership was predicted using Mahalanobis distance as a similarity measure. The Criterion for classifying a sample as a member of the group is that the Mahalanobis distance from the sample to the group centroid is smallest. The higher classification accuracy and the lower error imply that the discrimination between the groups is greater[32].

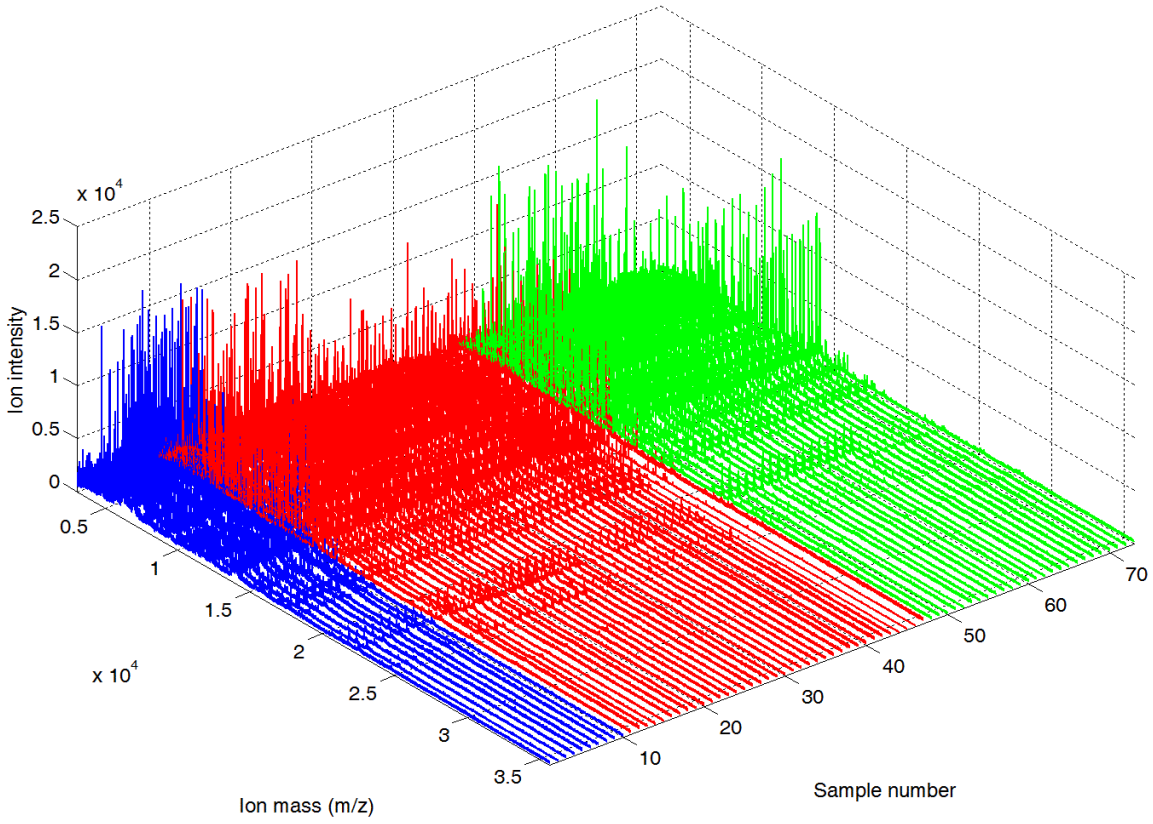

Figure 2.11 The 73 MALDI-TOF MS spectra (replicates) of six human breast cancer cell lines. 26 green spectra for the cancerous and metastatic cell lines, MDA-MB231 and MDA-MB468; 37 red spectra for the cancerous and non-metastatic cell lines, MCF-7, SKBR-3 and T47-D; and 10 blue spectra for the normal and transformed cell line, MCF-10A (control).

In Figure 2.10 samples in each of the three comparisons were clustered at 100% classification accuracy into two distinct groups, indicating discrimination by spectral fingerprints, as demonstrated by the 3 plots of projection of samples into the space of the first 2 PC's In each plot the PC scores representing replicate spectra are well demarcated by 95% ellipses. The plots provide visual summary of the relationships among the breast cancer cell lines being compared. The plots clearly show that all the 10 spectra normal cell line (MCF-10A) are different from the 37 spectra of the non-metastatic cell lines (MCF-7, SKBR-3 and T47-D), and so are the 10 spectra of the normal cell line compared to the 26 spectra of the metastatic cell lines (MDA-MB231 and MDA-MB468), as well as the 26 spectra of the metastatic cell lines compared to the 37 spectra of the of the non-metastatic cell lines. Slight overlapping of the group ellipses occurred on comparing the metastatic with non-metastatic in the last plot, indicating some similarity between these groups. No PC scores, however, lay in the intersection area of these 2 group ellipses.

The PC scores of few samples were found lying outside the ellipses. It is unlikely that these samples were misclassified given that the classification accuracy was 100% and also since they lie next to a particular cluster. It is likely though that these samples are outliers, however, no outlier tests were performed. Moreover, it is possible that clustering on a two PCs space was not optimal to orientate all the scores to have shorter Mahalanobis distances from cluster centroid and hence be in one cluster. This is evident from the discrimination of metastatic versus non-metastatic where the first two PCs explain only 50% of the variance and scores of about 10 samples lay outside of the ellipsoids. Projection of the scores on a three PCs space might have made them to be at

much more closer proximity to the cluster centroid as to have all of them included in ellipsoids as the remaining variance is sufficiently captured by the third PC.

Overall, the clusters of features of cell lines being compared are accurately separated when projected on the low dimensionality space made up of the first two principal components (Figures 2.8 and 2.9), indicating that the spectral fingerprints generated by MALDI-TOF-MS following the one-step cell sample processing, contain discriminating features. Although the in-house bioinformatics pipeline could distinguish between metastatic and non-metastatic as well as between these and normal transformed groups of cell line spectra, it gives limited information about comparable attributes of the spectra. For example, the data analytic process does not reveal the discriminating features neither does it show how related the member spectra are. Therefore, it is inadequate for MALDI-TOF MS characterization of breast cancer cells.

2.4.2.5 Peak Selection and Matching using BioNumerics Software

To investigate how related the spectra are and what features enable discrimination of the breast cancer cell lines, the 73 raw spectra of the six cell lines were reanalyzed using BioNumerics software (Austin, Texas; www.applied-maths.com) following the instructions provided. First, a database of the 73 spectra was created and next spectral data files were imported into the BioNumerics interface and preprocessed using the given methods. Upon peak detection, peak matching was done to create peak classes that could be used for comparisons. In BioNumerics a peak is defined on the basis of the spectrum during preprocessing while a peak class is defined on a basis of a group of spectra and peak classes are generated during peak matching. Many peaks may have been detected at a signal-to-noise ratio of 5 during spectral preprocessing, but about 100 peak classes were

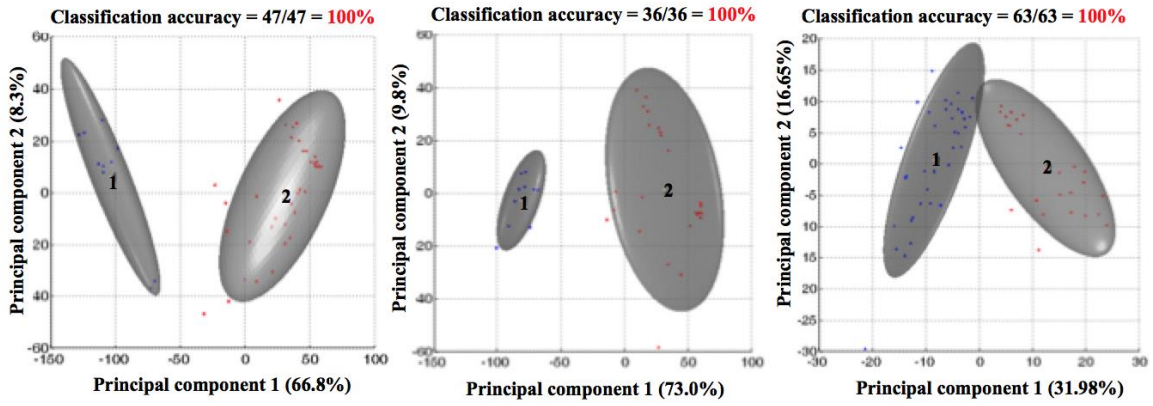

Figure 2.12 Principal component analyses and classification of 3 sets of data, first panel: normal against non-metastatic, second panel: normal against metastatic, and third panel: non-metastatic against metastatic

created during the subsequent peak matching. A binary table of presence and absence of peak classes showing expression of 110 proteins by the 6 cell lines (Figure 2.11) was exported in excel. The heatmap version of the table showing intensities of the peaks or expression levels in different colors was also generated but could not be exported because of limited access to this commercial data analytic software. In the binary table the presence of a peak or expression of a protein as well as absence of a peak or no protein expression is indicated by different colors. The cell lines are characterized by protein expression, where the pattern made by spectral features, peaks (proteins) and their relative intensities (expression levels) forms the fingerprint of the cells. It can be observed from Table 2.3 that none of the replicate spectra of the cell lines have identical peaks. This shows that there is some level of variability among the replicate spectra. However, different cell lines could still be distinguished by their spectral features as evidenced by the comparisons described below. It is also noteworthy from the table that MDA-MB468 lacks many of the peaks below m/z 7000 compared to all other cell lines. Our sample preparation method and reagents could have been unfavorable to cellular proteins of this cell line in that m/z range. It is strikingly evident though that absence of the peaks or lack of protein expression was highly repeatable among the replicates of MDA-MB468.

2.4.2.6 PCA Analysis using BioNumerics Software

The 73 mass spectral protein profiles were further analyzed by performing 2 different unsupervised clustering methods, principal component analysis (PCA) and hierarchical clustering. The unsupervised hierarchical clustering of the spectra and the proteins was done using Pearson correlation as the similarity metric. Its results were displayed as

Table 2.3 Binary representation showing presence and absence of protein peaks in the spectra of each of the 73 samples. Red – presence of a peak. White – absence of a peak.

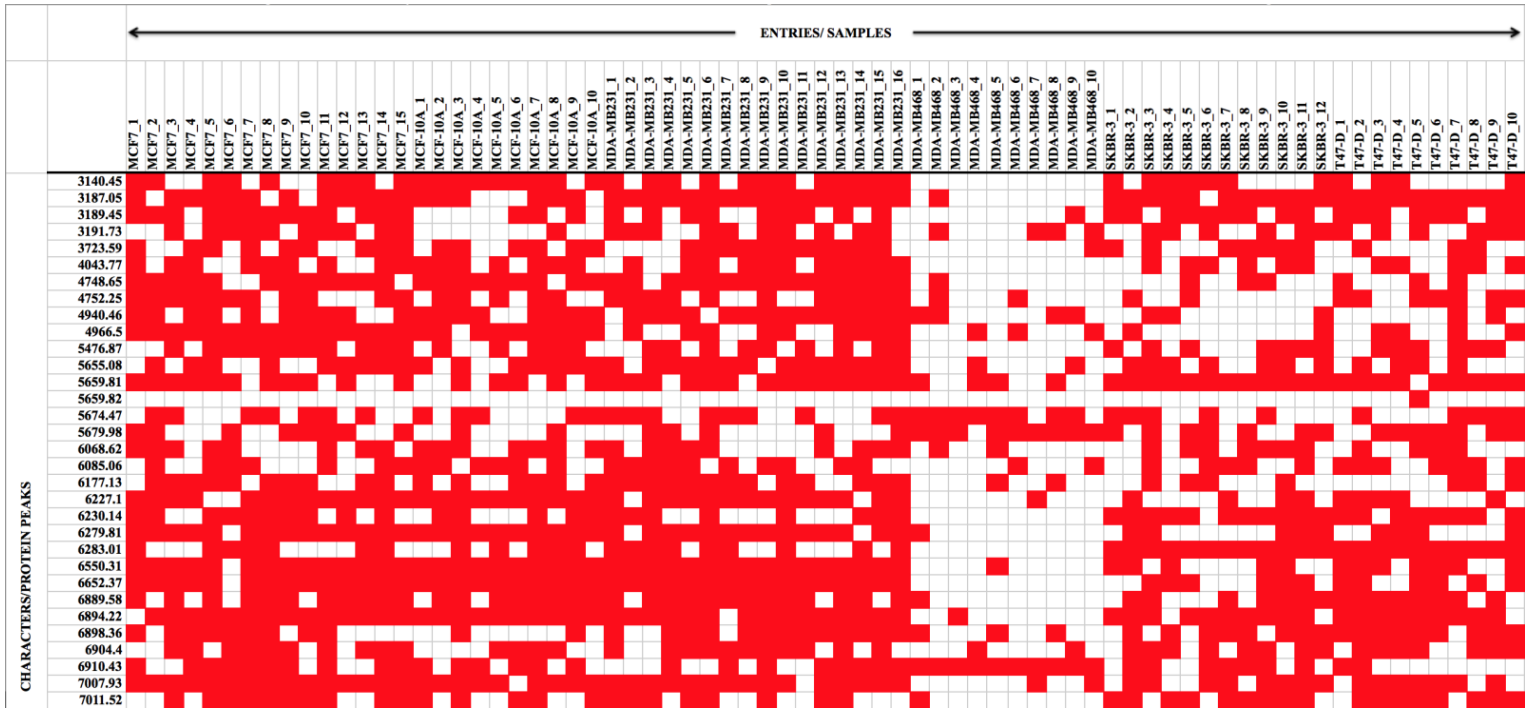

Table 2.3 Contd.

Table 2.3 Contd.

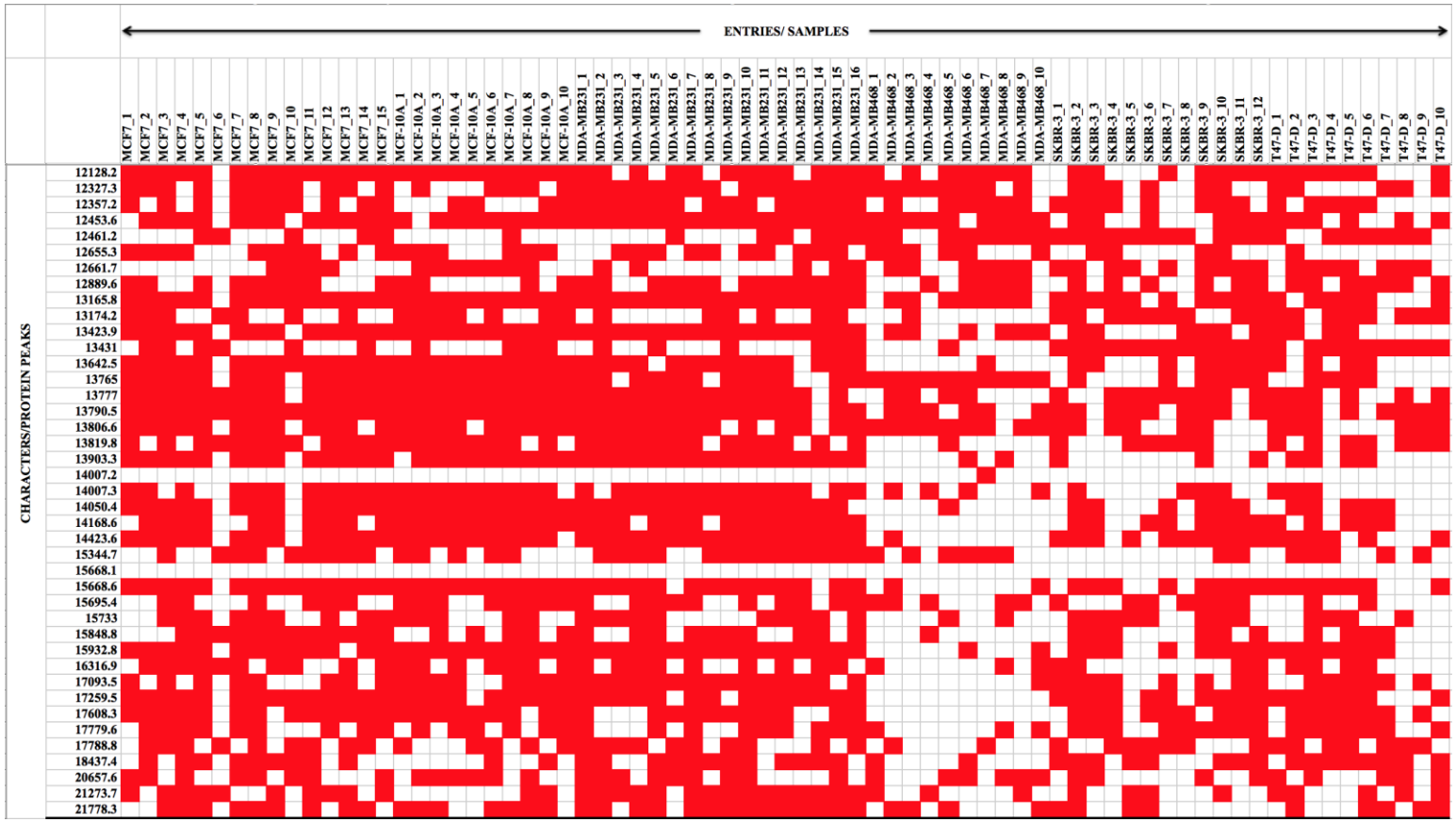

dendogram. PCA allowed data reduction and visualization of samples (spectra or entries) and proteins (peak classes or characters) on a 2 PC's space (for samples/entries and proteins/characters), and second on a 3 PC's space (for samples/entries only). On a 2 PC's space PC scores of samples appear on the 1st plot and PC loadings of the proteins on the 2nd plot. Both plots are complementary and superimposable. On a 2 PC's space distinct clusters of the cell lines could hardly be observed except for the MDA-MB468 (far right of the 1st bi-dimensional plot). However, no peak classes/characters were found to correspond with the MDA-MB468 cluster looking at the 2nd bi-dimensional plot. Hence, no unique peak classes of this distinct cluster could be observed. In general, owing to the inability to obtain distinct clusters for all the rest of the 5 cell lines, it is hard to locate unique peak classes of the cell lines, if any. The first 2 PC's space accounted for 50% of the variance while the first 3 PC's space described 60% of the variance. As a result visualization would be better on a 3 PC's space.

A distinct cluster of PC scores (turquoise dots) of MDA-MB468 spectra was observed with 3-D PCA. Two large mixed clusters, one of SKBR-3 and T47-D (yellow and purple dots, respectively), and the other of MCF-7, MDA-MB231 and MCF-10A (green, red and dark cyan dots, respectively) also resulted from 3-D PCA. While mixed clustering of SKBR-3 together with T47-D could be explained by shared characteristics of possessing luminal breast cancer behavior and being non-metastatic, co-cluster of MCF-7 and MDA-MB231, both of which are molecularly different, as one is luminal and the other basal B, is least expected. Such outcome could be explained by either lack of sufficiently discriminatory protein peaks from our methodical m/z range of profiling or insufficiency of a clustering that is based on all the proteins instead of a selected set that

is highly discriminatory. Co-clustering of MDA-MB231 with MCF-10A is reasonable because both possess basal characteristics of breast cancers. Although distinct clusters of the 5 cell lines (excluding MDA-MB468) were not obtained, majority of the PC scores of spectra of these cell lines seem to aggregate together showing that there may be more similar than dissimilar features among replicates of each cell line.

2.4.2.7 Hierarchical Clustering using BioNumerics Software

In support of the PCA results, hierarchical clustering divided the 73 samples into 2 large groups (represented by 2 big branches of the horizontal dendrogram, Figure 2.13) based on their similarity. The first branch is shared by all the MDA-MB468 and mixture of the SKBR-3 and T47-D replicates. All the MDA-MB468 are on one sub-branch showing that they are similar to one another than to spectra of other cell lines, hence they formed a distinct cluster as in the PCA analysis above. The mixture of SKBR-3 and T47-D on next sub-branch resembled a co-cluster of these two in PCA that could be explained by insufficient discriminatory peaks in the spectra of the two cell lines or inability of the used classifier to adequately separate the cell lines.

The second branch is shared by the remaining replicate spectra of SKBR-3 and T47-D, all the replicate spectra of MCF-7, MCF-10A and MDA-MB231. Similar to the PCA above it was least expected to have MCF-7 and MDA-MB231 in one branch. In general majority of the replicates of each of the cell lines MCF-7, MCF-10A and MDA-MB468 were clustered together showing that there was high similarity among them whereas many of the replicates of MDA-MB231, SKBR-3 and T47-D were not clustered together, instead were mixed up showing that there was low similarity among the replicates as a result of fewer discriminative features or inadequacy in the classification

model. These results are based on the clustering using all 109 proteins. It is possible that if the number of proteins had been reduced to include only highly discriminatory ones, the sizes and the components of the clusters would have changed. Probably even the replicate spectra of MCF-7 and MDA-MB231 would have been classified into 2 distinct groups.

Hierarchical clustering of 27 breast cell lines, based on their SELDI-TOF mass spectra, placed T47-D and MCF-7 in the first branch, and SKBR-3, MDA-MB231 and MCF-10A in second branch. The subsequent supervised classification of the 27 breast cell lines, based on only the significant differentially expressed protein peaks, placed MCF-7, SKBR-3 and T47-D in the first branch, and MCF-10A and MDA-MB231 in the second branch, where the first branch and second branch depict the luminal and basal subtypes, respectively. In that classification the 3 luminal cell lines were adjacent to one another showing that they were highly similar, while the 2 basal cell lines were distant from one another showing that they were less similar. MDA-MB468 was not included in that study. In the current study, supervised clustering was not accomplished due to limited access to the commercial software. Had the supervised clustering been performed, the clustering might have been refined and could have been comparable to that by Goncalves *et al*.[52] Supervised clustering methods can control within-group variance while maximizing beween-group separations to enhance discrimination between groups.[55]

Clustering of the 109 protein peaks (vertical dendogram, Figure 2.13) reveals that there may be similarities shared in intensities among peaks in the m/z ranges 3000-5000, 5000-25000, and 25000-30000. The remarkable observation from this pattern of clustering was the distinctly low intensities of the protein peaks of MDA-MB468

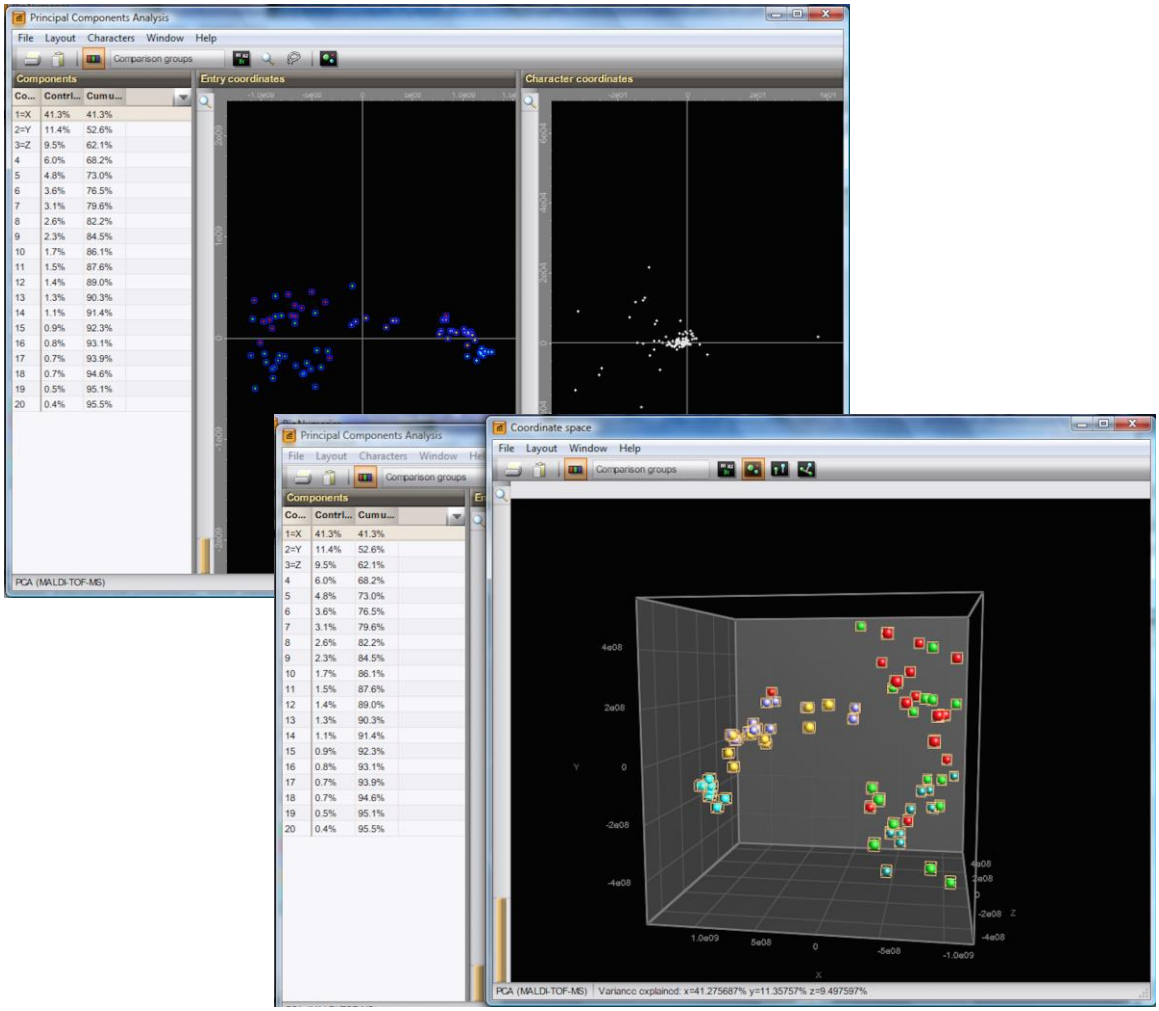

Figure 2.13 Projection of the PC scores for the 73 samples on a 2-dimensional (first panel) and 3-dimensional space (second panel) made up of 2 and 3 principal components, respectively. The first panel has 2 plots. The left one is the plot of PC scores of spectra/samples (hereby referred to as entries), and the right one is the plot of PC loadings showing protein peaks (hereby referred to as characters). The first 2 PC's account for 50% of the variance while the first 3 PC's explain 60% of the variance.

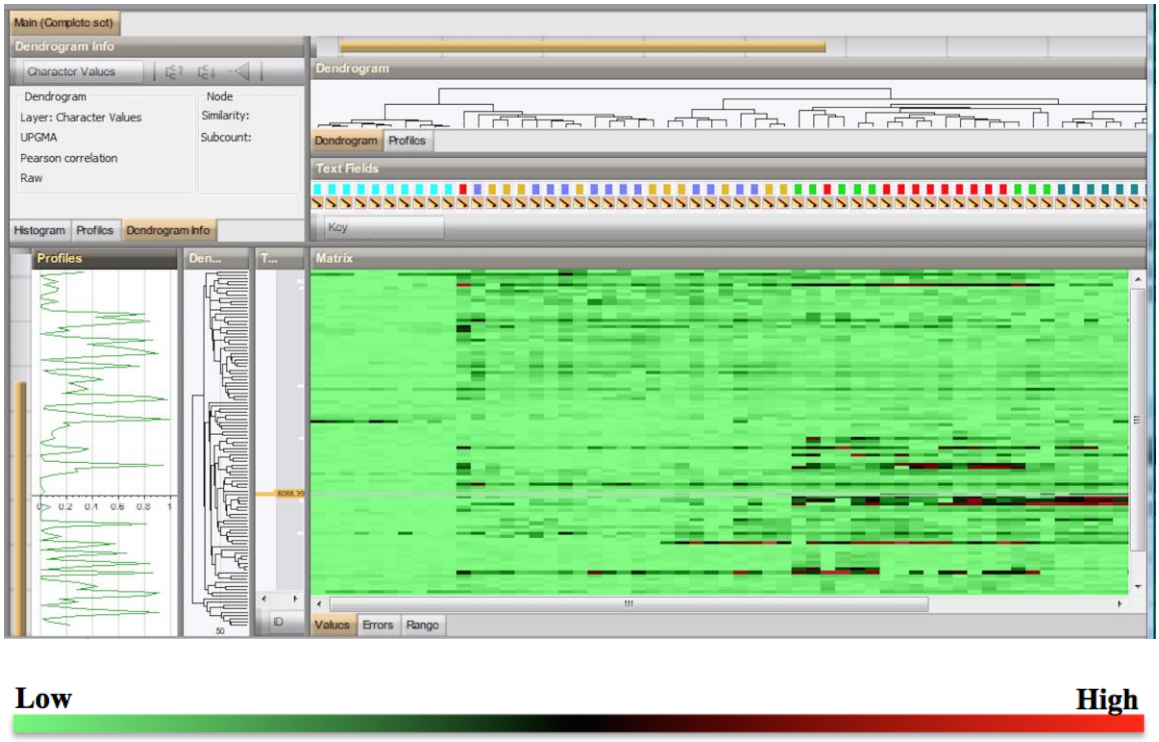

Figure 2.14. Protein expression profiling and hierarchical clustering of breast cancer cell lines (MCF-7/red, MCF-10A/dark cyan, MDA-MB231/green, MDA-MB468/turquoise, SKBR-3/purple, and T47-D/yellow) and 110 proteins based on MALDI-TOF mass spectral measurements. Each row represents a protein peak and each column represents a spectrum of a cell line. The expression level of each protein is relative to its median abundance across all cell lines and is shown according to a color scale. Black, red and green are levels on, above and below the median, respectively. The magnitude of deviation from median is represented by color saturation. The curve in the profiles panel depicts the change in p-values of differential expression between MCF-10A (the control) and the 5 breast cancer cells lines.

replicates and that these low expression levels underscore the observations shown in the binary table. Due to limited access to the commercial software, protein peaks that have significant differential expression among the cell lines are not known. However, several proteins were found to have significant differential expression between MCF-10A and all the 5 breast cancer cell lines at an adjusted p-value of ≤ 0.05.

2.5 CONCLUSIONS

Using NIH3T3 cell line, a novel one-step process method has been developed for whole cell analysis of mammalian cells using MALDI-TOF MS. The established method involves use of the optimized novel rinsing matrix solution of the composition 5 mg/mL DHB in isopropanol: acetonitrile: dH_2O (2:1:1 v/v/v) and the DHAP spotting matrix solution developed by Wenzel *et al*.[31]. Spectra generated had strong signals and consisted of the largest array of peaks ever to be reported from direct cell MALDI-MS in the mass range 3000-30000.The established method is simple, rapid , direct, and repeatable. Since it is a one-step process, it reduces the variables and complications that can lead to irrepeatable spectra. By the optimization of pre-analytical conditions such as organic solvent, matrix, temperature, inhibitor, time and concentration of cells as well as spotting approach, reproducible spectral fingerprints could be obtained. The novel one-step profiling was applied in the fingerprinting and discrimination of breast cancer cell lines. Four different mammalian cell lines 3T3, MCF-10A, MCF-7and MDA-MB231Three non-metastatic cell lines MCF-7, SKBR-3 and T47-D, two metastatic cell lines, MDA-MB231 and MDA-MB468, and one non-cancerous cell line, MCF-10A were investigated and differences among them were observed by comparing their mass spectra. Since the mass spectral data is highly dimensional it is mandatory[34] that multivariate pattern

recognition methods be employed to demonstrate the similarities and differences and to visualize some patterns in the data. Two different data analytic pipelines were employed to ensure confidence of the profiling results, one is the in-house methodology developed by Morgan *et al*.[32] and the other is a commercial BioNumerics software (www.applied-maths.com).

PCA analysis using Morgan *et al*. methodology distinguished the breast cancer cell lines into groups based whether they were metastatic, non-metastatic or non cancerous. The clustering was performed for two groups at a time where the samples were always classified with 100% accuracy. However, this pipeline could not demonstrate clustering of more than two groups and therefore was inadequate for differentiation of spectra of the six breast cancer cell lines in one analysis. BioNumerics on the other hand permitted hierarchical clustering and PCA of all the six cell lines, where distinct groups were observed for MDA-MB468 and MCF-10A. A co-cluster of SKBR-3 and T47-D showed that there are more similar than dissimilar features between these two. These cell lines have similar clinicopathological features so they are likely to co-cluster. A co-cluster of MCF-7 and MDA-MB231 was least expected since these have different clinicopathological properties. Although the unsupervised clustering methods demonstrated the potential to distinguish breast cancer cell line, the discrimination could have been improved by employment of supervised clustering that uses only a discriminatory set of variables (proteins) to cluster the samples.

REFERENCES

1. A. Bombonati, D. C. Sgroi, The molecular pathology of breast cancer progression. *J. Pathol.,* **2011,** 223, 307-317.

2. A. Journet, M. Ferro, The potentials of MS-based subproteomic approaches in medical science: the case of lysosomes and breast cancer. *Mass Spectrom. Rev.,* **2004,** 23, 393-442.

3. R. R. Drake, L. H. Cazares, E. E. Jones, T. W. Fuller, O. J. Semmes, C. Laronga, Challenges to Developing Proteomic-Based Breast Cancer Diagnostics. *OMICS: J. Integrative Biol.,* **2011,** 15, 251-259.

4. M. Lacroix, G. Leclercq, Relevance of Breast Cancer Cell Lines as Models for Breast Tumours: An Update. *Breast Cancer Res. Treat.,* **2004,** 83, 249-289.

5. J. Mladkova, M. Sanda, E. Matouskova, I. Selicharova, Phenotyping breast cancer cell lines EM-G3, HCC1937, MCF7 and MDA-MB-231 using 2-D electrophoresis and affinity chromatography for glutathione-binding proteins. *BMC Cancer,* **2010,** 10, 449.

6. R. M. Neve, K. Chin, J. Fridlyand, J. Yeh, F. L. Baehner, T. Fevr, *et al.,* A collection of breast cancer cell lines for the study of functionally distinct cancer subtypes. *Cancer Cell,* **2006,** 10, 515-527.

7. C. Laronga, R. R. Drake, Proteomic approach to breast cancer. *Cancer Control,* **2007,** 14, 360-368.

8. M. Karas, F. Hillenkamp, Laser desorption ionization of proteins with molecular masses exceeding 10,000 daltons. *Anal. Chem.,* **1988,** 60, 2299-2301.

9. J. H. van Adrichem, K. O. Bornsen, H. Conzelmann, M. A. Gass, H. Eppenberger, G. M. Kresbach, *et al.,* Investigation of protein patterns in mammalian cells and culture supernatants by matrix-assisted laser desorption/ionization mass spectrometry. *Anal. Chem.,* **1998,** 70, 923-930.

10. K. Tanaka, H. Waki, Y. Ido, S. Akita, Y. Yoshida, T. Yoshida, Protein and Polymer Analyses up to m/z 100000 by Laser Ionization Time-of-flight Mass Spectrometry. *Rapid Commun. Mass Spectrom.,* **1988,** 2, 151-153.

11. C. Fenselau, P. A. Demirev, Characterization of intact microorganisms by MALDI mass spectrometry. *Mass Spectrom. Rev.,* **2001,** 20, 157-171.

12. R. Kaufman, Matrix-assisted laser desorption ionization (MALDI) mass spectrometry: a novel analytical tool in molecular biology and biotechnology. *J. Biotechnol.,* **1995,** 41, 155-175.

13. B. L. Adam, Y. Qu, J. W. Davis, M. D. Ward, M. A. Clements, L. H. Cazares, *et al.*, Serum protein fingerprinting coupled with a pattern-matching algorithm distinguishes prostate cancer from benign prostate hyperplasia and healthy men. *Cancer Res.*, **2002,** 62, 3609-3614.

14. E. T. Fung, V. Thulasiraman, S. R. Weinberger, E. A. Dalmasso, Protein Biochips for Differential Profiling. *Curr. Opin. Biotechnol.*, **2001,** 12, 65-69.

15. J. M. Hettick, M. L. Kashon, J. E. Slaven, Y. Ma, J. P. Simpson, P. D. Siegel, *et al.*, Discrimination of intact mycobacteria at the strain level: a combined MALDI-TOF MS and biostatistical analysis. *Proteomics,* **2006,** 6, 6416-6425.

16. J. O. Lay, Jr., MALDI-TOF mass spectrometry of bacteria. *Mass Spectrom. Rev.*, **2001,** 20, 172-194.

17. T. L. Williams, D. Andrzejewski, J. O. Lay, S. M. Musser, Experimental factors affecting the quality and reproducibility of MALDI TOF mass spectra obtained from whole bacteria cells. *J. Am. Soc. Mass Spectrom.*, **2003,** 14, 342-351.

18. S. L. Cohen, B. T. Chait, Influence of matrix solution conditions on the MALDI-MS analysis of peptides and proteins. *Anal. Chem.,* **1996,** 68, 31-37.

19. K. O. Bornsen, M. A. Gass, G. J. Bruin, J. H. von Adrichem, M. C. Biro, G. M. Kresbach, *et al.*, Influence of solvents and detergents on matrix-assisted laser desorption/ionization mass spectrometry measurements of proteins and oligonucleotides. *Rapid Commun. Mass Spectrom.,* **1997,** 11, 603-609.

20. L. F. Marvin-Guy, P. Duncan, S. Wagniere, N. Antille, N. Porta, M. Affolter, *et al.*, Rapid identification of differentiation markers from whole epithelial cells by matrix-assisted laser desorption/ionisation time-of-flight mass spectrometry and statistical analysis. *Rapid Commun. Mass Spectrom.,* **2008,** 22, 1099-1108.

21. R. Knochenmuss, F. Dubois, M. J. Dale, R. Zenobi, The matrix suppression effect and ionization mechanisms in matrix-assisted laser desorption/ionization. *Rapid Commun. Mass Spectrom.,* **1996,** 10, 871-877.

22. J. Rappsilber, M. Moniatte, M. L. Nielsen, A. V. Podtelejnikov, M. Mann, Experiences and perspectives of MALDI MS and MS/MS in proteomic research. *Int J Mass Spectrom,* **2003,** 226, 223-237.

23. T. C. Cain, D. M. Lubman, W. J. Weber, Differentiation of Bacteria Using Protein Profiles from Matrix-Assisted Laser-Desorption Ionization Time-of-Flight Mass-Spectrometry. *Rapid Commun. Mass Spectrom.,* **1994,** 8, 1026-1030.

24. S. Vaidyanathan, C. L. Winder, S. C. Wade, D. B. Kell, R. Goodacre, Sample preparation in matrix-assisted laser desorption/ionization mass spectrometry of whole bacterial cells and the detection of high mass (>20 kDa) proteins. *Rapid Commun. Mass Spectrom.,* **2002,** 16, 1276-1286.

25. A. J. Madonna, F. Basile, I. Ferrer, M. A. Meetani, J. C. Rees, K. J. Voorhees, On-probe sample pretreatment for detection of proteins above 15 KDa from whole cell bacteria by matrix-assisted laser desorption/ionization time-of-flight mass spectrometry. *Rapid Commun. Mass Spectrom.,* **2000,** 14, 2220-2229.

26. E. E. Balashova, D. I. Maxim, P. G. Lokhov, Proteomics Footprinting of Drug-Treated Cancer Cells as a Measure of Cellular Vaccine Efficacy for the Prevention of Cancer Recurrence. *Mol. Cell. Proteomics*, **2012**, (10.1074/mcp.M111.014480).

27. H. Dong, W. Shen, M. T. Cheung, Y. Liang, H. Y. Cheung, G. Allmaier, *et al.*, Rapid detection of apoptosis in mammalian cells by using intact cell MALDI mass spectrometry. *Analyst,* **2011,** 136, 5181-5189.

28. H. T. Feng, L. C. Sim, C. Wan, N. S. Wong, Y. Yang, Rapid characterization of protein productivity and production stability of CHO cells by matrix-assisted laser desorption/ionization time-of-flight mass spectrometry. *Rapid Commun. Mass Spectrom.,* **2011,** 25, 1407-1412.

29. P. Lokhov, E. Balashova, M. Dashtiev, Cell proteomic footprint. *Rapid Commun. Mass Spectrom.,* **2009,** 23, 680-682.

30. X. Zhang, M. Scalf, T. W. Berggren, M. S. Westphall, L. M. Smith, Identification of mammalian cell lines using MALDI-TOF and LC-ESI-MS/MS mass spectrometry. *J. Am. Soc. Mass Spectrom.,* **2006,** 17, 490-499.

31. T. Wenzel, K. Sparbier, T. Mieruch, M. Kostrzewa, 2,5-Dihydroxyacetophenone: a matrix for highly sensitive matrix-assisted laser desorption/ionization time-of-flight mass spectrometric analysis of proteins using manual and automated preparation techniques. *Rapid Commun. Mass Spectrom.,* **2006,** 20, 785-789.

32. S. L. Morgan, E. G. Bartick, Discrimination of Forensic Analytical Chemical Data Using Multivariate Statistics. In *Forensic Analysis on the Cutting Edge: New Methods for Trace Evidence Analysis*, Blackwell, R. D., Ed. John Wiley & Sonds: New York, 2007, pp 331-372.

33. G. Caprioli, G. Cristalli, E. Ragazzi, L. Molin, M. Ricciutelli, G. Sagratini, *et al.*, A preliminary matrix-assisted laser desorption/ionization time-of-flight approach for the characterization of Italian lentil varieties. *Rapid Commun. Mass Spectrom.,* **2010,** 24, 2843-2848.

34. A. C. Tas, J. Vandergreef, Mass-Spectrometric Profiling and Pattern-Recognition. *Mass Spectrom. Rev.,* **1994,** 13, 155-181.

35. C. Shui, A. M. Scutt, Mouse embryo-derived NIH3T3 fibroblasts adopt an osteoblast-like phenotype when treated with 1alpha,25-dihydroxyvitamin D(3) and dexamethasone in vitro. *J. Cell. Physiol.,* **2002,** 193, 164-172.

36. C. F. Franco, M. C. Mellado, P. M. Alves, A. V. Coelho, Monitoring virus-like particle and viral protein production by intact cell MALDI-TOF mass spectrometry. *Talanta,* **2010,** 80, 1561-1568.

37. O. Sedo, I. Sedlacek, Z. Zdrahal, Sample preparation methods for MALDI-MS profiling of bacteria. *Mass Spectrom. Rev.,* **2011,** 30, 417-434.

38. F. Hillenkamp, M. Karas, R. C. Beavis, B. T. Chait, Matrix-Assisted Laser Desorption/Ionization Time-of-Flight Mass Spectrometry of Biopolymers. *Anal. Chem.,* **1991,** 63, 1193-1203.

39. M. W. Duncan, H. Roder, S. W. Hunsucker, Quantitative matrix-assisted laser desorption/ionization mass spectrometry. *Brief Funct Genomic Proteomic,* **2008,** 7, 355-370.

40. Z. Wang, L. Russon, L. Li, D. C. Roser, S. R. Long, Investigation of Spectral Reproducibility in Direct Analysis of Bacteria Proteins by Matrix-assisted Laser Desorption/Ionization Time-of-Flight Mass Spectrometry. *Rapid Commun. Mass Spectrom.,* **1998,** 12, 456-464.

41. R. J. Arnold, J. P. Reilly, Fingerprint matching of E. coli strains with matrix-assisted laser desorption/ionization time-of-flight mass spectrometry of whole cells using a modified correlation approach. *Rapid Commun. Mass Spectrom.,* **1998,** 12, 630-636.

42. Q. Liu, A. H. Sung, M. Qiao, Z. Chen, J. Y. Yang, M. Q. Yang, *et al.*, Comparison of feature selection and classification for MALDI-MS data. *BMC Genomics,* **2009,** 10 Suppl 1, S3.

43. J. Qian, J. E. Cutler, R. B. Cole, Y. Cai, MALDI-TOF mass signatures for differentiation of yeast species, strain grouping and monitoring of morphogenesis markers. *Anal. Bioanal. Chem.,* **2008,** 392, 439-449.

44. F. Bertucci, D. Birnbaum, A. Goncalves, Proteomics of breast cancer - Principles and potential clinical applications. *Mol. Cell. Proteomics,* **2006,** 5, 1772-1786.

45. C. M. Perou, T. Sorlie, M. B. Eisen, M. van de Rijn, S. S. Jeffrey, C. A. Rees, *et al.*, Molecular portraits of human breast tumours. *Nature,* **2000,** 406, 747-752.

46. P. T. Simpson, J. S. Reis-Filho, T. Gale, S. R. Lakhani, Molecular evolution of breast cancer. *J. Pathol.,* **2005,** 205, 248-254.

47. T. Sorlie, C. M. Perou, R. Tibshirani, T. Aas, S. Geisler, H. Johnsen, *et al.*, Gene expression patterns of breast carcinomas distinguish tumor subclasses with clinical implications. *Proc. Natl. Acad. Sci. U. S. A.,* **2001,** 98, 10869-10874.

48. C. Sotiriou, S. Y. Neo, L. M. McShane, E. L. Korn, P. M. Long, A. Jazaeri, *et al.*, Breast cancer classification and prognosis based on gene expression profiles from a population-based study. *Proc. Natl. Acad. Sci. U. S. A.,* **2003,** 100, 10393-10398.

49. L. A. Liotta, E. F. Petricoin, Beyond the genome to tissue proteomics. *Breast Cancer Res.,* **2000,** 2, 13-14.

50. J. Kao, K. Salari, M. Bocanegra, Y. L. Choi, L. Girard, J. Gandhi, *et al.*, Molecular profiling of breast cancer cell lines defines relevant tumor models and provides a resource for cancer gene discovery. *PLoS One*, **2009,** 4, e6146.

51. E. Charafe-Jauffret, C. Ginestier, F. Iovino, J. Wicinski, N. Cervera, P. Finetti, *et al.*, Breast cancer cell lines contain functional cancer stem cells with metastatic capacity and a distinct molecular signature. *Cancer Res.*, **2009,** 69, 1302-1313.

52. A. Goncalves, E. Charafe-Jauffret, F. Bertucci, S. Audebert, Y. Toiron, B. Esterni, *et al.*, Protein profiling of human breast tumor cells identifies novel biomarkers associated with molecular subtypes. *Mol. Cell. Proteomics*, **2008,** 7, 1420-1433.

53. H. D. Soule, T. M. Maloney, S. R. Wolman, W. D. Peterson, Jr., R. Brenz, C. M. McGrath, *et al.*, Isolation and characterization of a spontaneously immortalized human breast epithelial cell line, MCF-10. *Cancer Res.*, **1990,** 50, 6075-6086.

54. K. Subik, J. F. Lee, L. Baxter, T. Strzepek, D. Costello, P. Crowley, *et al.*, The Expression Patterns of ER, PR, HER2, CK5/6, EGFR, Ki-67 and AR by Immunohistochemical Analysis in Breast Cancer Cell Lines. *Breast Cancer (Auckl.)*, **2010,** 4, 35-41.

55. M. Hilario, A. Kalousis, C. Pellegrini, M. Muller, Processing and classification of protein mass spectra. *Mass Spectrom. Rev.*, **2006,** 25, 409-449.

CHAPTER 3

AFFINITY ENRICHMENT AND LC-MS/MS ANALYSES OF O-LINKED-N-ACETYLGLUCOSAMINE PROTEOME

3.1 ABSTRACT

Investigation of O-GlcNAc epithelial-mesenchymal transition (EMT) proteomics is critical in understanding how aberrant O-GlcNAc PTM promotes cancer invasion and metastasis, as well as in the identification of early stage therapeutic targets. Until now the role of O-GlcNAc PTM in TGF-β-induced EMT is unknown. To explore the O-GlcNAc EMT proteome, we developed a cleavable azide-reactive dibenzocyclooctyne-disulphide agarose-based beaded resin by coupling DBCO-SS-NHS ester to two commercial available NH_2-terminated resins. Prior to utilization of these affinity probes, robust bead washing was established to minimize the non-specific protein binding to affinity resins. Protein extracts from GalNAz-fed, metabolically labeled cells were conjugated onto the affinity resin via SPAAC for 18 h at 37 ºC. Using NIH3T3, a cell line that has been previously GalNAz labeled, the affinity-enriched proteins were detected by SDS-PAGE and in-gel fluorescence scanning. The GalNAz labeling and affinity purification were repeated on NMuMG cells undergoing EMT. The five samples tested were as follows: 1) DBCO-beads+GalNAz+TGF-β; 2) beads+GalNAz+TGF-β; 3) DBCO-beads+GalNAz-TGF-β; 4) beads+GalNAz-TGF-β; and 5) DBCO-beads-GalNAz-TGF-β, where samples 2, 4 and 5 were negative affinity controls, and 1 and 2 were TGF-β induced. Following

affinity enrichment and bead washing the non-O-GlcNAc peptides were obtained by tryptic digestion and analyzed by LC-MS/MS with CID fragmentation. Using the intact and fragmented peptide ion profiles, label-free quantification and identification were performed with MaxQuant and Andromeda search engine. Based on the MaxQuant-generated LFQ intensities, biochemical enrichment factor of each protein was calculated and employed in filtering nonspecific binding proteins. Out of 196 proteins identified, 125 constituted the affinity enriched proteins. 75% of these have been identified among O-GlcNAc affinity enrichment samples in other studies. Bioinformatics gene ontology analyses were performed using Ingenuity Pathway Analysis to determine cellular localization, functions and processes represented by the data. *In silico* protein-protein interactions revealed a regulatory network for metastasis, and cell cycle and proliferation, among the highly represented cellular processes. *In silico* canonical pathways analysis revealed glycolysis among the highly represented metabolic pathways and several signaling pathways that cooperate with TGF-β/SMAD signaling in accomplishing EMT. A metastatic regulatory network that features core regulators β-Catenin and cyclin-D1 both of which are regulated by OGT has led us to hypothesize that TGF-β signaling cooperates with O-GlcNAc signaling in promoting EMT, invasion and metastasis, pending validation and O-GlcNAc site-mapping.

3.2 INTRODUCTION

Cancer metastasis is the major cause of high breast cancer mortality[1-2]. Therefore understanding of molecular mechanisms leading to cancer cell invasion and metastasis is very essential. Epithelial-Mesenchymal Transition (EMT), a process by which cells lose their epithelial features and acquire mesenchymal and migratory behavior, is known to

initiate invasion leading to metastasis[3]. In addition, EMT supports cancer phenotypes by promoting angiogenesis, immune response escape, and stem cell properties[4]. Targeting molecular events of EMT has been perceived to be helpful in mitigating propagation of malignancies. Research on proteomic studies of EMT is aimed at identifying molecular signatures that allow detection of the transition from normal mammary epithelial cells to malignant invasive cells[5]. Such signatures are critical in the development of diagnostic, therapeutic and preventative strategies against breast cancers[5-6]. While proteomic investigations provide platform for protein-level probing of gene expression as compared to DNA-, and RNA-based studies, it is envisaged that study on functional proteomics involving PTMs can generate newer and more useful insights on complex diseases than other molecular profiling approaches have so far elucidated[7-8].

Recently O-GlcNAc PTM has been considered as a link between abnormal glucose metabolism and metastasis[9]. However, its role in TGF-β-induced EMT is not fully understood. In cancer cells, alteration in glucose metabolism leads to aberrant glycosylation and plays a role in disease progression[10]. Due to "Warburg effect" elevation of glucose uptake resulting from de-regulation of glucose metabolism upregulates glucose flux through HBP leading to increase in UDP-GlcNAc[11], the nucleotide-sugar substrate for enzymatic tagging of target proteins with O-GlcNAc. Increase in UPD-GlcNAc stimulates the expression and activity of the tagging enzyme, uridine diphospho-N-acetylglucosamine: polypeptide beta-N-acetylglucosaminyltransferase (O-GlcNAc Transferase [OGT]) which will then glycosylate target nucleocytoplasmic proteins to modulate activity, localization, stability and interactions of O-GlcNAc-regulated proteins, mainly transcription regulators[10, 12-14].

Upregulation of O-GlcNAcylation in this manner modulates the expression of target proteins to favor cancer growth and metastasis[9].

The role of O-GlcNAcylation on protein function as well as on cancer progression has been reported. Reference to O-GlcNAcylation of Snail1, at protein level, OGT overexpression resulting from hyperglycaemia, increased the amount of Snail1 protein and enhanced the O-GlcNAc modification without changing the Snail mRNA levels[10]. Together with Snail1, several other cellular proteins were also O-GlcNAcylated as many bands were resolved on SDS-PAGE of lectin-based sWGA-affinity purified total cell lysates. OGT overexpression stabilized O-GlcNAcylated Snail1 through inhibition of phosphorylation-mediated ubiquitination resulting in Snail1 transcriptional repression of E-cadherin. In a different study on O-GlcNAcylation in breast tumors, at cellular and tissue level, OGT overexpression was associated with elevated global O-GlcNAcylation, E-cadherin downregulation, and invasion and metastasis both in vitro and in vivo, as shown by immunohistochemical analyses[9]. Based on these observations, it is likely that the elevated OGT expression and O-GlcNAcylation cooperate with the known signaling cascades in promoting invasion and metastasis.

In TGF-β-induced EMT, the mediators of the TGF-β induced signal, namely, the Smad proteins are weak in binding DNA[1, 15]. They only bind strongly to the promoters of target genes upon interacting with the transcription regulators, some of which are O-GlcNAc regulated. By interacting with the Smads to form EMT-promoting Smad complexes, these O-GlcNAc-regulated transcription cofactors facilitate recognition and binding to target promoter elements, ensure nuclear retention and prevent degradation of the Smads[16]. Many studies have shown that transcription cofactors of the Smads

including Hmga-2, c-Myc, Snail1, and Foxm1, among others, are upregulated in cancers synergistically with O-GlcNAcylation and they may be O-GlcNAcylated[14, 16-18]. However, only the O-GlcNAc modifications of Snail1 and c-Myc have been characterized in relation to phosphorylation, and the interplay between these two modifications in controlling breast cancer progression has been recognized[10, 19]. The oncogenic protein Foxm1 is upregulated in high O-GlcNAc levels but its O-GlcNAc site has not been established[14, 20]. The impact of O-GlcNAc, if any, at specific sites on these transcription regulators and other key proteins in the context of TGF-β-induced EMT is still unknown. Since a combination of affinity enrichment and mass spectrometry is widely acceptable as a suitable approach for identification of O-GlcNAc-modified proteins and mapping the site of modification to understand the role of O-GlcNAc modification in protein function[11], it was hereby applied in investigating the O-GlcNAc-modified proteins from cells undergoing EMT.

In previous studies proteomic characterization of cells undergoing EMT has revealed protein expression changes reflecting cellular reprogramming regardless of the source of the EMT-inducing signal. Biarc and coworkers have performed targeted proteomics of mutant K-Ras^{v12}-, and TGF-β-induced MCF-10A cells[8]. Proteomic profiles from both treatments reflected EMT features including upregulation of cytoskeletal proteins, translation and degradation machineries, as well as metabolic enzymes, and down-regulation of cell-cell adhesion proteins. Their study, however, did not demonstrate the role of PTMs such as, in providing the link between metabolic changes and EMT, specifically in revealing which proteins during EMT might be modulated by abnormal metabolic regulation elicited by TGF-β. Examination of the O-GlcNAc proteome in

discovery LC-MS/MS has a potential to reveal a wealth of information pertaining to new candidate disease biomarkers, as well as insights on regulation of protein function by O-GlcNAc PTM in the context of EMT and metastasis.

To explore the O-GlcNAc molecular signatures in TGF-β-induced EMT, we developed a cleavable "click"-chemistry-based affinity enrichment probe, azide-reactive DBCO-SS-resin. Of all the O-GlcNAc enrichment strategies including immunoaffinity-based[21], WGA lectin-based[22-23], chemoenzymatic biotin/avidin-based[24-25], azide-reactive cyclooctyne resin (ARCO)-based[26], and resin-alkyne-based[27], our affinity probe is ARCO-resin-based. However, unlike the ARCO-resin that was suited for O-GlcNAc-modified peptides, our probe is aimed at enrichment of intact proteins following the strategy employed for the commercial resin-alkyne (Click-iT® Protein Enrichment kit, Invitrogen)[27]. In that strategy, the GlcNAz modified intact cellular proteins were captured via CuAAC onto the resin-alkyne, thus as an alternative, we propose a SPAAC-based strategy in which the GlcNAz modified proteins are enriched by capture onto DBCO-SS-resin probe and released from the resin by reductive cleavage[28]. Previous studies have shown that the ARCO-resin that selectively enriches proteins by SPAAC is more suited to peptides since it avoids the toxic effect of Cu (I)[26]. Extension of the SPAAC-based bead conjugation to intact proteins allows expansion of the utility of such probes. Temming *et al*. briefly characterized a "capture and release" bicyclononyne-resin possessing a hydrazine-cleavable levulinoyl linker[29]. Our cleavable DBCO-SS-resin probe is hereby characterized and applied in EMT O-GlcNAc proteomics.

In this chapter affinity enrichment of O-GlcNAc proteins from NMuMG cell line using the approach of metabolic labeling of cellular O-GlcNAc PTM with azido-sugar

and ligation of azido-sugar labeled proteins to resin-strained-alkyne by SPAAC is described. The overall analytical workflow involves metabolic labeling, affinity O-GlcNAc protein enrichment and shotgun proteomics (Figure 3.1). Prior to enrichment, metabolic labeling of O-GlcNAc proteins with azido-GalNAc was confirmed by chemo-selective staining with alkyne-conjugated fluorescein dyes and imaging by fluorescence microscopy. The stability of the O-GlcNAz PTM in cell lysates was confirmed by a similar dye-labeling strategy, and the proteins were resolved using 1D SDS-PAGE and visualized by in-gel fluorescence scanning. The resin strained-cleavable-alkyne-conjugated probe was prepared following the reaction scheme on Figure 3.2, by coupling dibenzo-cyclooctyne-disulphide-N-hydroxysuccinimide ester to epoxy-activated amine-terminated sepharose or ω-aminohexyl agarose. The efficiency of coupling was evaluated by UV-Vis spectrophotometry while the reactivity, not the reaction kinetics, of the modified bead probe was tested by MALDI-TOF MS analysis of the reduced and cleaved glycoconjugate products. To detect O-GlcNAc proteins during TGF-β1-induced EMT, azido-GlcNAc-tagged proteins in pre-fractionated protein extracts from induced and non-induced cells were enriched via SPAAC onto the alkyne-modified bead probe. The selectivity of the enrichment strategy was assessed through evaluation of the bead washing protocol to ensure that non-specific binding is minimized. The selectivity is further demonstrated by biochemical enrichment factors of the identified proteins. The specificity of the enrichment strategy was assessed in two ways; 1) by detection of affinity enriched proteins from metabolically labeled NIH3T3 cells, and 2) by LC-MS/MS quantification and identification of enriched O-GlcNAz-proteins from on-resin tryptic digests of metabolically labeled NMuMG cells undergoing EMT. These peptides

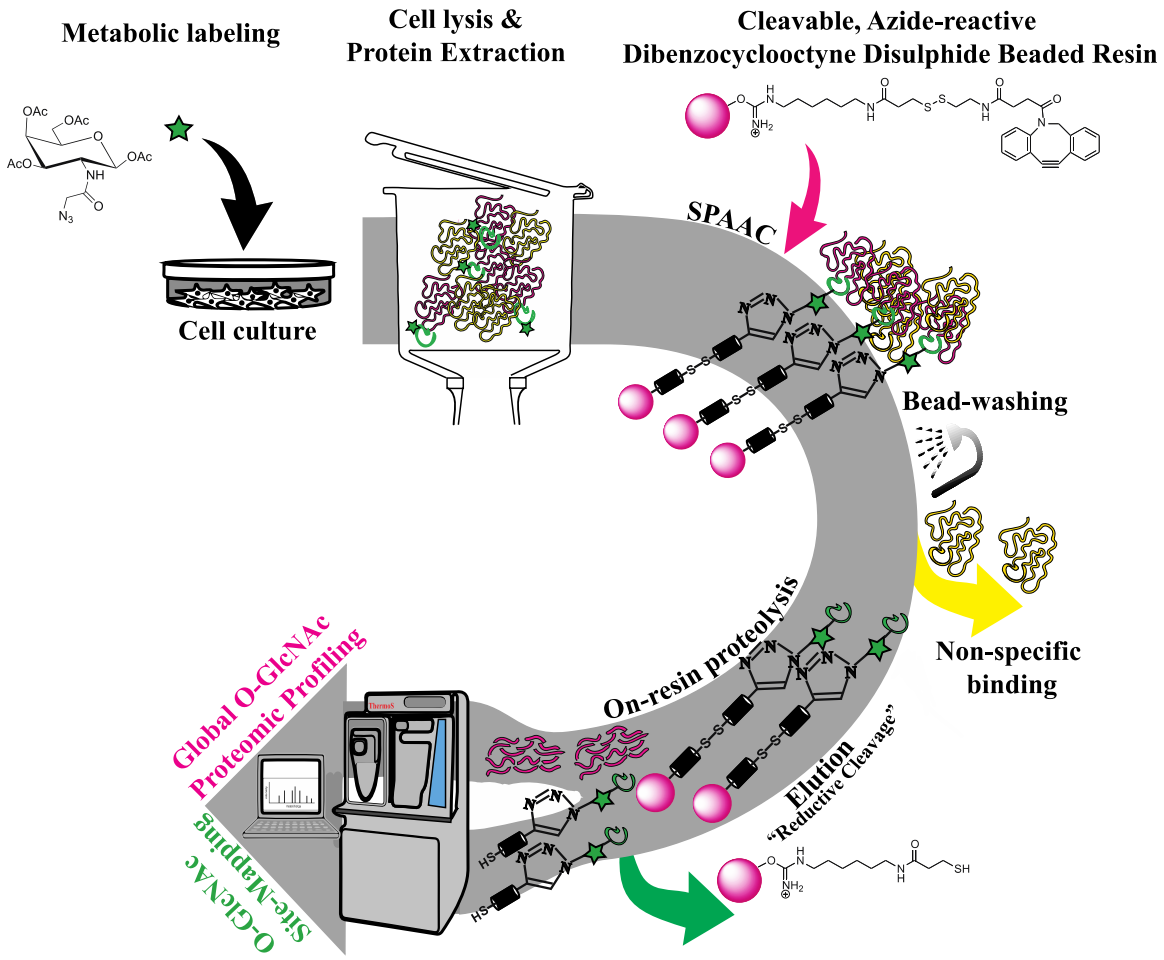

Figure 3.1 Schematic representation of the combined Cu-free Click chemistry-based O-GlcNAc affinity enrichment and shotgun proteomics approach for O-GlcNAc LC-MS/MS glycoproteomic profiling.

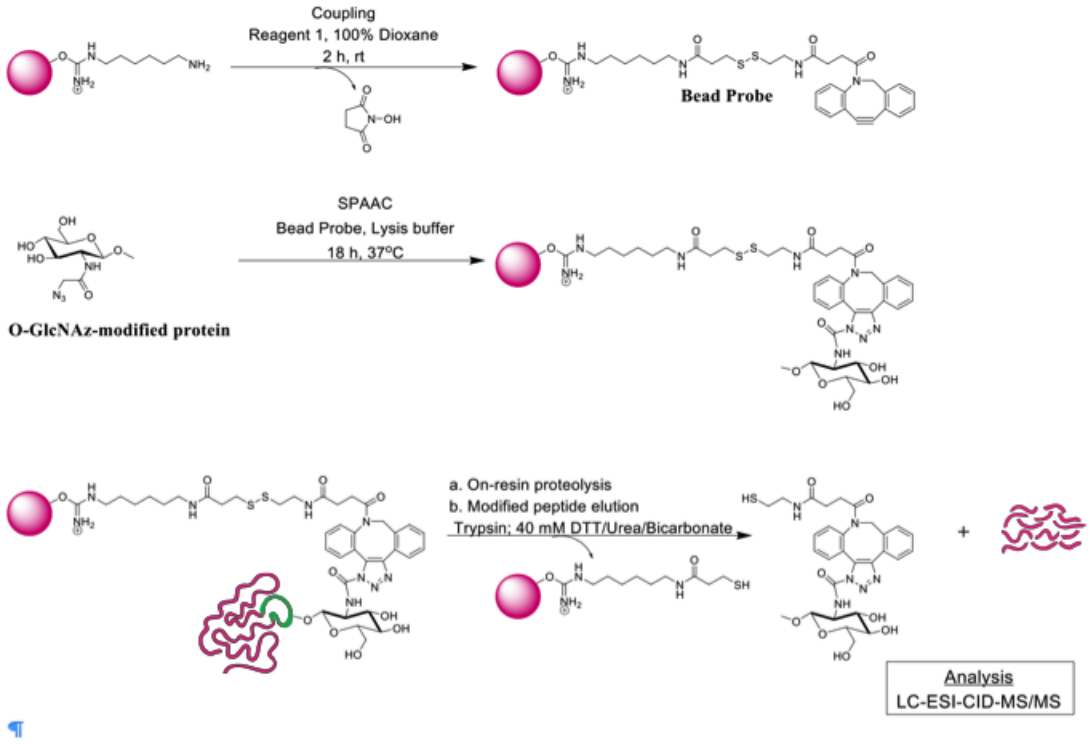

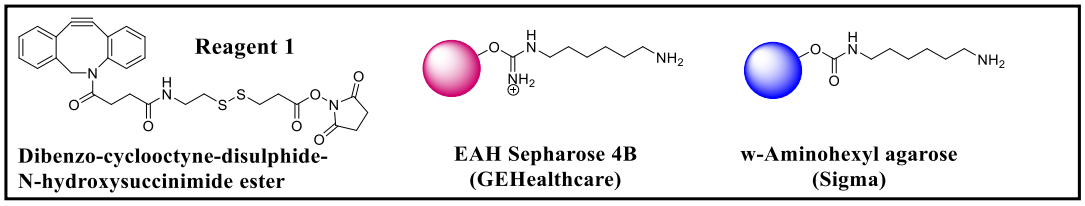

Figure 3.2 Reaction scheme for the O-GlcNAc glycoproteomic profiling showing the preparation of the "click-able" and cleavable bead probe and its application in affinity enrichment of O-GlcNAc PTM. Two different raw bead resins, namely; EAH sepharose 4B and ω-aminohexyl agarose were used.

were not directly attached to the beads and were analyzed as the first fraction. The second fraction consisted of the O-GlcNAz-modified peptides that were directly linked to the beads by the triazolyl linkage and these were eluted via reduction of the disulphide linker using DTT and saved for O-GlcNAc site-mapping. Analysis of this fraction required a different kind of fragmentation method, electron transfer dissociation, and due to time not permitting, the O-GlcNAc site-mapping was not accomplished in this study. However, data from O-GlcNAc proteomic profiling based on the tryptic digests alone revealed EMT and O-GlcNAc characterization that underscores findings from many previous studies.

3.3 EXPERIMENTAL SECTION

3.3.1 Materials

ω-Aminohexyl agarose and dibenzocyclooctyne-disulphide-N-hydroxysuccinimide ester were purchased from Sigma and EAH Sepharose 4B came from GE Healthcare. FITC-alkyne, DBCO-naphthalimide, peracetylated N-azidoacetylgalactosamine, peracetylated N-acetylgalactosamine and 3-azido-7-hydroxycoumarin were synthesized in-house. Click-iT L- homopropargylglycine, was purchased from Gibco Invitrogen. NMuMG and NIH3T3 were purchased from ATCC (Manassas, VA). DBCO-Fluorescein was purchased from Click Chemistry Tools (Scottsdale, AZ). Cell scraper was obtained from BioTang Inc. (Lexington, MA). Benzonase and sequencing trypsin were purchased from Promega (Madison, WI). Protease and phosphatase inhibitor and immunoblotting reagents were purchased from Thermo Fisher Scientific (Grand Island, NY). SDS-PAGE materials and RNA extraction kit were obtained from Biorad (Hercules, CA).

Transforming Growth Factor beta-1 was purchased from R&D Systems (McKinley, NE). Anti-Snail1 antibody was purchased from Cell Signaling (Danvers, MA). All other chemicals were purchased from Sigma (St. Louis, MO).

3.3.2 Coupling of DBCO-SS-NHS Linker to ω-Aminohexyl Agarose and EAH Sepharose 4B Resins

3.3.2.1 Synthesis of the Strained Alkyne-resin and Evaluation of the Efficiency of Coupling

Three 250 μL (1.75-3 μmol active amino groups) aliquots of bead slurry were placed in empty spin columns. Synthesis of the bead probe was done through coupling of DBCO-SS-NHS to commercial beads following the manufacturer's instructions, where available. Prior to coupling, the beads were prepared by washing 1× with acidified water (pH 4.7) and 1× with 0.5 M NaCl. Next, the beads were rinsed 2× with coupling buffer (50% dioxane in acidified water, pH 4.7). The wash flow-throughs were collected by centrifugation (200 × g, 30 s) to obtain drained bead matrix. 20 mM solution containing 4.18 μmol DBCO-SS-NHS was added to each of the three drained bead samples and coupling was allowed at room temperature for 24 h on an end-over-end rotator. After coupling the beads were washed 4 times with coupling buffer, 1× with acidified water and 1× with 0.5 M NaCl. The absorbance of the DBCO linker in the series of wash flow-throughs were determined by UV-Vis spectrophotometry at a wavelength of 302 nm. Thus, the amount of DBCO linker retained on the beads was estimated. To facilitate the estimation, a standard curve was prepared from ≤100-fold diluted aliquots of the starting

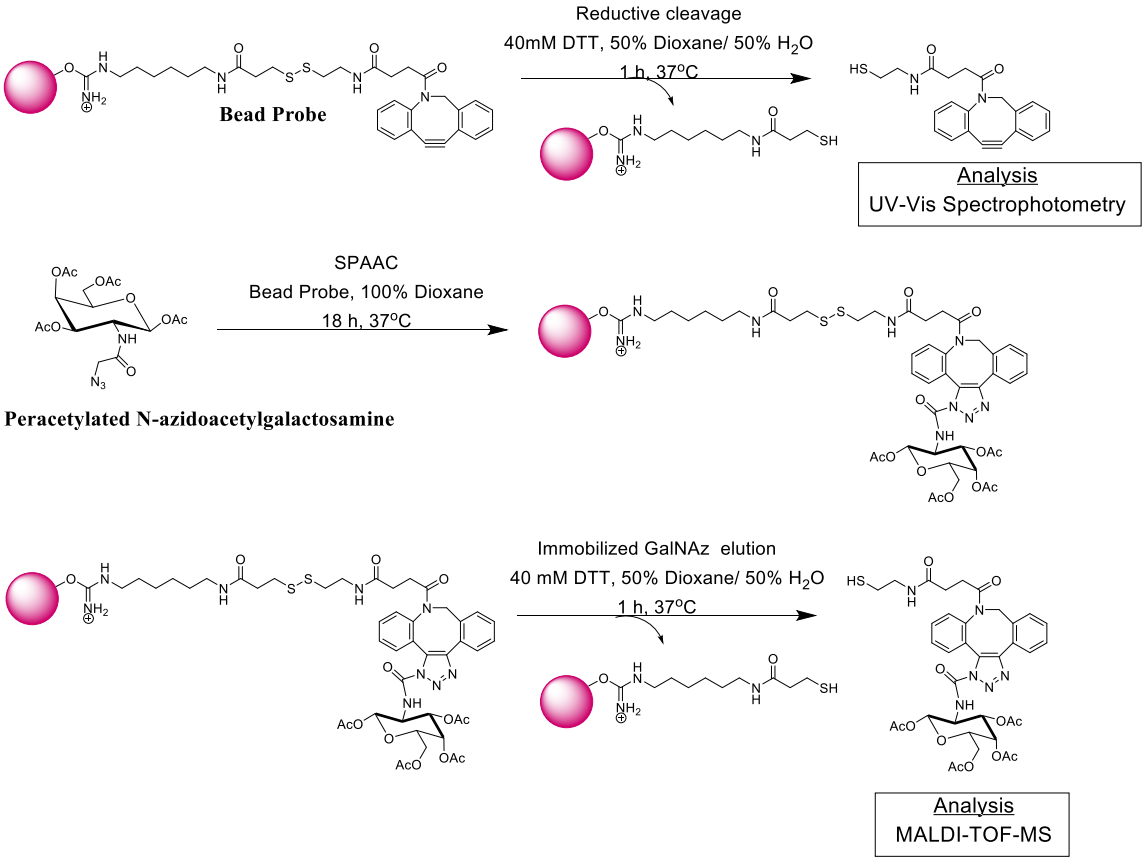

Figure 3.3 Reaction scheme for evaluation of the "click-able" and cleavable bead probe using UV-vis spectrophotometry and MALDI-TOF MS.

solution. The first four wash flow-through samples used were blanked with coupling buffer.

Initially coupling of DBCO-SS-NHS to ω-aminohexyl agarose was performed using different conditions, none of which were from the manufacturer as these were not available. Coupling was done with excess linker (equivalent to 2× μmol of active amino groups in beads) in 70% DMSO/30% PBS with incubation for 2 h on end-over-end rotator.3.3.2.2 Determination of Suitable Conditions for Cleavage of Bead-conjugated Product

The reductive cleavage elution buffer consisting of 20 mM DTT, 1 M Urea and 50 mM NH_4HCO_3 was adopted from Howden *et al*. who used it for elution of biotin-avidin enriched proteins[28]. The cleavage conditions were initially determined for the ω-aminohexyl agarose but used later with the EAH Sepharose. After coupling of DBCO-SS-NHS linker to resin beads, 20 μL aliquots of slurry of modified and unmodified beads were placed in 1.5 mL Eppendorf tubes. The beads were briefly centrifuged (200 × g, 30 s) and the supernatant was removed from the top of the slurry. The beads were rinsed with water, which was removed too. Next the modified and unmodified beads were incubated with DTT in different solutions: 1) 40 mM DTT in 60% DMSO containing 1 M Urea and 50 mM NH_4HCO_3; 2) 40 mM DTT in 0% DMSO containing 1 M Urea and 50 mM NH_4HCO_3; 3) 40 mM DTT in 60% DMSO only. The samples were kept in a shaker at 37ºC for 1 hr. After the first fraction of eluents was collected, fresh DTT solution was added and the beads were incubated again to get the second fraction. The cleaved DBCO conjugate was detected by UV-Vis spectrophotometry.

3.3.2.3 Testing Whether the Beaded Resin Probe is Azide-reactive

MALDI-TOF MS analysis of the eluted GalNAz conjugate was performed according to the procedure on MALDI analysis of starch hydrolysis by Grant *et al*[30]. After coupling of DBCO-SS-NHS linker to resin beads, 50 μL aliquots of slurry of modified and unmodified beads were placed in 1.5 mL eppendorf tubes. The beads were rinsed 2× with 50% dioxane (EAH Sepharose) or 50% DMSO (ω-aminohexyl agarose) and supernatant was removed by pipetting from the top of the slurry. Next, the beads were incubated with 10 mM AC_4GalNAz (50 μL) in 50% Dioxane or 50% DMSO for 24 h on a shaker at 37°C for SPAAC conjugation of AC_4GalNAz to alkyne on beads. The SPAAC conditions used here were based on the on-bead SPAAC kinetics reported in Temming *et al*[29]. After SPAAC the supernatant was removed and beads were washed 5× with the coupling buffer to get rid of unbound AC_4GalNAz. Subsequently the beads were incubated with 40 mM DTT in coupling buffer for 1 h at 37°C for reductive cleavage of the covalently bound AC_4GalNAz. The eluent (cleavage GalNAz conjugate = m/z 817.4) was analyzed by MALDI-TOF MS. A mixture of 2 μL eluent, 100 μM AC_4GalNAc and 10 mM NaCl in 50% dioxane or DMSO was made. An aliquot of this mixture was mixed 1:1 with DHB matrix solution, spotted on the MALDI target plate and air-dried, before analysis. External calibration was done using AC_4GalNAc ($[M+Na]^+$ = 411.547 Da). Spectra were acquired from 200 shots in positive linear mode in the m/z range 200-2000.

3.3.3 Cell Culture

NIH3T3 cells were cultured in high-glucose DMEM media (Hyclone, ThermoScientific) supplemented with 10% FCS (Hyclone, ThermoScientific). NMuMG cells were cultured

in low-glucose DMEM media containing 10% FBS and 10 μg/mL insulin. All cells were seeded at a density of 1 million cells in 10-cm culture plates and were maintained in a humidified incubator at 37°C and 5.0% CO_2.

3.3.4 Metabolic Labeling with AC_4GalNAz

After 24 h and at about 70% confluence, all media were replaced with low-glucose DMEM containing 200 μM AC_4GalNAz (200 mM stock in DMSO) of DMSO vehicle, and the labeling was done for 16 h. NMuMG cells were induced with 100 pM TGF-β1 or 1% BSA in 4 mM HCl vehicle and 200 μM AC_4GalNAz was added 8 h after induction with TGF-β1 so that the duration for induction was 24 h and that for AC_4GalNAz labeling was 16 h.

3.3.5 Metabolic Labeling and Pulse-Chase with HPG

Double and single metabolic labeling and pulse-chase with HPG were carried out according to the procedures in Duan *et al*.[31-32] Beatty *et al*.[33] and Liu *et al*.[34] Briefly two 12-well plates were seeded with 6×10^4 cells per well on sterile microscope cover slips immersed in high-glucose DMEM supplemented with 10% FBS, 1% penicillin/streptomycin, and 10 μg/mL insulin, and containing 100 μM AC_4GalNAz or DMSO vehicle. Cells were cultured for 48 h and in the last 6½ h cells were starved for 30 min, pulsed with HPG for 4 h and chased with L-Methionine for 2 h before fixing and staining.

3.3.6 Fluorescence Visualization of GalNAz-tagged Proteins in Fixed NIH3T3 and NMuMG Cells

Cells were seeded in 12-well plates on sterile microscope cover slips disinfected by immersion in 70% ethanol and UV irradiation for 20 min. After 16 h of AC_4GalNAz labeling, wells were washed 3 times with warm PBS, and then fixed with 4% paraformaldehyde in PBS for 10 min. Cells were permeabilized with 0.1% Triton X-100 in PBS for 30 min, rinsed with PBS and blocked with 0.1 M Glycine in PBS for 30 min. Dye-labeling was carried out with 10 μM DBCO-fluorescein or FITC-alkyne for 30 min. For double metabolic labeling, cells were stained with multiple stains, first, DBCO-fluorescein or FITC-alkyne for the GalNAz tag, then Azide-42 for HPG tag, and then DAPI or propidium iodide for nuclear DNA. After dye-labeling the wells were washed four times with a wash solution containing 1% Tween 20 and 0.5 mM EDTA in PBS, and once with ddH_2O.

3.3.7 Preparation of Cellular Protein Extract for Immunoblotting

Cellular protein extracts were prepared according to the procedure by Zaro *et al*. modified. Cells were resuspended in hypotonic buffer (10 mM HEPES, pH 8.0, 1.5 mM $MgCl_2$, 10 mM KCl, 1X protease and phosphatase inhibitor), and disrupted with a homogenizer. The samples were incubated on ice for 30 min for lysis to be completed. Crude nuclei were pelleted by centrifugation (500 × g, 5 min). To prepare cytoplasmic extracts, this nuclei- depleted supernatant was centrifuged at 20,000 × g to pellet insoluble (i.e. membrane and small organelle) material and the resulting supernatant was saved. To prepare nuclear extracts, the crude nuclear pellet was resuspended in sucrose

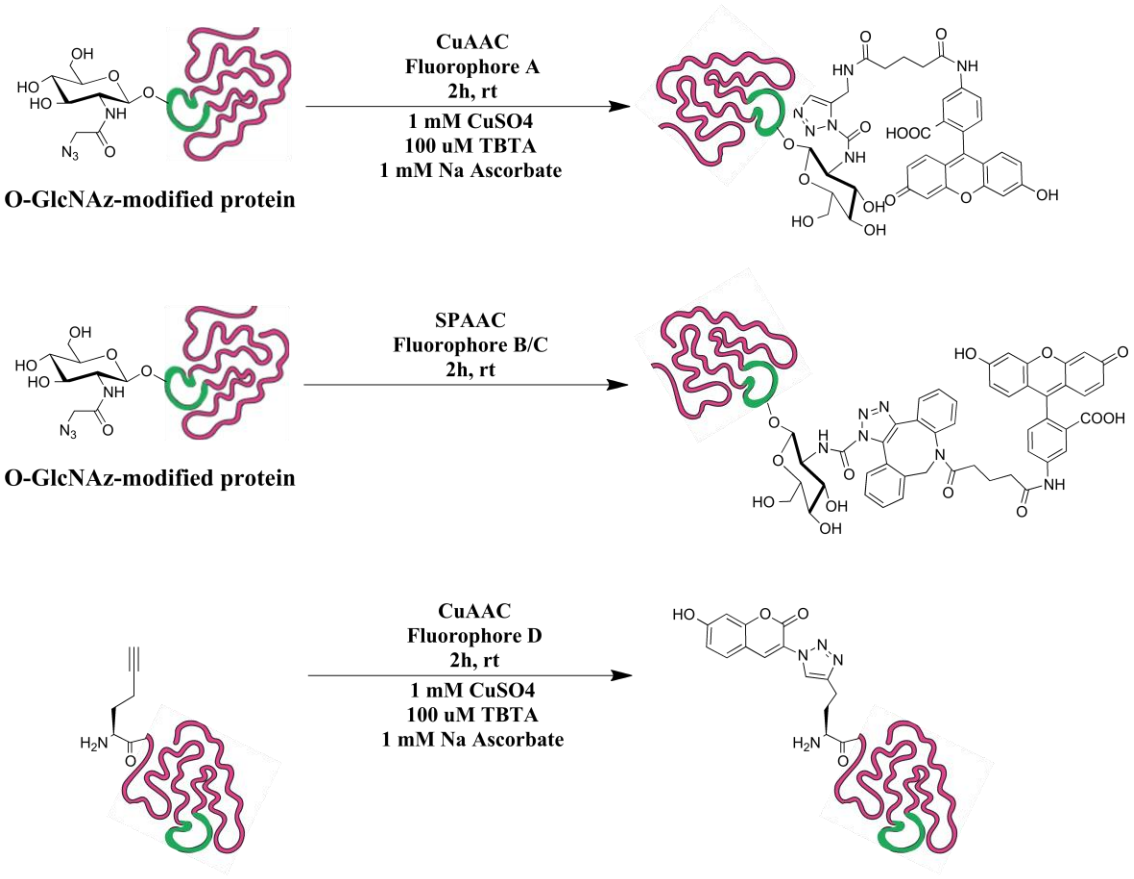

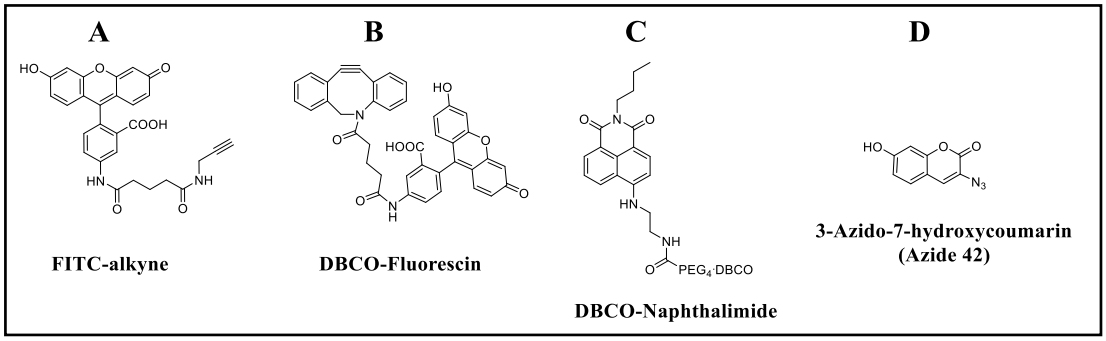

Figure 3.4 Reaction scheme for bio-orthogonal dye labeling of azido- and alkyne-modified proteins employing a given panel of fluorophores A-D.

buffer A (250 mM sucrose, 10 mM $MgCl_2$), layered over an equal volume of sucrose buffer B (880 mM sucrose, 0.5 mM $MgCl_2$) and pelleted by centrifugation (2,800 × g, 10 min). This highly purified nuclear pellet was resuspended in 1% Triton X-100, 300 mM NaCl, 20 mM Tris pH 7.4. All samples were sonicated and cleared by centrifugation (10,000 × g, 10 min).

3.3.8 Western Blotting

Alternatively, cells were lysed in RIPA buffer with protease and phosphatase inhibitors, and then prepared and immunoblotted according to the procedure by Lamouille *et al*. modified[35]. Protein concentration was determined using a modified Bradford protein assay (Pierce, ThermoScientific). 20 mg of protein was separated by SDS-PAGE and transferred to nitrocellulose membranes which were blocked with 5% dry milk TBST for 1 h before overnight incubation with primary antibody diluted in 3% BSA in TBST. HRP-conjugated secondary antibody (Jackson ImmunoResearch Laboratories) was applied and detected by ECL (Pierce, ThermoScientific) and BioMax film (Kodak).

3.3.9 RNA Extraction and Reverse-Transcription Quantitative Polymerase Chain Reaction (RT-qPCR)

RT-qPCR was performed following the procedure in Saha *et al*. Briefly total RNA was extracted from NMuMG cells induced with 0, 2 and 5 ng/μL TGF-β1 after 2 days of culture using RNeasy mini purification kit (Qiagen) and subsequently reverse-transcribed with qScript cDNA synthesis kit (Quanta Bioscience, inc.). RT-qPCR was carried out for 45 cycles of PCR (95 ºC for 15 s, 58 ºC for 15 s and 72 ºC for 30 s) with iQ5 SYBR Green Supermix (Biorad) using the Snai1 and Gapdh primers shown in Table 2. The

reaction mixture of 25 μL total volume included 200 nM of both forward and reverse primers (Integrated DNA Technologies, inc.) and the cDNA template at a final concentration of 0.25 ng/μL. Data analysis was performed using $2^{-\Delta\Delta C}$T method for relative quantification. The samples were normalized to Gapdh as the internal control. The reaction was repeated using another batch of NMuMG samples.

3.3.9 Preparation of Nonidet P-40 (NP-40)-Soluble Lysates for SDS-PAGE and In-gel Fluorescence Visualization

Preparation of NP-40-soluble lysates was done following the method of Zaro *et al*. modified[36]. Briefly, after 16 h or labeling cells harvested in ice-cold PBS using cell scraper after washing plates with ice-cold PBS. The cell suspension was centrifuged at 100 × g for 5 min at 4 ºC. The pellet was washed again in ice-cold PBS before re-suspension in about 100 μL 1% NP-40 lysis buffer containing 1 × protease and phosphatase inhibitor solution. Samples were incubated on ice for 30 min for cell lysis to be completed. Samples were then centrifuged at 10,000 × g for 10 min at 4 ºC. The pellet was discarded while supernatant was used for labeling of GalNAz-tagged proteins. Total protein in the supernatants of the GalNAz-labeled and control cell lysates was quantified by Bradford assay using BSA as standard.

3.3.10 In-gel Fluorescence Visualization of GalNAz-tagged Proteins from NIH3T3 Cell Lysates

A 200 μL reaction mixture containing 1 mg/mL cell lysate protein in the presence of 100 μM DBCO-fluorescein or DBCO-naphthalimide dye was set up. Alternatively the amount of cell lysate protein was mixed with click chemistry reagents; 100 μM FITC-

alkyne, 1 mM ascorbic acid, 1 mM TBTA and 1 mM $CuSO_4.5H_2O$. Dye-labeling reaction was carried out at 10 ºC for 10 h. An additional condition of room temperature 1 h was included to find out the suitable conditions for dye labeling with DBCO-naphthalimide. When labeling was completed, 1 mL of ice-cold methanol was added and the mixtures placed at -80 ºC for 2 h to precipitate the proteins. The cold mixtures were centrifuged at 10,000 × g for 10 min at 4 ºC. The supernatant was discarded and the pellet air-dried. The proteins were re-solubilized in 50 µL of 4% SDS buffer [4% SDS, 150 mM NaCl and 50 mM Tris, pH 7.4] in a bath sonicator. The samples were diluted accordingly and total protein quantified by Bradford assay, using BSA as standard. Samples were further diluted 2-fold by adding 50 µL of 4 × SDS-free loading buffer containing 1.4% β-mercaptoethanol. 30 µg protein of each sample was loaded onto gel for SDS-PAGE analysis. Prestained protein standards were used as weight markers while FITC-IgG was used as a positive for fluorescence.

3.3.11 Optimization of Washing Protocol of the Beads to Remove Non-specifically Bound Proteins

Different bead-washing conditions were tested to aid in establishing an optimized in-house bead-washing method. In each test about 200 µL bead slurry (ω-aminohexyl agarose, Sigma) was added to at least two empty spin columns (Pierce, Thermo Scientific). The beads were washed twice with PBS and once with the protein conjugation buffer. One tube was loaded with 2 mg of cell lysate protein and the other tube (control) was loaded with conjugation buffer without protein. Both tubes were incubated under SPAAC conditions and then washed according to the washing conditions

under test. The bead washing was evaluated by SDS-PAGE to check the protein content of the wash flow-throughs, the DTT-eluted fraction and the denatured beads. To a gel with 30 μL well capacity was loaded a mixture of 15 μL wash sample and 15 μL SDS loading buffer containing 5% β-mercaptoethanol. Prestained protein standards solution was loaded in weight markers' lane.

To two sets (A and B) of three empty spin columns each was added 400 μL bead slurry (EAH Sepharose, GE Healthcare). The bead bed was washed with acidified water, pH 4.7 and 0.5 M NaCl to prepare it for loading. The first tube of each set was loaded with 10 mg cell lysate protein, the second was loaded with 10 mg BSA while the third was loaded with same lysis buffer as was used for samples in the first and second tubes (0.01 × Urea buffer), but no protein. All tubes were incubated under SPAAC conditions (37 ºC for 24 h, on a shaker) to mimic coupling of GalNAz-tagged proteins to DBCO-modified beads. At the end of incubation, the SPAAC supernatant was removed and beads in set A tubes were washed according the manufacturer's protocol while beads in set B tubes were washed according to the in-house protocol. The bead-washing protocols were evaluated by measuring the amount of protein in DTT-eluted fraction (Bradford assay, with BSA as standard) and by SDS-PAGE profile of denatured beads. Before Bradford assay, the DTT eluents were dialyzed against 0.1M PBS, pH 7.4 overnight.

3.3.12 Preparation of Cellular Protein Extract and Affinity Enrichment of Cellular O-GlcNAc Proteins

For analysis of affinity-enriched proteins using SDS-PAGE, azido-GalNAc-labeled and control, NIH3T3 cells were harvested as indicated above. 5×10^6 cells per sample were

lysed in 1% SDS/PBS buffer containing 1× protease inhibitor and benzonase. 800 μL lysate was added to DBCO-SS-modified beads and incubated on a shaker under SPAAC conditions for the azido-labeled proteins to be conjugated to the beads. After SPAAC the beads were washed 3 times with alternate low and high pH SDS wash buffer, 5 times with urea/bicarbonate wash buffer, 5 times with 20% acetonitrile in H_2O. For each wash the beads were incubated 5 min on shaker at 37 °C. The washing procedure used here was applied before establishment for the in-house washing protocol. After washing, the conjugated proteins were eluted by incubation for 1 h at 37 °C in 40 mM DTT elution buffer. Elution was repeated to collect the 2nd fraction. A total of 200 μL of the eluents was reduced and concentrated in a SpeedVac to 20 μL.

For analysis of affinity-enriched protein using LC-MS/MS, Azido-GalNAc-labeled and control, TGF-β1-induced and non-induced cells (5-10 × 10^7) were harvested as indicated above. The cell extracts and protein samples were prepared according to procedures used in Hahne *et al*. and Boyce *et al*[27, 37]. The cell pellets were re-suspended in 500 μL hypotonic lysis buffer [10 mM HEPES, 1.5 mM $MgCl_2$, 10 mM KCl, 1× protease and phosphatase inhibitor and 20 μM PUGNAc] and cells were homogenized for 1 min using 3 out 5 power. The samples were incubated on ice for 30 min for lysis to be completed. Crude nuclei were pelleted by centrifugation (500 × g, 15 min, 4 °C). The supernatant was used for fractional enrichment of Cytosolic extracts while the pellet was further processed for isolation of nuclear extracts.

The 1-mL nuclei-depleted supernatant was transferred to 10-mL ultra-centrifuge tube and the volume was adjusted to about 9 mL using cold water. The samples were

centrifuged at 145,000 × g for 1 h at 4 ºC. The clarified supernatant was placed in a 4 mL chamber of a 15-mL MWCO (3K) centrifugal tube and centrifuged at 10,000 × g for 10 min at 4 ºC. The retentate was re-suspended in 8M Urea buffer [8 M Urea, 100 mM Tris, pH 8, 4% CHAPS, 1 M NaCl, 1 × protease and phosphatase inhibitor solution].

The pellet containing crude nuclei (obtained after homogenization) was re-suspended in sucrose buffer A [250 mM sucrose, 10 mM $MgCl_2$], layered onto sucrose buffer B [880 mM sucrose, 0.5 mM $MgCl_2$] and centrifuged at 2800 × g for 10 min at 4 ºC. The resultant pellet contained purified nuclei. The pellet was re-suspended in hypotonic lysis buffer supplemented with 0.1% SDS. The nuclei were lyses with a probe-tip sonicator for 30 sec at the lowest speed. The nuclear proteins were precipitated using chloroform/methanol method and the precipitate was re-solubilized in 8M Urea lysis buffer. The nuclear extracts were mixed with the cytosolic extract to create a sample from which O-GlcNAc proteins could be 'fished out'. The concentration of protein in this sample was determined by Bradford assay using BSA as standard.

Each of the five 1 mg protein samples was reduced using 10 mM DTT at 30 ºC for 1 h and alkylated using 50 mM iodoacetamide at 37 ºC for 1 h in the dark. The protein solutions were centrifuged in MWCO (3K) spin columns to remove DTT. The retentates were suspended in water and loaded to the respective bead samples. Samples were incubated on a shaker at 37 ºC for 24 h to allow conjugation of Azido-GlcNAc proteins to the beads by SPAAC. After SPAAC, the supernatant was removed by centrifugation at 200 × g for 1 min at room temperature. All the bead samples were washed according the manufacturer's protocol using 4 cycles of alternate solutions of high and low pH. These solutions were 0.1 M Sodium acetate buffer, pH 4 containing 0.5 M NaCl and 0.1 M Tris

buffer, pH 8 containing 0.5 M NaCl. The beads were next rinsed with acidified water, pH 4.7 before incubation with 20 ng/μL Trypsin for about 16 h at 37 °C. The fraction of peptides was collected by centrifugation. The beads were rinsed with acidified water and the rinses were pooled together with their respective fractions. Before DTT elution, bead washing was repeated following the 4 cycles of alternate solutions of high and low pH. After rinsing with acidified water, the beads were incubated with 50 mM DTT in 1 M urea and 50 mM NH_4HCO_3. The eluent was collected by centrifugation. The beads were rinsed with elution buffer and the rinses were pooled together with their respective fractions. All peptide samples were desalted using iSEP tips. The eluents obtained were concentrated by vacuum drying in a SpeedVac, and re-diluted with 0.1% formic acid to about 10 μL. 1 μL aliquots of the eluents were mixed with CHCA matrix and analyzed by MALDI-TOF MS to ensure presence of peptide before LC-MS/MS analysis.

3.3.13 LC-MS/MS Analyses

Mass spectrometry was performed on an LTQ Orbitrap Velos mass spectrometer (Thermo Fisher Scientific, Germany) connected to a nanoLC Ultra 1D+ liquid chromatrography system (Dionex,) using both pre-column and analytical column packed with ReproSil-Pur C18 (New Objective, Germany). The mass spectrometer was equipped with a nanoelectrospray ion source (Pico Chip,), and the electrospray voltage was applied via a liquid junction. All measurements were performed in positive ion mode. Intact peptide mass spectra were acquired at a resolution of 7500 at a normal mass range, and an automatic gain control target value of 106, followed by fragmentation of the most intense ions by collision-induced dissociation. CID was performed in the FTMS for up to 8 MS/MS (4 h gradient) per full scan with 35% normalized collision energy and an AGC

target value of 5000. Both full scans and tandem mass spectra were acquired in profile mode. Singly charged ions and ions without assigned charge state were excluded from fragmentation, and fragmented precursor ions were dynamically excluded (4 h gradient, 30 s). Internal calibration was performed using Pierce LTQ Velos ESI positive ion calibration solution (Pierce,). The raw MS1 and MS2 spectra were generated using Proteome Discoverer software (Thermo Fisher Scientific) and saved as .RAW files.

Intensity-based label-free quantification and protein identification from on-resin digestion experiments were achieved with the MaxQuant computational proteomics platform and its integrated search engine, Andromeda (Max Planck Institute of Biochemistry, Martinsried, Germany). The .RAW files were loaded into MaxQuant version 1.2.5.6 interface where detected features were preprocessed through alignment of the retention times and m/z across samples and recalibration of precursor ion peak intensity outputted as LFQ intensity. Andromeda automatically searched the resulting peak lists of precursor and fragment ions against Mouse Fasta database (UniProtKB) using search parameters that included a precursor tolerance of 2 ppm and a fragment tolerance of 0.5 Da for CID spectra. Enzyme specificity was set to trypsin, and up to 2 missed cleavage sites were allowed. The variable modifications allowed were oxidation of Met and phosphorylation of Ser and Thr while the fixed modification was carbamidomethylation of Cys. Tables of detailed results showing protein identities and search parameters, mass spectrometric parameters, peptide sequences and their LFQ quantities were automatically generated.

3.3.14 Data Analysis

Prior to data analysis, contaminants were discarded from the protein list if identified as trypsin or if they had no gene name. The biochemical O-GlcNAc protein enrichment factors of the proteins were determined based on label-free quantification following the procedures by Hahne *et al*[27]. Briefly, the biochemical enrichment factor of a given protein was calculated as the ratio of its LFQ intensity in the O-GlcNaz-labeled sample compared to that in the control (unlabeled) sample. The LFQ intensity of each protein represents the summed intensities of unique peptides including the razor signal. In the case of missing values, where a protein was present in either the labeled or unlabeled and not in the other, 3000 was used as the smallest value to avoid zero and infinite ratios. The biochemical enrichment factors were then converted to Log_2 ratios. All proteins with log_2 enrichment factor <2 were considered non-specifically bound since they were found in the unfunctionalized beads, hence they were discarded. The list of bead-enriched O-GlcNAc proteins was subjected to downstream bioinformatics analysis to understand the protein expression changes in our system and the relevance of these changes to EMT and metastasis.

Gene Ontology enrichment analysis was performed using the Ingenuity Pathway Analysis, proprietary software that maps experimental data to the Ingenuity Knowledge Base and provides four basic outputs; canonical pathways enriched in the data, biological functions and diseases overrepresented in the data, plausible molecular networks showing molecular interactions, as well as upstream regulators that might explain changes observed in the data. As parameters for the analyses, settings were made to explore direct and indirect relationships among proteins/genes in our data reference to mouse mammary

gland or breast cancer cell lines. The threshold and level of significance was set to $p < 0.05$. Fisher's Exact Test p-value was used to demonstrate significant enrichment or overrepresentation while activation and inhibition were predicted based on the z-score. Each of these two statistical measures was used depending on the analysis type. The Fisher's Exact Test compares the similarity between proportions of significant molecules that map to a function/pathway in the experimental data to that of the molecules in the reference data that map randomly to a similar function/pathway. The Z-score determines the overall prediction direction based on expression values of individual proteins.

3.4 RESULTS AND DISCUSSION

A SPAAC click-chemistry-based strategy for affinity enrichment and identification of proteins modified by the post-translational O-GlcNAc glycosylation has been described. The enrichment scheme is summarized in Figure 3.1. The present strategy was adopted from a CuAAC click-chemistry-based affinity enrichment of O-GlcNaz-modified proteins onto resin-alkyne bead probe, developed and commercialized by Invitrogen[27]. Application of the commercial resin-alkyne in large-scale enrichment of HEK293 cellular O-GlcNaz-modified proteins has been demonstrated. In comparison, our strained-cleavable alkyne was prepared in-house by coupling DBCO-SS-NHS ester to amine-terminated Sepharose beads via amidation reaction. The efficiency of coupling and the azide-reactivity of the strained-cleavable-alkyne bead probe were evaluated by UV-Vis spectrophotometry and MALDI-TOF MS, respectively. Our enrichment strategy is unique in three ways: 1) coupling of O-GlcNAz-labeled proteins onto the bead probe occurs by SPAAC, 2) coupling takes place in an aqueous buffer (e.g. Urea/Tris buffer) with neither copper catalyst, reducing agent nor ligand, and 3) the bead probe possesses a

disulphide bridge for easy and reproducible elution of covalently coupled proteins under mild reducing conditions. Overall, several measures were taken to maintain selectivity toward O-GlcNAc purification. Many precautions including growing cells under low glucose conditions to reduce azide tagging of N-linked and O-linked mucin glycans, and ultracentrifugation of cell lysate to clear away potentially unspecific protein background, were borrowed from Zaro *et al*. and Hahne *et al*[27, 38]. Details of evaluations of the coupling reactions, metabolic-, and dye-labeling of fixed cells and cell lysates, bead washing optimization, enrichment, and identification of cellular O-GlcNAz-labeled proteins from a TGF-β1-induced EMT model, are described below.

3.4.1 Evaluation of coupling DBCO-SS-NHS linker to ω-Aminohexyl agarose and EAH Sepharose 4B beads

Preparation of strained-alkyne agarose beads was accomplished by coupling DBCO-SS-NHS to EAH Sepharose 4B (GE Healthcare) and ω-aminohexyl agarose (Sigma) under their respective optimum conditions that are different between the two. The goal of the synthesis was to obtain 100% degree of modification so that the loading of the DBCO in the bead probe is the same as the loading of the NH_2 groups in the unmodified bead resin. We also aimed at reproducing this high DOM. Given that the reaction stoichiometry is 1:1, the UV-Vis measurements of uncoupled DBCO-SS-NHS washed from beads show that coupling was most efficient and repeatable when starting with excess amount of DBCO-SS-NHS ester since two molar equivalent of the ester to that of the reactive NH_2 groups on the beads resulted in 100% DOM. Furthermore, we used MALDI-TOF analysis to show that the bead probe is azide reactive. The MALDI spectra of DTT-eluent obtained after coupling azido-GalNAc to the modified bead probe revealed a [DBCO-

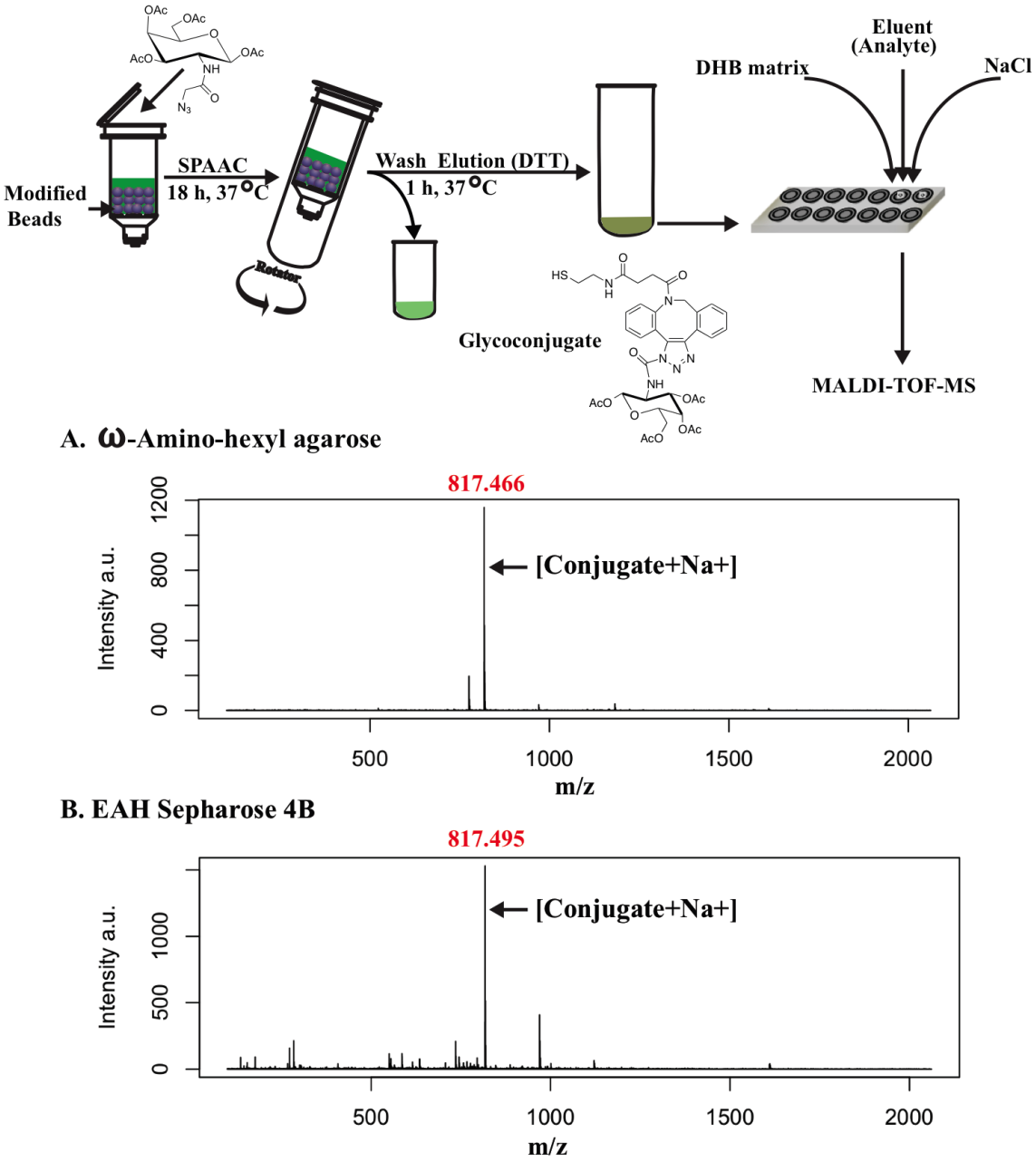

Figure 3.5 MALDI evaluation of the "click-able" and cleavable bead probe. The workflow shows the steps involved in the evaluation. Spectra A and B were obtained from the two modified resins used in this study showing that they were azide-reactive. The MALDI peak at m/z 817.4 for the reduced and cleaved O-GalNAc glycoconjugate was obtained with both Sepharose- and agarose-based bead probes. "a.u" = arbitrary intensity units.

SH-triazolyl-GalNAz + Na]$^+$ cleavage product at m/z = 817.4 that was not obtained from the control bead. This product is indicative of the reactivity of the strained-alkyne agarose bead probe. The product was obtained from both EAH sepharose and ω-Aminohexyl agarose showing that the reactivity of the strained-alkyne agarose bead probe is the same regardless of the length of the linker and conditions that were involved in coupling alkyne to the bead. In addition, the azide-reactivity test makes it confident to use the strained-alkyne agarose bead probe for affinity capture and enrichment of Azido-GlcNAc tagged proteins from complex biological samples of metabolically labeled cells.

UV-Vis spectrophotometry was also employed in the determination of the suitable conditions for reductive cleavage of bead-bound linker (Table 3.1). It was estimated that ~ 60% of the product was cleaved in the first fraction, obtained by incubation of modified beads with 40 mM DTT for 1 h at 37 ºC on a shaker, in the presence or absence of urea and NH_4HCO_3. This indicates that urea and NH_4HCO_3, the likely components of a DTT elution buffer for enriched proteins are not inhibitory to the reductive cleavage reaction. The remaining bead-bound linker was recovered in the second fraction. DTT, Urea and NH_4HCO_3 were components of a reductive cleavage elution buffer previously used in the selective isolation of enriched proteins from drugged immune cells in a quantitative non-canonical amino acid tagging strategy. Presence of DMSO or 1,4-dioxane in the cleavage solution ensured solubility of the cleaved linker. However, these solvents will not be needed in elution of actual bead-bound proteins.

Table 3.1 Relative Amounts of DBCO Residues Cleaved from the DBCO-functionalized Resin under Different Conditions

Elution (Reductive Cleavage) Conditions	**μmol equivalents in 20 μL (out of 200 μL total bead slurry)**			
	1-h eluent		**2-h eluent**	
Modified beads+40mM DTT+60% DMSO+Urea+NH_4HCO_3	0.063/0.1	63%	0.037/0.1	37%
Modified beads+40mM DTT+60% DMSO	0.066/0.1	66%	0.031/0.1	31%
Modified beads+40mM DTT+0% DMSO+Urea+NH_4HCO_3	0.038/0.1	38%	0.018/0.1	18%
Control beads+40mM DTT+60% DMSO+Urea+NH_4HCO_3	0	0%	0	0%
Control beads+40mM DTT+0% DMSO+Urea+NH_4HCO_3	0.0012/0.1	0.12%	0.0024	0.24%

Table 3.2 Evaluation of Coupling of DBCO-SS-NHS ester to EAH Sepharose resin

Bead sample	Starting linker	Wash Flow-throughs (μmol)				Total μmol in Washes	Retained μmol
		A	B	C	D		
1	4.180	0.288	0.103	0.179	0.0046	0.4401	3.780
2	4.180	0.834	0.154	0.177	0.0043	1.0693	3.111
3	4.180	0.369	0.129	0.0312	0.00647	0.536	3.640

3.4.2 Dye-labeling and fluorescence microscopy of Azido-O-GlcNAc-tagged proteins in fixed cells

Metabolic labeling of proteomes in cells using an unnatural sugar and a non-canonical amino acid was followed with dye-labeling and fluorescence microscopy. The unnatural sugar, GalNAz, non-canonical amino acid, HPG and their bioorthogonal fluorophores have been successfully used elsewhere for labeling subsets of proteomes. As applied and recognized in Duan *et al*., fluorescence of fluorophores used in this study is quenched by the surrounding groups such as azide, and recovers upon formation of the triazole ring via CuAAC and SPAAC reactions[31, 39-40]. The fluorogenic nature ensures minimal background noise and high signal-to-noise ratio of detection[41]. Like many cell lines that have been metabolically labeled with GalNAz in previous studies, our results show that both NMuMG and NIH3T3 cells are amenable to metabolic labeling by azido-sugars and to dye-labeling that tags the azido moiety with fluorescent alkyne dyes via CuAAC or SPAAC[36, 38, 42]. In both cell cultures the green fluorescence arising from the FITC-alkyne-Tagging of azido-labeled proteins colocalized with nuclear staining (Figures 3.7 and 3.8). NMuMG was metabolically labeled with two bioorthogonal chemical reporters, azido-GalNAc and homopropargylglycine (HPG) while NIH3T3 was labeled with one bioorthogonal chemical reporter, azido-GalNAc. HPG is an analogue of the amino acid Methionine and therefore tags the newly synthesized proteome, while Azido-GlcNAc tags the PTM following synthesis of the proteome[34]. The blue fluorescence stain for HPG-tagged proteins colocalized with green fluorescence stain azido-GlcNAc PTM and the red fluorescence stain for nuclei.

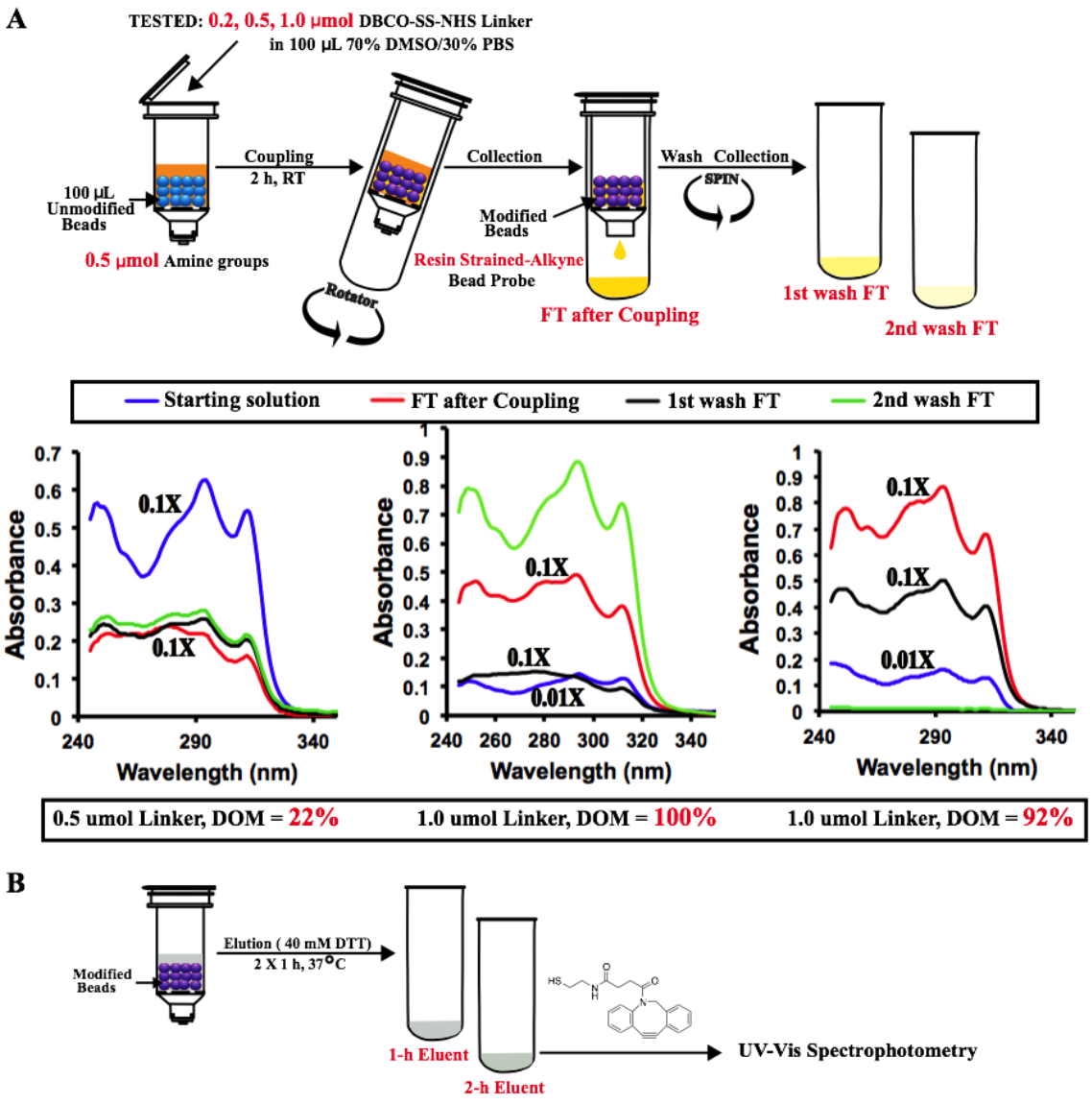

Figure 3.6 UV-Vis spectrophotometric evaluation of the coupling of the DBCO-SS-NHS ester to raw beads to produce the affinity bead probe. A) The workflow for the coupling and the UV-Vis profiles obtained with different ester concentrations are shown. B) The workflow for testing the elution conditions. The coupling was efficient when two equivalent of ester (in related to the terminal amine groups on the beads) was added. The characteristic absorbance profile was maintained by nearly all samples but seemed to change at continued washing due to dilution.

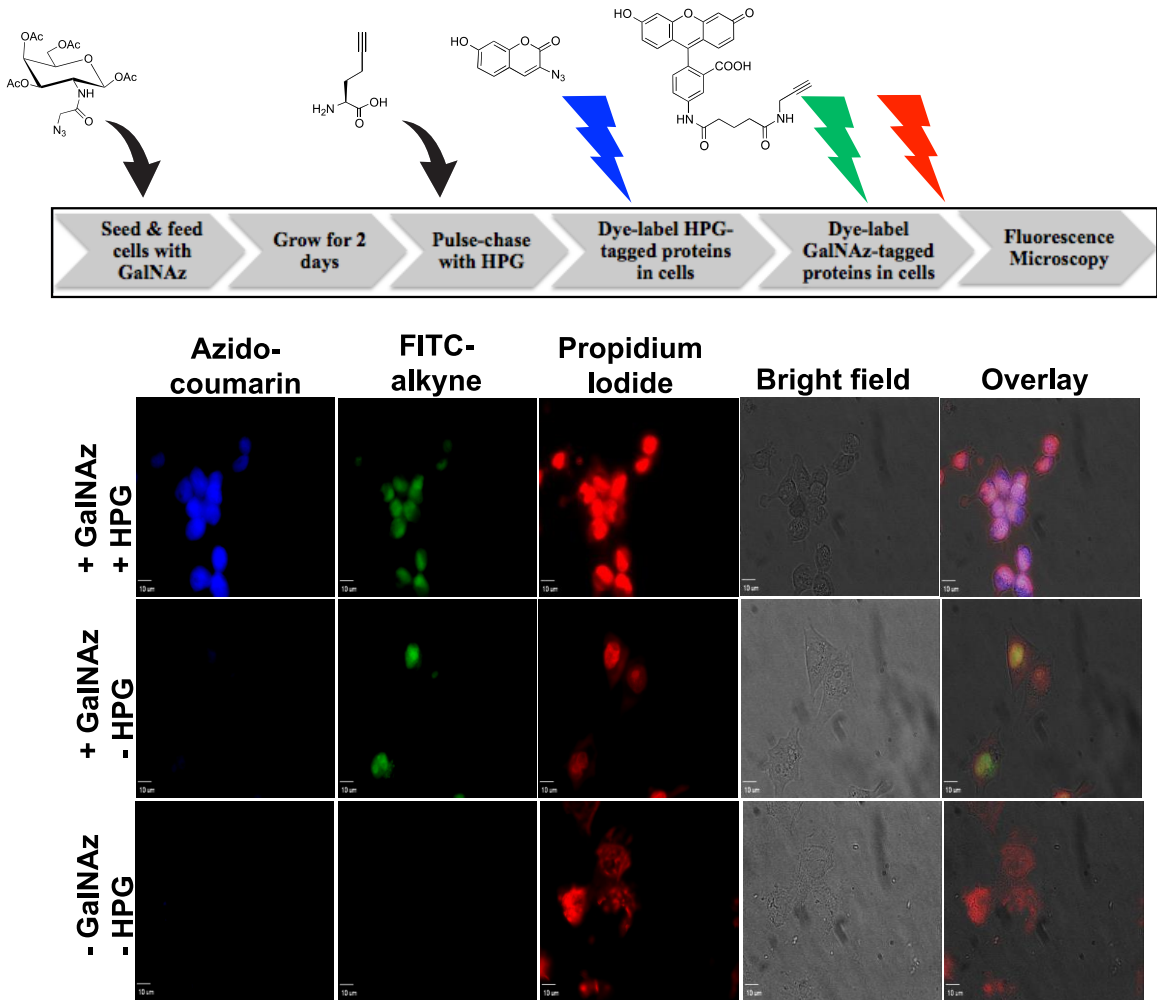

Figure 3.7 Fluorescence imaging of O-GlcNAc proteins (green) and newly synthesized proteins (blue) in double-metabolically-labeled fixed NMuMG cells. Nuclei were stained with propidium iodide (red). Scale bar = 10 μm.

Fluorescence microscopy examination of dye-labeled HPG-tagged proteome and azido-GlcNAc tagged PTM in fixed cells confirmed the metabolic labeling and aided in the localization of the labeled proteome. In Figure 3.8 co-localization of DAPI with FITC-alkyne in azido-GalNAc-fed NIH3T3 cells and not in the control, showed the labeling of both nuclear proteome and its PTM. Cell population in the GalNAz-labeled cultures was found to be lower than that in the control. A similar observation was previously made by Duan *et al*[32]. In Figure 3.7, the three dye stains; namely, azido-coumarin for HPG labeling, FITC-alkyne for azido-GalNAc labeling and propidium iodide for nuclear staining, all colocalized in multiply-stained NMuMG cells, showing azido-GlcNAc PTM of the newly synthesized proteome around the nucleocytoplasmic region. The exent of FITC-alkyne staining is smaller than that of azido-coumarin staining showing that not all the newly synthesized proteome has the O-GlcNAc PTM. The results demonstrate that NMuMG cells can be metabolically labeled with bioorthogonal chemical reporters to probe the O-GlcNAc PTM. Fluorescence Microscopy of dye-labeled, HPG pulse-chased and azido-GlcNac tagged NMuMG cells was initially aimed at monitoring dynamic glycosylation in TGF-β1-induced EMT similar to the work of Liu *et al*[34]. However, multiple staining seemed laborious and could not be easily reproduced, hence it was not applicable to cells undergoing EMT. To overcome this limitation cells undergoing EMT could have been followed by: 1) monitoring glycosylation of a target protein, or 2) studying changes in global glycosylation using dye-labeling of azido-GlcNAc PTM in cell lysates.

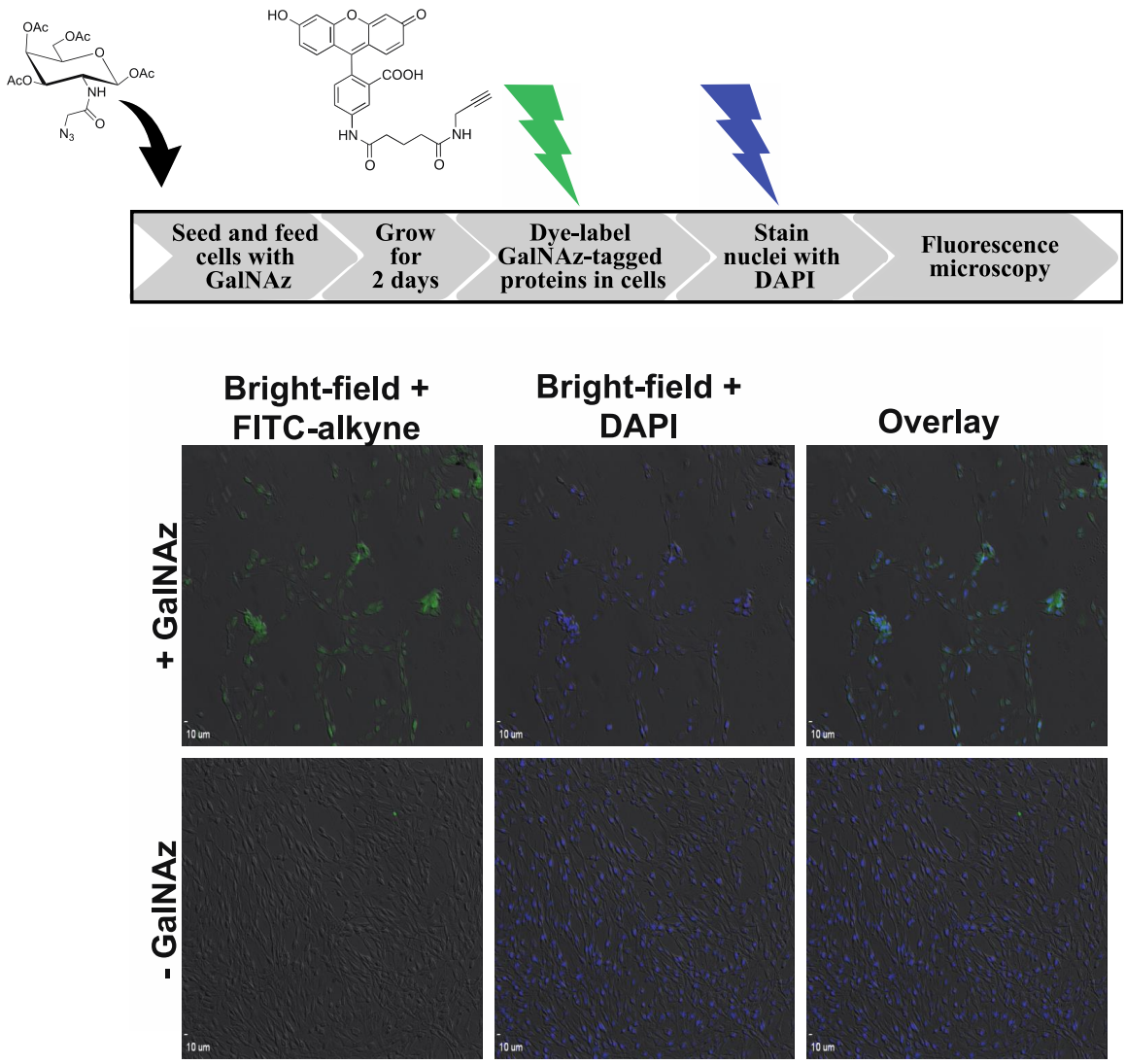

Figure 3.8 Fluorescence imaging of O-GlcNAc proteins (green) in metabolically-labeled fixed NIH3T3 cells. Nuclei were stained with DAPI (blue). Scale bar = 10 μm.

3.4.3 Fishing for Snail1 protein

Snail protein might be the only key transcription factor and EMT marker whose O-GlcNAc in relation to phosphorylation has been well studied. Park *et al*. showed that the presence of O-GlcNAc stabilizes Snail1 expression by inhibiting O-phosphorylation and that O-GlcNAc PTM on Snail1 occurs in various cell lines. In addition, these researchers demonstrated the presence of O-GlcNAc-modified Snail1 by immunoblotting following succinylated Wheat Germ Agglutinin-affinity purification from total cell lysates[10]. For this reason we were interested in using the strained-alkyne-cleavable bead probe to enrichfor Snail1 from metabolically labeled NMuMG cells using the O-GlcNAz as a handle for bead capture and enrichment, and to subsequently determine whether TGF-β1-induction of EMT has effect on how the O-GlcNAc PTM level changes. The goal was to resolve using 1D SDS-PAGE, bead-enriched proteins from TGF-β1-induced cellular extracts and among them detect Snail1 using immunoblotting with anti-Snail1 antibody.

From preliminary work aimed at demonstrating presence of Snail1 without enrichment, we failed to detect Snail1 by immunoblotting, despite an attempt to follow a procedure that has been used previously[35]. On troubleshooting by analyzing positive control cell lysates, Snail1 was detected (Figure 3.9 C) showing that the procedure worked. In addition, Snail mRNAs were detected by qRT-PCR analysis of NMuMG TGF-β1-induced and control lysates using the same optimized forward and reverse primers for Snail and Gapdh (house-keeping gene) as were employed in Saha *et al*[43]. Snail mRNA levels were 3-5 fold higher in induced cells than in the control (Figure 3.9B). The change in mRNA levels paralleled morphological change (Figure 3.9A) during TGF-β1 induction, and both seemed to be dose-dependent. It was surprising that

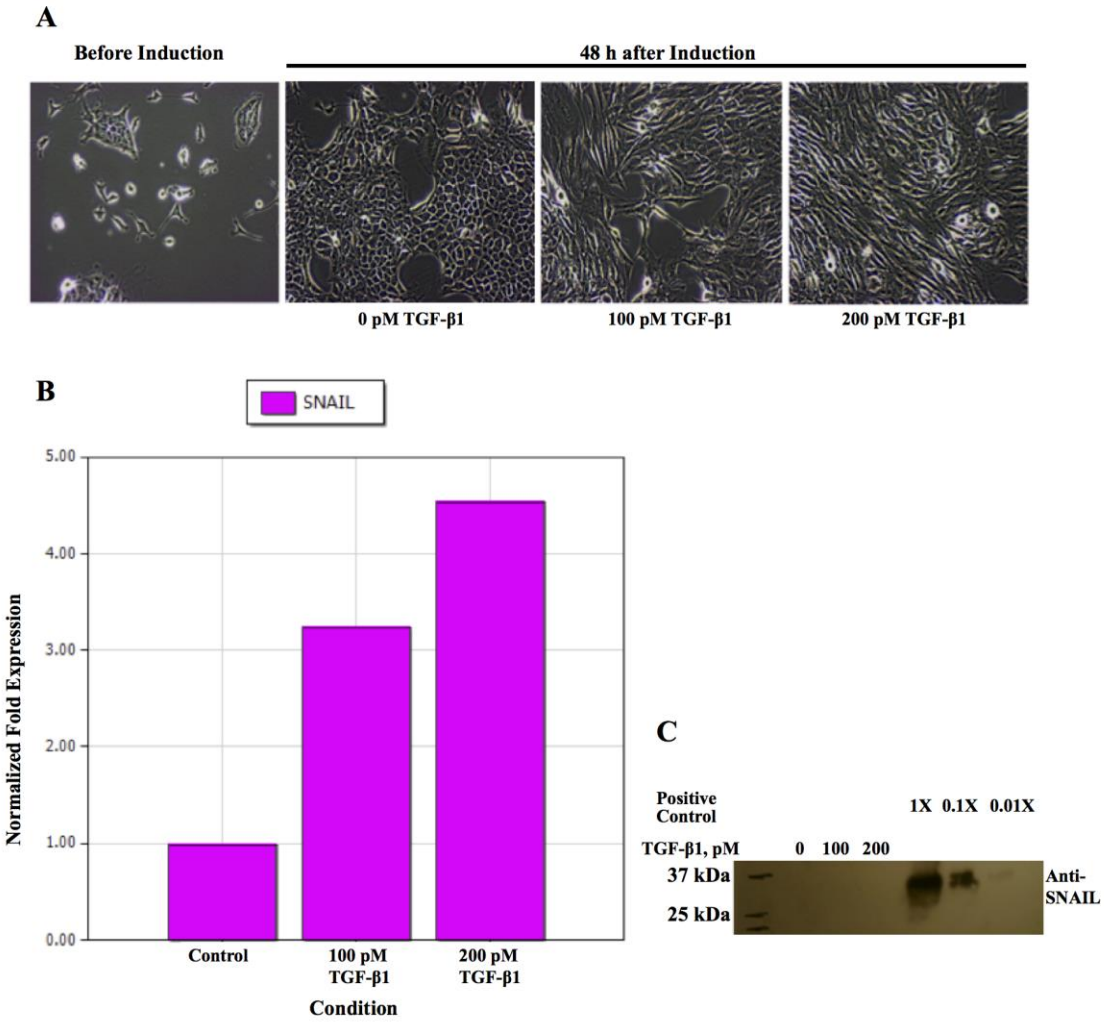

Figure 3.9 (A) Light microscope images showing changes in cell morphology between induced and control samples after 48 hours of TGF-β1-induced EMT. (B) Snail mRNA levels were higher in the induced sample than in the control. Both the cell morphology and mRNA changed in a dose-dependent manner. (C) Absence of Snail1 protein in both the induced and control samples.

despite these changes associated with Snail expression, Snail protein could not be detected. Perhaps, the presence of Snail should have been monitored through following its localization using immunofluorescence microscopy prior to isolation from cellular extracts. Alternatively immunoprecipitation or succinylated Wheat Germ Agglutinin (sWGA)-affinity purification of Snail should have been carried out to facilitate detection as has been demonstrated in Park *et al*[10]. Failure to detect Snail paralleled inability to see consistent morphological changes characteristic to EMT from different batches of the 48-h TGF-β1-induced cell cultures, a problem that could be attributed possibly to some inactive TGF-β1 protein aliquots among the refrigerated stock. As a consequence, the work on Snail1 was discontinued.

3.4.4 Dye-labeling, SDS-PAGE and Fluorescent Scanning of Azido-O-GlcNAc-tagged Proteins

Despite failure in detecting our target O-GlcNAc modified Snail, enrichment of global O-GlcNAc proteins from the nucleocytoplasmic cellular fractions was pursued. We sought to find out if Azido-O-GlcNAc tagged proteins in cell lysates could be detected through dye-labeling via SPAAC since this has never been reported. We hypothesized that successful labeling of Azido-O-GlcNAc tagged proteins in cell lysates with DBCO-functionalized dye via SPAAC would indicate that such proteins could be attached to any strained-alkyne in cell lysates regardless of whether the reaction environment is liquid phase or solid phase. Prior to bead-based enrichment, Azido-O-GlcNAc tagged proteins in cell lysates were directly labeled with an alkyne-conjugated fluorescein dye, and subsequently detected by in-gel fluorescence scanning. Dye-labeling here, not only confirmed the presence of azido functionality, but it proved that the azido group on

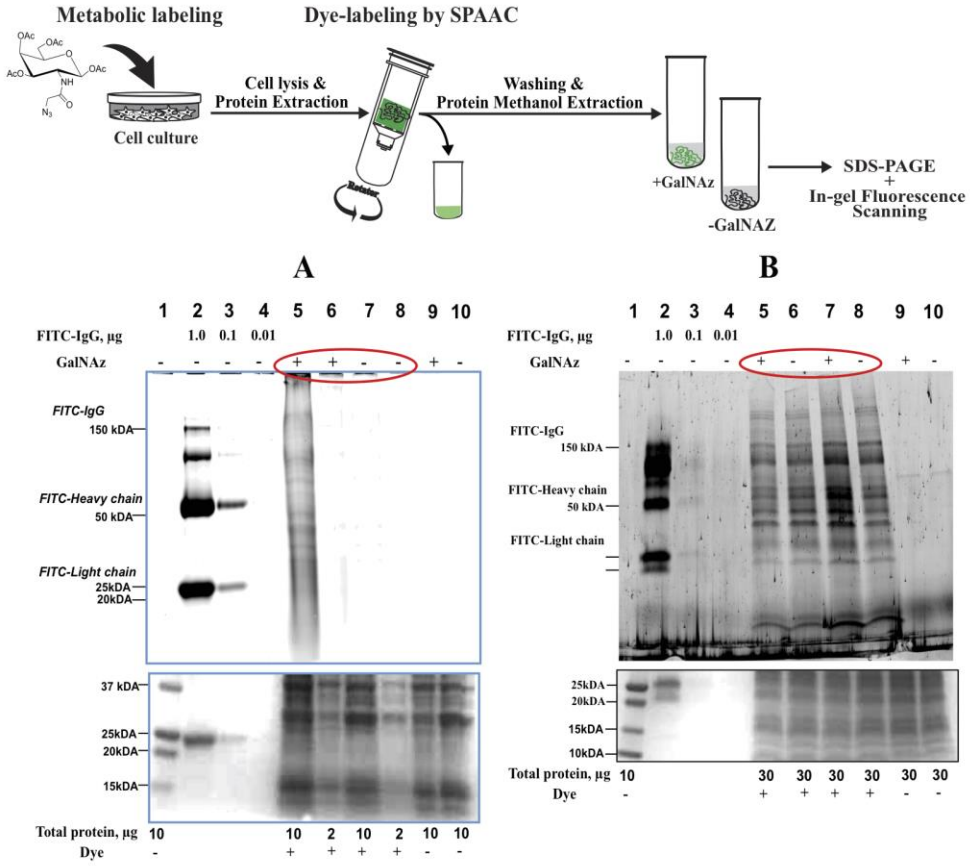

Figure 3.10 In-gel fluorescence detection of O-GlcNAz-modified proteins. Protein lysates from metabolically labeled cells were dye-labeled with (A) DBCO-fluorescein and (B) DBCO-naphthalimide and imaged with fluorescence scanner. Alongside dye-labeling, different conditions tested were (A) two different amounts of protein, 2 and 10 µg; and (B) two dye-labeling conditions, room temperature for 2 h and 10 °C for 10 h. Test loadings were made in lanes 5-8 of each gel. Lane 1 contains protein weight makers. Lanes 2-4 has FITC-IgG (positive control). Lanes 9-10 contains dye-unlabeled lysates (negative control).

proteins can be probed via SPAAC in cell lysates, even though previous studies exploitedonly the Cu-catalyzed click chemistry. Two dyes available in the lab, DBCO-fluorescein and FITC-alkyne, were used for dye-labeling of proteins in cell lysates. The dyes were tested on NIH3T3, a cell line that has been previously labeled in other studies[38]. Labeling was done by incubation at 10 ºC for 10 h on a shaker. No signal was observed from FITC-alkyne-labeled samples in a preliminary experiment comparing dye-labeling of proteins in lysates using FITC-alkyne and DBCO-fluorescein. The FITC-alkyne might have been out dated and inactive and its use was therefore discontinued. Figure 3.10 A shows that GalNAz-tagged proteins were detected with a loading of 10 compared to 2 g total protein using DBCO-fluorescein dye. The protein bands were however faint, as a result dye-labeling was repeated. To improve the signal obtained using DBCO-fluorescein labeling and to demonstrate that azido-GlcNAc proteins could be coupled to a strained-alkyne probe via SPAAC in cell lysates, a newly prepared dye, DBCO-naphthalimide (by Dr. Honglin Li) was used. Two conditions were tested with DBCO-naphthalimide: 1) incubation at room temperature for 2 h on end-over-end rotator, and 2) incubation at 10 ºC for 10 h on a shaker. Incubation at room temperature resulted in unspecific binding since the signal of the test samples was the same as that of control samples. The 2 h room temperature and the 10 h 10 ºC conditions have been previously employed in Cu catalyzed dye-labeling of GlcNAz-tagged NIH3T3 cell lysates using Tamra-alkyne dye, and that of azidohomoalanine-tagged Jurkat cells with Alkynyl Alexa-647 dye, respectively, without any unspecific protein background[34, 36]. Although unspecific protein background was the challenge in this study, a difference in the signal between test sample and control was observed with the 10 h 10ºC incubation, indicating

that the azido-GlcNAc proteins that had been coupled via SPAAC to alkyne dye probe in cell lysate were detected. Perhaps the poor signals observed in this work justify why none of these three alkyne-functionalized fluorescent dyes (DBCO-fluorescin, FITC-alkyne and DBCO-naphthalimide) are listed among the dyes known for robust labeling of azido-GlcNAc proteins in cell lysates.

3.4.5 Bead Washing

In bead-based enrichment of proteins, thorough washing of beads is crucial for removal of nonspecific protein background. Inability to remove these bead-adsorbed proteins can result in contamination of the bead-bound fraction and false positives. Owing to lack of washing instructions for the ω-Aminohexyl agarose beads, we attempted to formulate washing buffers and develop washing protocol based on the known wash buffers and protocols. Several bead-based affinity enrichment strategies have their own optimized washing protocols that differ from study to study. The only common thing among them is the repeated use of detergent- and salt-containing buffers. Detergents and salts in the wash buffers are good agents for solubilization of proteins and can thus cause desorption of non-covalently adsorbed proteins. A washing protocol or condition was evaluated by comparing SDS-PAGE protein profiles of the original SPAAC feed, first washes, final washes, DTT eluent and denatured beads. We considered a washing protocol ideal and efficient if proteins are observed in the first washes, and none in the final washes, DTT eluents as well as denatured beads. Since nonspecific binding proteins on affinity resins cannot be avoided, presence of protein bands from denatured beads was expected. However, reduction in protein bands in this fraction was preferable.

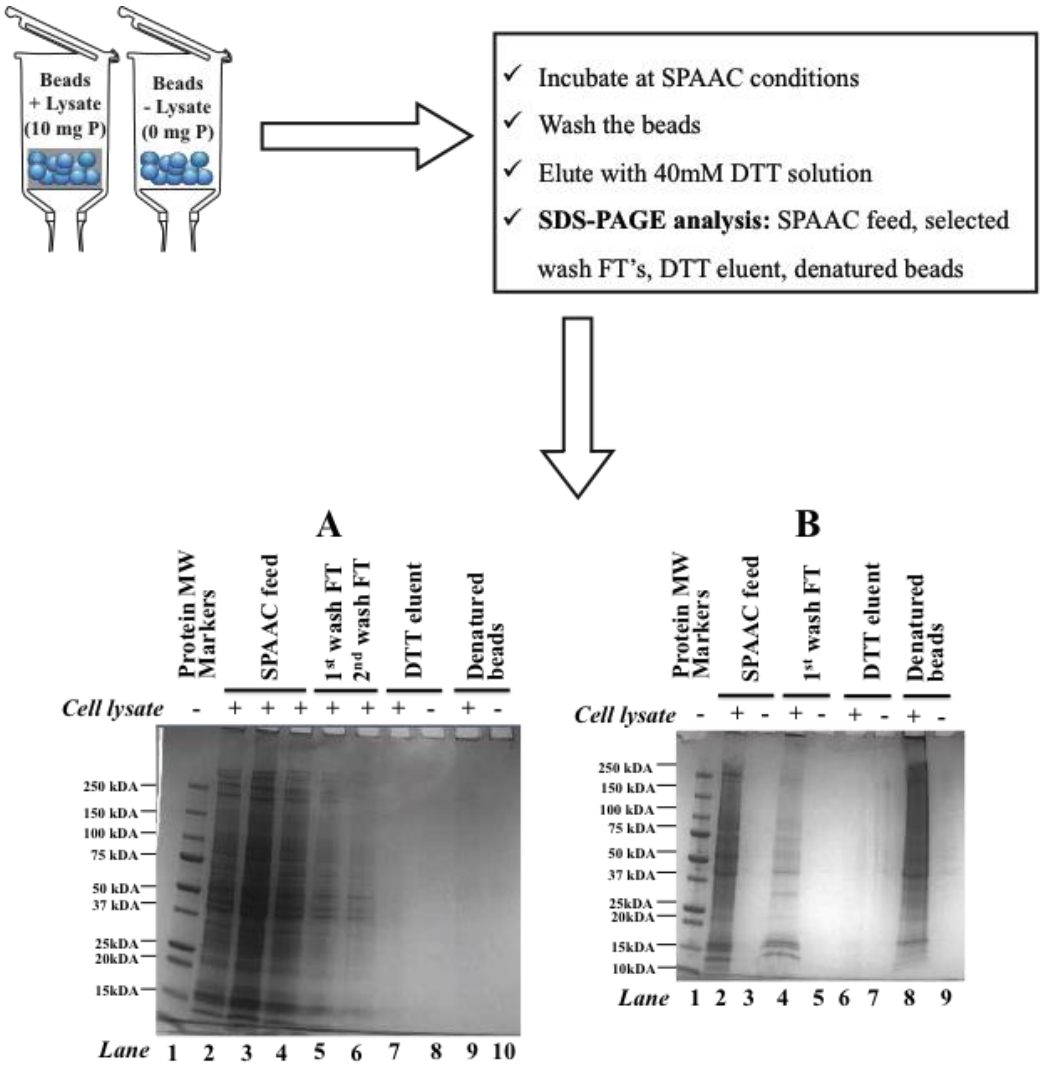

Figure 3.11 Evaluation of the RIPA wash buffer against an in-house bead-washing protocol. (A) RIPA wash buffer cleaned the beads permitting no contamination of the DTT eluent and no proteins remaining on the beads. (B) The complete elimination of proteins from denatured beads (lanes 8 and 9) was not repeatable with RIPA wash buffer and could not be achieved with the in-house bead-washing protocol.

Through recommended series of trail-and-error experiments testing and combining different bead washing strategies, the washing protocol illustrated on fig. 3.12B was formulated. Some of the wash buffers and protocols tested prior to formulation included RIPA wash buffer[21], Click-iT® bead-washing protocol that uses SDS and 8M Urea/100 mM Tris, pH 8 wash buffers (Click-iT® Enrichment Kit, Invitrogen) and TBST that is commonly used to remove non-specific binding proteins in immunoassays. TBST and Click-iT® wash buffers did not work at all while RIPA wash buffer did clean up the beads resulting in undetectableproteins in the DTT eluent and denatured beads (Fig. 3.11A). The absence of non-specifically bound proteins remaining on beads was however not repeatable (Fig. 3.11B). Taken together, we developed a wash buffers comprising components from known wash buffers. Our in-house bead-washing procedure (Figure 3.13B) resulted in no contamination in the DTT eluent and some detectable proteins in the denatured bead fraction.

We evaluated the in-house procedure against the EAH Sepharose 4B manufacturer's bead-washing procedure (Protocols – Figure. 3.13B). We compared the efficiency of removing cell lysate proteins and BSA from the beads after a typical SPAAC protein coupling reaction. The resin employed in the evaluation as well as in the previous trial-and-error bead-washing tests consisted of unmodified beads. On Figure 3.12, it was observed that both bead-washing protocols resulted in no detectable proteins in the DTT eluent, but that some proteins remained on the denatured beads. In analyses where proteins were not quantifiable by Coomassie blue absorbance method, an aliquot was mixed 1:1 with SDS loading buffer and loaded on the gel. On lane 8 of each gel, we observed that thick BSA bands remained on the beads after applying our in-house bead-

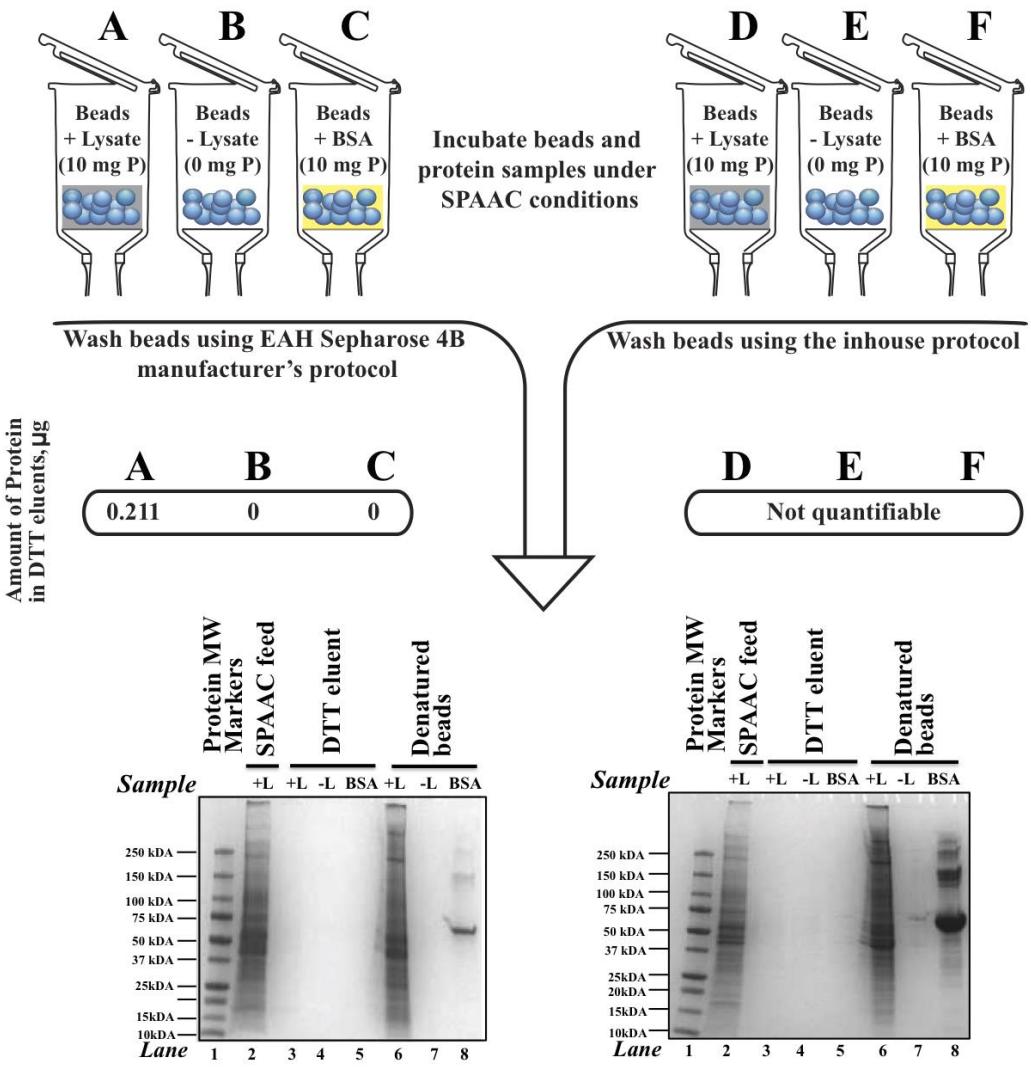

Figure 3.12 Evaluation and comparison of effectiveness of the two bead-washing protocols. The effectiveness is based on removal of cell lysate proteins and BSA from beads that have been incubated with protein sample under SPAAC conditions. "+L" means cell lysate added to beads; "-L" means no lysate added (negative control). DTT eluents and denatured beads fractions are used to show removal of proteins from beads.

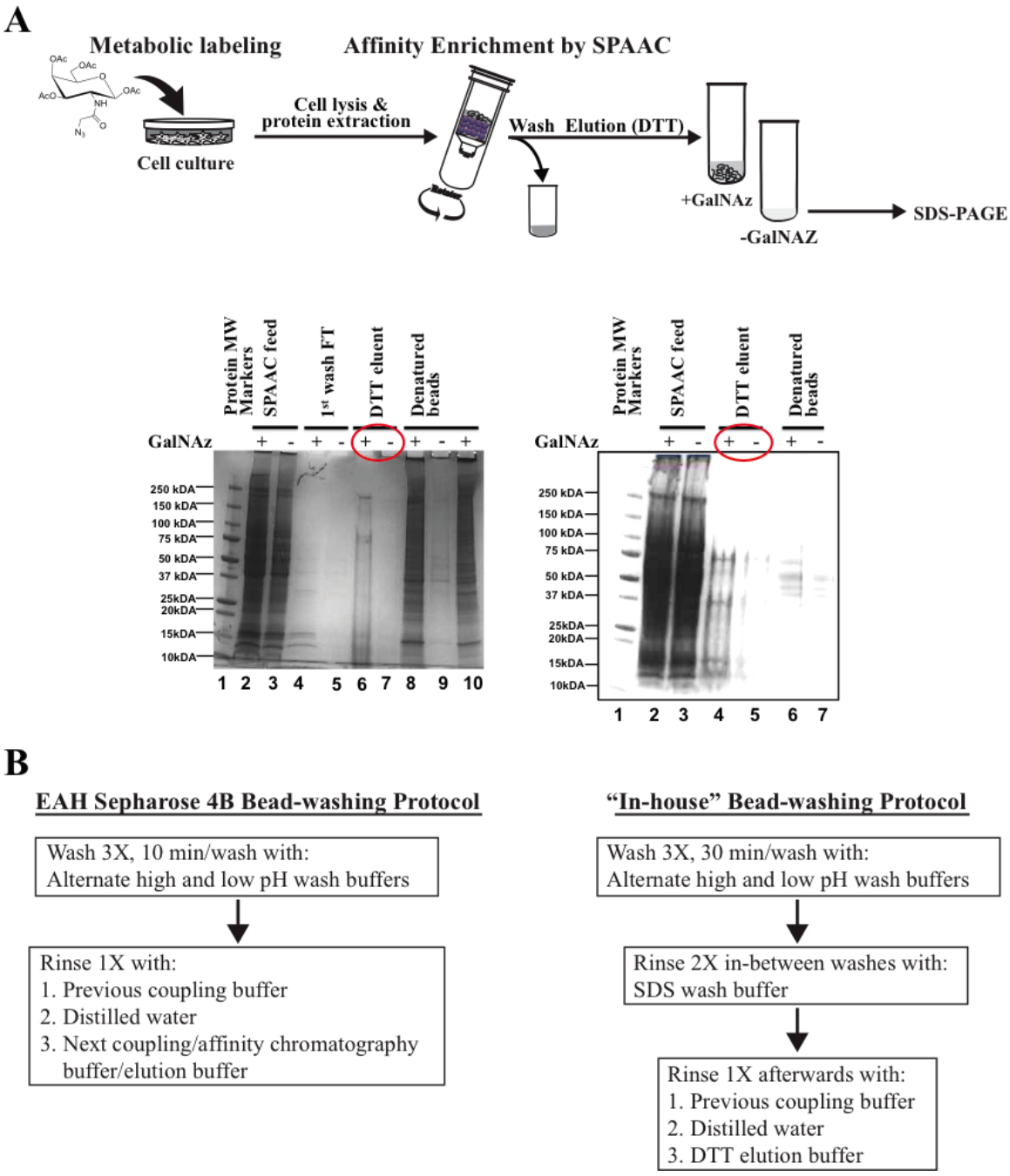

Figure 3.13 (A) Resin strained-alkyne-based O-GlcNAc affinity enrichment was repeatable and resulted in faint protein bands (lanes 6 [*right gel*] and 4 [*left gel*]). (B) The two bead-washing protocols of choice in our study, namely; the in-house and the EAH Sepharose 4B manufacturer's bead-washing protocols.

washing protocol compared with the manufacturer's protocol. This observation and the fact that the washing steps of the manufacturer's protocol are very short motivated us to select the manufacturer's protocol for subsequent enrichment experiments.

3.4.6 Affinity Enrichment of Cellular O-GlcNAc Proteins and Label-free LC-MS/MS Quantification and Identification

Following optimization of the bead washing, selectivity of the O-GlcNAc enrichment strategy was assessed by resolving the enriched fraction using 1D SDS-PAGE. Figure 3.13A shows protein bands of the azido-labeled samples and not the control from DTT eluents. The selectivity was further assessed by comparing the label-free LC-MS/MS quantified intensities of the proteins from the azido-labeled (O-GlcNAz-modified) and the control (O-GlcNAc-modified) samples, both TGF-β1-induced and non-induced. The summed intensities, the enrichment factors and their logarithmic values were utilized for comparisons. The summed intensities were initially corrected for by removing proteins identified to be contaminants and had no mouse gene name associated with them. All of the keratin proteins seem to be listed among the proteomics contaminants in the UniProtKB database. However, only those with no mouse gene name associated with them were discarded, and the others were retained since some cytokeratins are epithelial markers and are relevant to cancer and EMT biology. Intensities of the discarded proteins were reminiscent of biochemical noise and obscured observation of the actual differences between the azido-labeled and control samples, as seen on Figure 3.14. In both the TGF-β1-induced and non-induced sample the summed intensity of the azido-labeled was about 3-fold higher than that of the control. However, the median enrichment factors were different, 3.2 in TGF-β1-induced and 1 in non-induced samples. Although the data

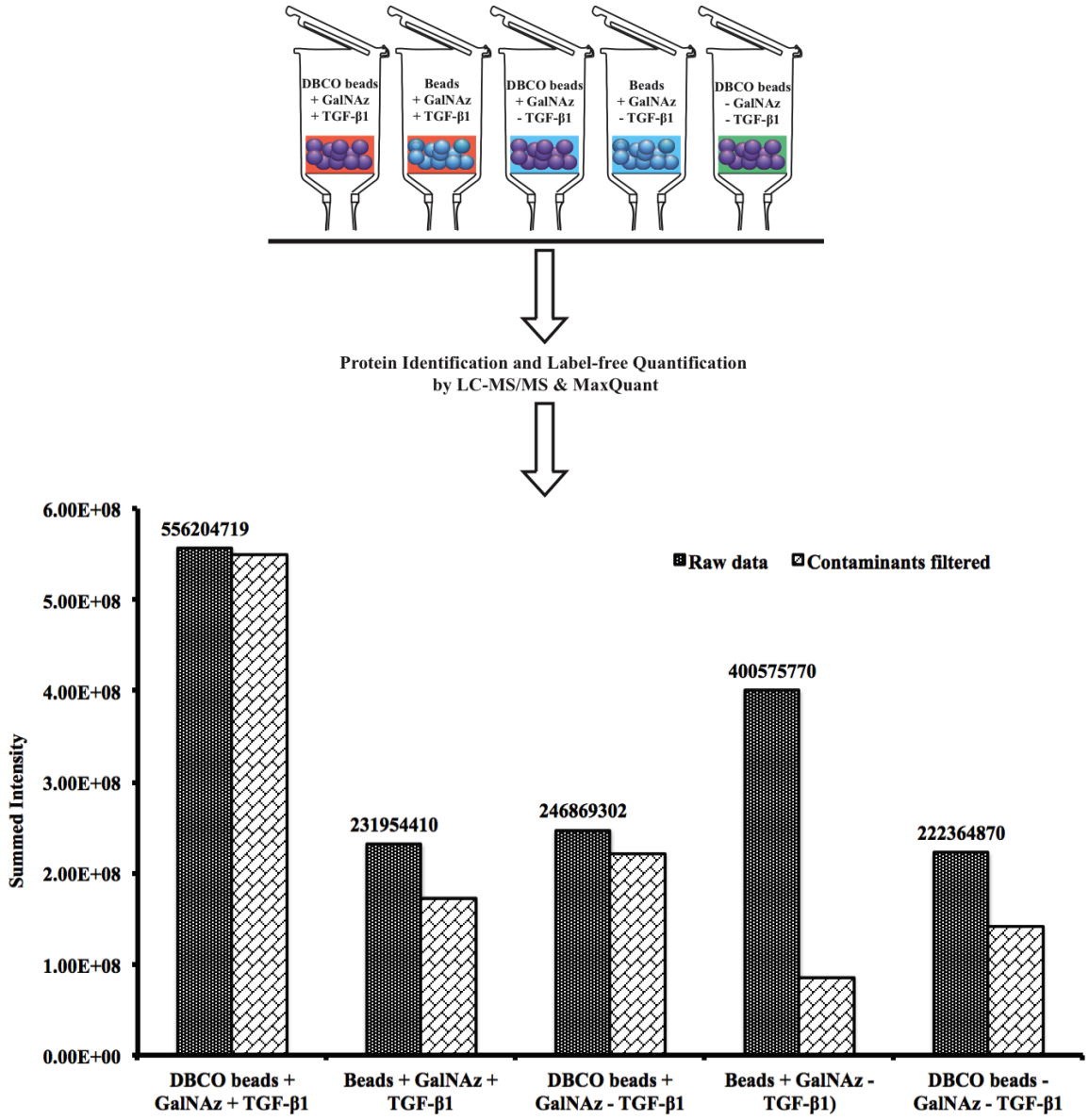

Figure 3.14 Summed intensities of identified proteins from raw and "contaminants-filtered" data generated from five samples with modified or unmodified beads, with or without metabolic labeling in NMuMG cells induced or non-induced with TGF-β1.

suggests that enrichment was not consistent between the TGF-β1-induced and non-induced samples, it is inconclusive to rate the efficiency of enrichment since the experiment was not repeated. Using the commercial resin-alkyne, Hahne *et al*. reported efficient enrichment showing 60-fold higher summed intensity in azido-labeled than the control and a median enrichment factor of 260. Although their enrichment efficiency is higher, the degree of modification of their resin is unknown. Hence, the click chemistry-based affinity enrichment reported in Hahne *et al*. and this study cannot be compared.

The distribution of protein intensities as a function of $\log_2$ [EF] is complex but has the same sigmoidal pattern across all samples with many proteins having minimum intensities covering a stretch of $\log_2$ [EF] values from -5 to 5, and beyond that the intensities increase exponentially. For the non-induced sample majority of the proteins (~120) had $\log_2$ [EF] around zero showing that they were not enriched. For the induced sample the number of proteins with $\log_2$ [EF] around zero is still high but the number of proteins $\log_2$ [EF] >0 forms a normal distribution that seems to peak around $\log_2$ [EF] = 3. Given that all the experimental conditions were the same, the data suggests that there might have been fewer O-GlcNAc-modified proteins in non-induced than in the induced sample. However, the global O-GlcNAcylation between TGF-β1-induced and non-induced NMuMG was not determined. All the proteins with $\log_2$ [EF] around zero and below were discarded from further analysis since they represented non-specifically bound proteins. Out of about 200 proteins identified, 125 were regarded as the bead-enriched O-GlcNAc proteome.

In a study on global profiling of O-GlcNAc proteome from HEK293 cells using the commercial resin-alkyne, Hahne *et al*. identified about 1500 proteins (Ref). In this

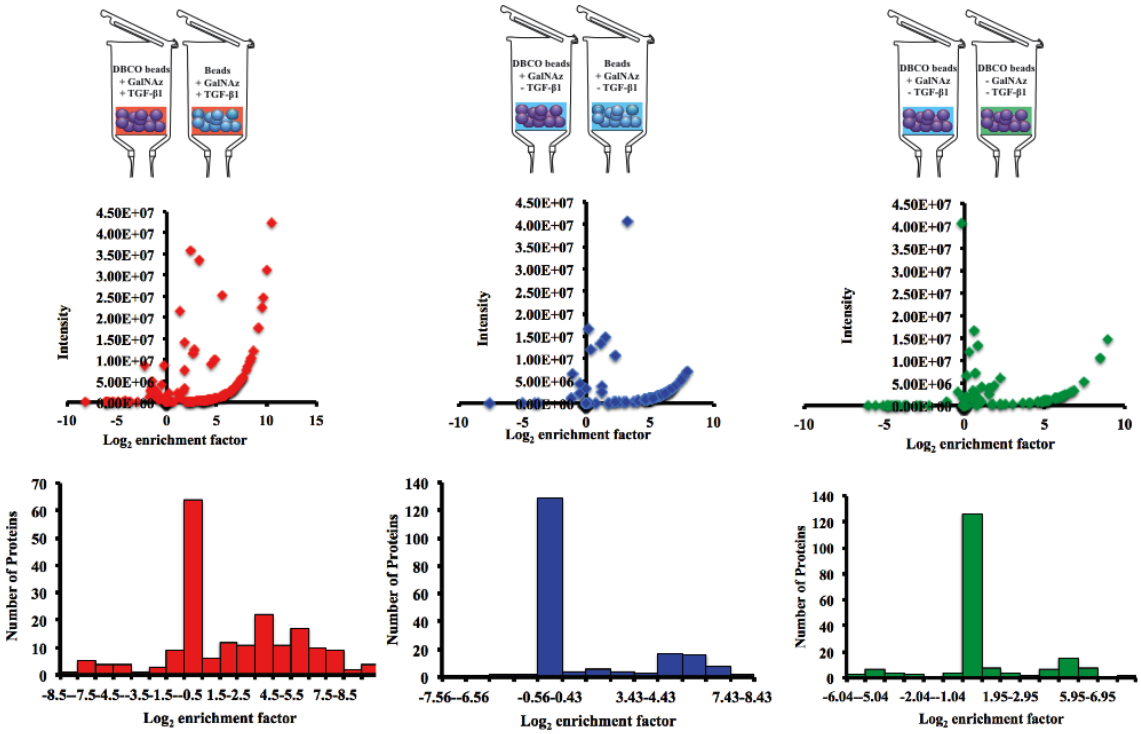

Figure 3.15 Global identification of potentially O-GlcNAc proteins in TGF-β1-induced EMT. (*Upper panel*) Pairs of tubes showing the samples used for determining the biochemical enrichment factors of the identified proteins are displayed. Red panel: Modified/Unmodified beads, +GalNAz, +TGF-β1; Blue panel: Modified/Unmodified beads, +GalNAz, -TGF-β1; Green panel: Modified beads, +/-GalNAz, -TGF-β1. (*Middle panel*) Scatter plots of intensity and log2 biochemical enrichment factors of identified potentially O-GlcNAc proteins. (*Lower panel*) Distribution of the biochemical enrichment factors. More proteins were enriched in the TGF-β1-induced compared to non-induced samples.

study, only about 200 proteins out of the entire O-GlcNAc proteome of NMuMG cells were identified. Unlike the commercial resin-alkyne, strained-alkyne resin employed in affinity enrichment of the O-GlcNAc proteome in this study was applied for the first timein proteomics. Although some parts of the enrichment procedure such as the conjugation of the affinity tag to the agarose-cleavable linker, as well as the bead washing were rigorously tested and optimized, the mass spectrometric component was not optimized. The proteomics results therefore represent only a once-off measurement that could have been preliminary and needed to be replicated for sufficient evaluation of the selectivity of the enrichment strategy. Typical proteomic studies using high-resolution orbitrap instruments generate massive data comprised of several thousands of proteins. Such studies often involve extensive pre-fractionation of the cells and tissue samples. In this study, only one subcellular fraction comprising nucleocytoplasmic proteins was analyzed. The number of proteins would have been increased if the nuclear and cytoplasmic fractions were analyzed separately. Also further fractionation to extract the mitochondrial fractions should have been considered since the OGT resides in the nucleus, cytoplasm and mitochondria where it carries out the O-GlcNAcylation of target proteins.

3.4.7 Gene Ontology Analyses

3.4.7.1 Subcellular Localization

Of all the protein ID's mapped by the IPA, 90% are nucleocytoplasmic proteins while 10% are plasma membrane and extracellular proteins. Although extensive pre-fractionation of the samples was not carried out prior to affinity enrichment, the results of

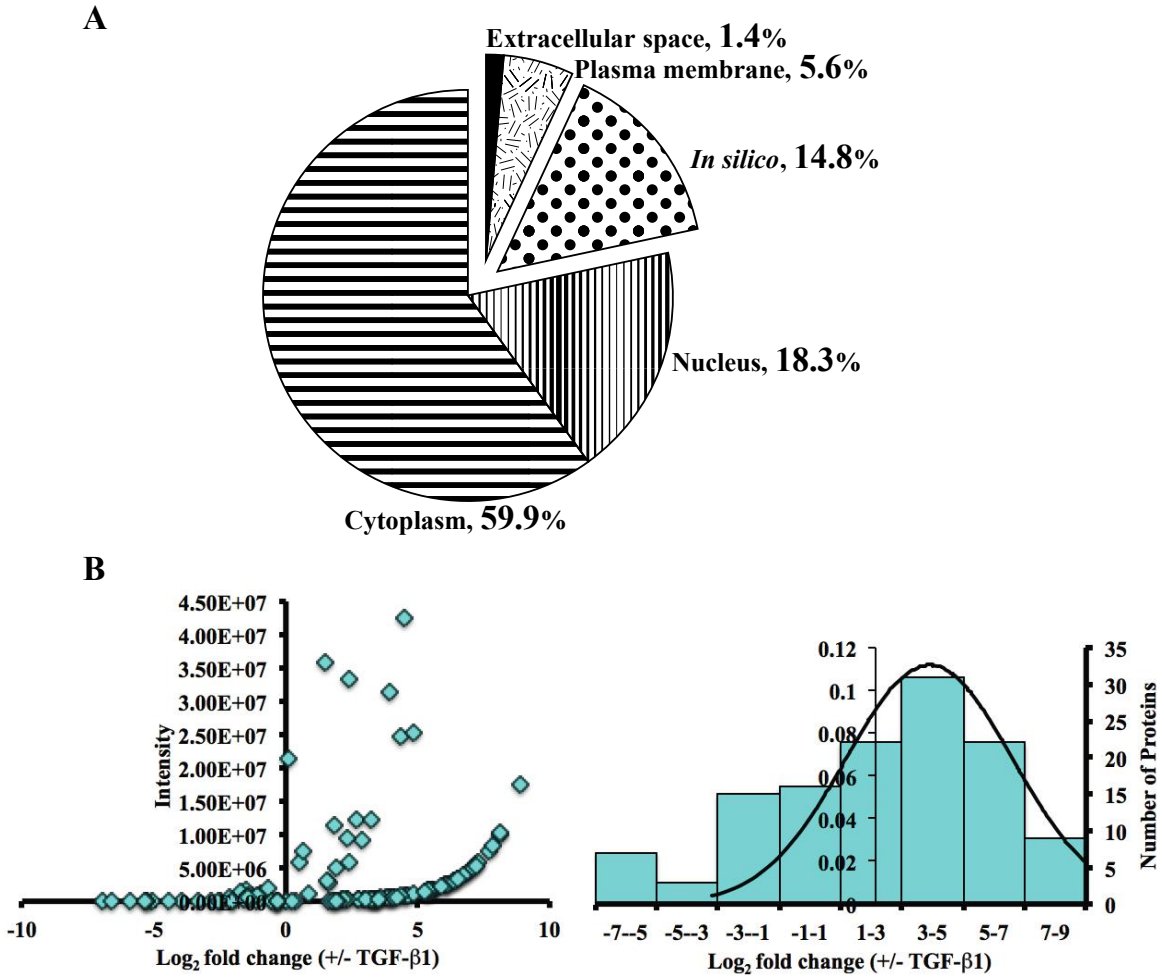

Figure 3.16 (A) Subcellular localization of the identified proteins. (B) Left panel: Scatter plot of intensity and log2-fold change of TGF-β-induced protein expression; Right panel: The distribution of log2 ratio (+/-TGF-β1) of the identified proteins. More proteins were upregulated than downregulated during TGF-β1-induced EMT in NMuMG cells.

the GO term analysis are in agreement with the fact that the O-GlcNAc is a PTM of nucleocytoplasmic proteins. However, some few plasma membrane and extracellular proteins bearing O- and N-glycans were also enriched. This is not surprising because the bioorthogonal reporter used this study, namely AC4GalNAz, is likely to be incorporated in glycans where GalNac occurs thereby resulting in proteins with complex glycans being enriched in mixture with the O-GlcNAc modified proteins. Nevertheless, efforts to minimize azido-labeling of O- and N-glycans were undertaken as suggested and done in other studies. Such efforts were successfully implemented since our data consists mostly of nucleocytoplasmic proteins.

3.4.7.2.Canonical Pathways

The results of the GO analyses show that the highly represented and/or enriched biological functions and diseases and well as pathways and networks in our data support breast cancer and cancer metastasis. Figure 3.17 (*Left panel*) is a bar chart showing canonical metabolic pathways that are significantly enriched in the experimental data. Out of the 16 metabolic pathways that were significantly enriched, the first two, Glycolysis I and Gluconeogenesis I, corresponding to glucose metabolism, are enriched 3-4 fold higher than the others. This corroborates proteomic findings in other studies and supports the fact about elevation of glucose metabolism in cancer cells. Majority of the metabolic pathways had 30% representative proteins (ratio=0.3) in the experimental data. Figure 3.17 (*Right panel*) is a bar chart showing canonical signaling pathways that are significantly enriched in the experimental data. A total of 68 signaling pathways were significantly enriched in our data set. Of the first 6 highly enriched pathways, 3 have been implicated in proteomic studies pertaining to TGF-β1-induced EMT. These are

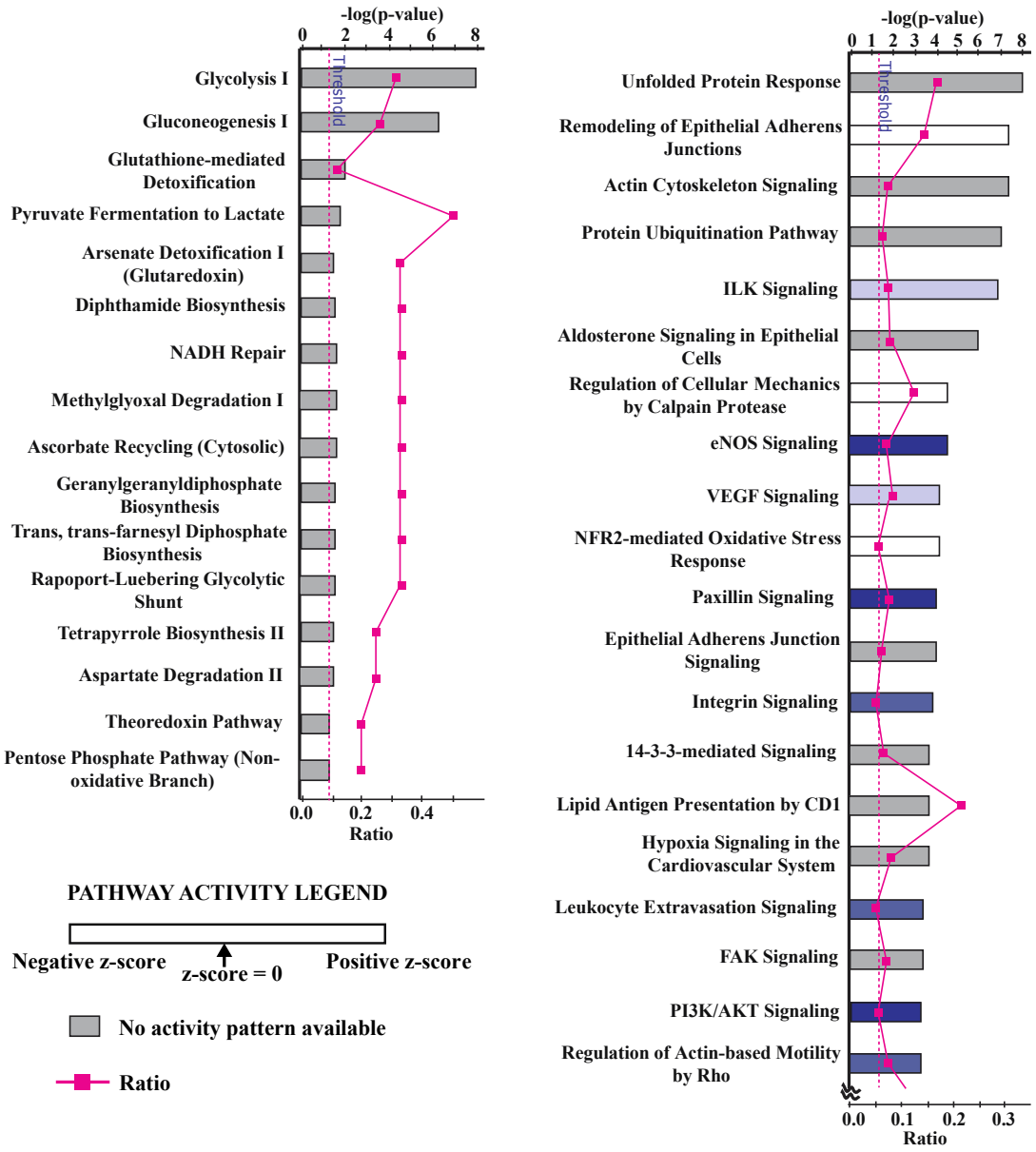

Figure 3.17 Cellular metabolic (left panel) and signaling (right panel) pathways responding to TGF-β1 induction in NMuMG cells. The y-axis represents the pathways identified. The x-axis (upper) represents significance of each pathway based upon the p-values determined using Right-tailed Fisher's exact test with threshold less that 0.05 ($p < 0.05$). The ratio of the number of proteins in a given pathway satisfying the cutoff to the total number of proteins present in that pathway was determined. In addition, each pathway's activity pattern represented by a Z-score showing decrease on increase in the overall activity as contributed by individual proteins in the pathway has been displayed as colored bars. Only a few signaling pathways had their activity patterns available.

Remodeling of Epithelial Adherens Junctions, Actin Cytoskeleton signaling and Protein Ubiquitination pathway. Different to metabolic pathways, majority of the signaling pathways have only about 5%representation in the experimental data, but similar to metabolic pathways, many signaling pathways show no pattern of prediction direction.

3.4.7.3 Biological Functions and Networks

The biological functions that were most significant to the enriched networks were determined and using the Fisher's exact test, the probability that each biological function assigned to a network was due to chance alone was calculated. Table 3.2 shows that the top interacting networks of TGF-β1-responsive gene products were significantly enriched for molecular and cellular functions of cancer metastasis, cell cycle, cellular movement and carbohydrate metabolism, among others. Examination of the visualized network reveals the observed functions. The upstream regulators in this network are genes for β-Catenin, Cyclin D1, Caveolin 1, and Receptor tyrosine-protein kinase erbB-2 (also known as human epidermal growth factor receptor 2). These regulators either singly or associatively modulate activity of several genes relevant to EMT and cancer metastasis in response to TGF-β1.

β-Catenin interacts with E-cadherin in the adherens junctions and both are down-regulated during TGF-β1 treatment. In the experimental data such interactions resulted in upregulation of ACTB, BTF3, CD44 and PSAP among the O-GlcNAc-modified proteins. Simultaneousy the scaffolding protein Caveolin 1 indirectly modulates several keratins, HSPA8 and Cyclin D1. All, but Cyclin D1 were upregulated in the experiment. The only upstream regulator of E-cadherin in this network is Protein Kinase AMP-Activated,

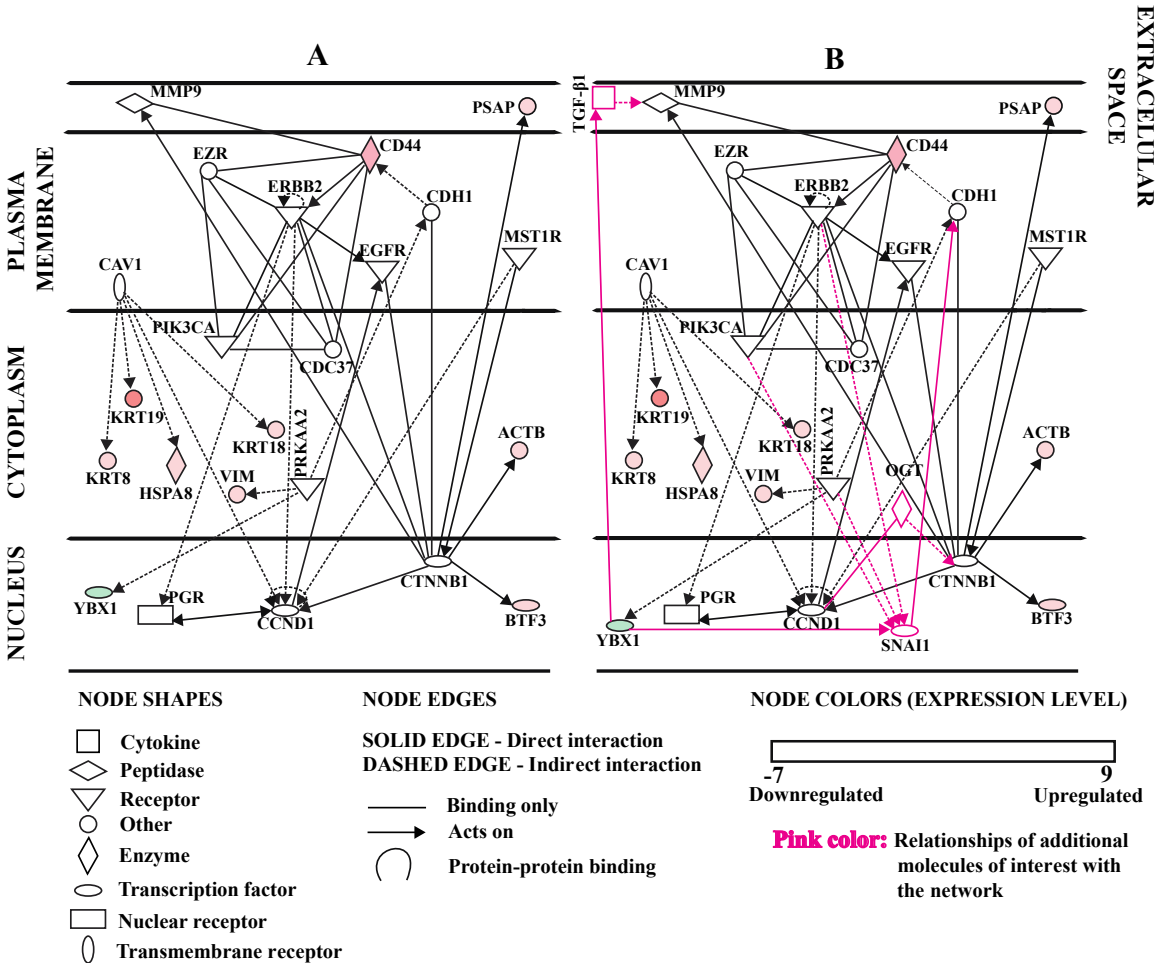

Figure 3.18 (A) Ingenuity Pathway Analysis was used to extract and display nodes overlaid with expression levels for proteins belonging to the top regulatory network enriched in the experimental data. This network is involved in metastasis. The upregulated proteins are displayed in red while the down-regulated proteins are in green. The colorless nodes represent proteins extracted *in silico*. The scale bar shows the range of fold changes. (B) Additional proteins SNAIL, TGF-β1 and OGT were included and their relationships with the proteins in the network are displayed.

alpha 2 (PRKAA2), a molecule that also indirectly upregulated Vimentin and down-regulated YBX1. Three extra genes, SNAI1, OGT and TGF-β1 were added to the network occurring in breast cancer cell lines to see if they might interact with the existing genes. These three regulators barely interact with any of the genes expressed in the dataset. However, SNAI1 regulates several genes in the network including E-cadherin gene. The down-regulated YBX1 acts upstream of SNAI1 and TGF-β1. The regulatory activity of TGF-β1 in this network is limited to modulation of ECM protein MMP9 while that of OGT includes interaction with Cyclin D1 and modulation of β-Catenin. The network does not show any crosstalk between regulatory activities of OGT and TGF-β1. However, there may be co-regulation on MMP9 originating from SNAI1 and TGF-β1.

3.4.8 Relevance of the Proteomics Data to EMT

In the post-genomic era proteome-wide genome-scale studies report gene expression maps for understanding mechanisms underlying biological functions and disease processes, the same way large-scale transcriptional analyses do. However, there are only a few proteomic studies of EMT compared to genomic and transcriptomic studies. In such proteomic analyses, tumor tissues undergoing EMT have been probed using tandem mass spectrometry techniques to identify differentially expressed and hence EMT-regulated proteins. *In silico* analyses of the protein-protein networks of these signatures have enabled establishment of the roles of proteins involved in EMT and metastasis, thus shedding new insights to the understanding of EMT. Biarc and co-workers have provided comprehensive EMT signatures obtained from proteomic profiling of MCF-10A cells following induction of EMT by two different signals, mutant K-Ras^{v12} and TGF-β[8]. Gene Ontology classification of these signatures pointed to enhancement of cellular processes

and functions that support cancer progression. Among the functional classes of proteins differentially expressed were EMT inducers, ECM proteins, adhesion proteins, cytoskeletal proteins, degradation machinery, translation machinery and glucose metabolic machinery. The revelation of increase in glucose metabolism during EMT raises a question about the influence of such metabolic changes to O-GlcNAcylation of nucleocytoplasmic proteins, a possible alternate route for upregulation of EMT regulators such as transcription factors through changing their localization and stability due to the O-GlcNAc PTM. To this end no large-scale O-GlcNAc proteomic studies have been reported on TGF-β1-induced EMT.

In this study we hypothesized that focusing functional proteomics to O-GlcNAc signatures would provide insights into the crosstalk between TGF-β1-induced EMT and O-GlcNAcylation, since both processes cause repression of E-cadherin leading to invasion and metastasis. The O-GlcNAc signatures reported herein are only putative since their O-GlcNAc modification sites were not mapped. The label-free quantification was not replicated hence the level of confidence of differential expression as a result of TGF-β1 induction could not be statistically determined. Moreover, the identification and the O-GlcNAc PTM of the proteins were not validated by western blotting as well as ETD-MS/MS for O-GlcNAc site-mapping. As a result, the novel analytical method is not sufficiently comprehensive. However, despite these shortcomings, the proteomic results obtained using the strained-alkyne terminated bead probe underscore several published EMT and O-GlcNAc reports (Figure 3.19). As described in detail below, our potential O-GlcNAc signature consists of functional classes of proteins shown in previous studies to support EMT and metastatic phenotypes. Figure 3.19A shows that 75% of the identified

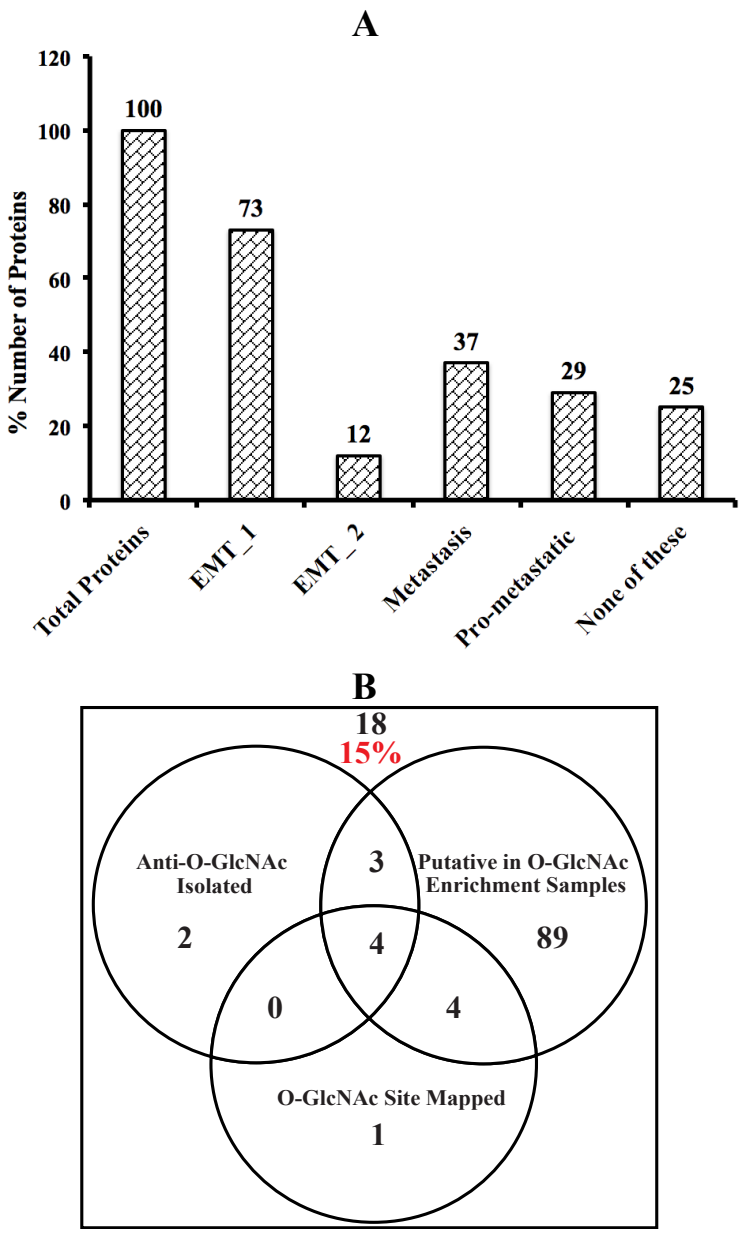

Figure 3.19 (A) 75% of the potentially O-GlcNAc proteins in a TGF-induced EMT have been previously identified in other related signatures[2, 8, 44-45]. EMT_1 (EMT signatures); EMT_2 (EMT-associated signature). (B) Out of 121, 100 proteins have been previously identified in putative O-GlcNAc enrichment samples[23, 36, 46-47]. Some of these proteins have O-GlcNAc sites mapped while others have been isolated by anti-O-GlcNAc immunoprecipitation[21, 23, 46]. 18 proteins do not appear in any of the O-GlcNAc literature.

proteome appears in EMT and metastatic signatures presented in other studies. However, unlike previous studies that demonstrated a set of proteomic EMT signature, our study shows only a subset that is potentially O-GlcNAcylated.

EMT is regulated at different levels of gene expression: transcriptionally and epigenetically, post-transcriptionally by non-coding RNAs and alternative splicing, translationally as well as post-translationally[48]. Our data contains some evidence of EMT regulation. The heterogenous nuclear ribonucleoproteins HNRNPA2B1, HNRNPC and HNRNPK were upregulated. This family of proteins is RNA-binding and is involved in the regulation of EMT-specific differential splicing[48]. An mRNA-binding protein, transcription factor, YB1 was downregulated. This protein controls translation of EMT-associated transcription factors SNAIL and ZEB family members[48]. Its overexpression in breast cancer is known to induce EMT. Its downregulation in our data suggests that translation of EMT-associated transcription factors might have been controlled by other factors. However, the *in silico* analysis shows that YB1 is upstream of SNAIL1 suggesting that at the time when the cells were harvested, i.e. towards completion of EMT in NMuMG cells, YB1 was no longer in control and was downregulated.

Successful EMT relies on the ability of the EMT-associated transcription factors to trigger cellular reprogramming[49]. Transcriptional regulation of EMT centers around the activities of the nuclear factors SNAIL, ZEB and TWIST families, which interact with several proteins in highly regulated networks to accomplish EMT[50]. None of these nuclear factors were observed in our data. Epigenetically, the activity of the EMT-associated transcription factors is known to be enhanced by their close interaction with chromatin modifiers such histone deacetylases[48]. Although no epigenetic modifiers were

upregulated in our data, several histones, including histone H3 were upregulated suggesting that they could be products of deacetylation associated with regulation of EMT. One chromatin modifier HMGB1 was downregulated probably because by the end of EMT it was no longer expressed and hence was downregulated.

Despite being tightly regulated, the EMT program involves many cellular changes that include loss of E-cadherin-mediated intercellular adhesion, loss of apical-basal polarity and concomitant acquisition of migratory behavior, as well as reorganization of the actin cytoskeleton[51]. Similar to other proteomic studies[2, 8], our data support EMT-associated changes. Among the canonical pathways, remodeling of epithelial adherens junctions and actin cytoskeleton signaling were over-represented. Some cytoskeletal proteins of the intermediate filaments, keratins (KRT8/18/19) and vimentin were upregulated. Keratins 8/18 pair, and vimentin are well characterized EMT markers[52] that are also O-GlcNAc proteins[23, 46]. Vimentin, in particular, is often ubiquitously isolated from EMT and metastasis samples of many cancers[2, 45]. Actin microfilament associated proteins, profilin-1, cofilin-1 and vinculin were upregulated. Microtubule-associated proteins, annexin A8 and microtubule-associated protein R/B 1 were also upregulated

EMT is associated with elevated levels of translation[8]. In eukaryotic cells, translation machinery occurs as translasome, the supercomplex structures within eIF3 interactome[53]. These structures contain proteins involved in translation initiation, translation elongation, ribosome biogenesis, quality control and transport, all linked together to facilitate efficient protein synthesis. In this study, representative proteins indicative of these processes were identified. Although no translation initiation factors were obtained, the translation elongation factors EEF1D and EEF2 were upregulated.

EEF2 has previously been associated with breast cancer metastasis[45]. For ribosome biogenesis, ADP-ribosylation factor 5, a GTP-binding protein that is involved in protein trafficking was upregulated. Ribosomal protein SA required for assembly and stability of 40S ribosomal subunit was upregulated. For quality control and transport, Importin-β, a nuclear transporter was upregulated. Several components of the degradation machinery were observed in our data and the proteasomal ubiquitination canonical pathway was significantly overrepresented. Different Chaperonin-containing TCP1 subunits (CCT7 experimentally and CCT3/4/5/6/8 *in silico*), as well as heat shock proteins 90 kDA (HSP90 AA1/AB1/B1), 70 kDA (HSPA 4//5/8/9) and 60 kDA (HSPD1) were upregulated. HSP90B1 has been previously associated with breast cancer metastasis[54]. Together with other heat shock proteins, calreticulin, an ER resident protein and calcium-binding chaperone, was highly upregulated. The unfolded protein response, a canonical pathway for cellular adaptation to ER stress was highly overrepresented in our data. The cellular defense response to oxidative stress was also overrepresented since members of the NRF2-mediated oxidative stress response pathway such as the Glutathione S-transferase proteins were upregulated. Only 1of the 5 proteasomal subunits was upregulated. Our data suggests that TGF-β induction might be inhibitory to expression of the proteasomal proteins.

Due to a plethora of molecular changes, cells undergoing EMT have higher energy requirements, especially for protein synthesis and general anabolism[8]. Both glycolysis and gluconeogenesis I were among significantly enriched canonical pathways. 32% of Glycolytic enzymes were observed while 3% of the gluconeogenetic enzymes were obtained. All these proteins were upregulated by TGF-β induction. Interestingly the

Glycolysis pathway enzymes observed among the O-GlcNAc proteome include the series of enzymes from triose phosphate isomerase down to pyruvate kinase. Glycolysis provides both energy and metabolic intermediates while Gluconeogenesis recycles non-sugar intermediary carbon sources back to glucose for feeding into glycolysis[55]. Malate dehydrogenase was upregulated in our data and it is known for producing NADPH for fatty-acid synthesis[8]. The fatty-acid binding protein 5 was upregulated too.

Still on carbohydrate metabolism, CD44 a hydrolytic enzyme for hyaluronic acid (HA) and a membrane receptor for HA and ECM proteins was upregulated. CD44 appears here as part of the metastatic regulatory network that was overrepresented in the experimental data. CD44 is a glycoprotein with N-linked and O-linked complex glycans. However, since the O-GlcNAc PTMs of proteins in the data have not been validated by site-mapping, it is difficult to tell whether CD44 falsely appears in the O-GlcNAc proteome or that CD44 has an unknown O-GlcNAc site. However, presence of CD44 in the data is in line with a study showing that cells that have undergone EMT have stem-like properties and TGF-β1 induction is known to promote stemness[56-57]. CD44 is a marker for stemness and the expression pattern of $CD44^{high}/CD24^{low}$ is characteristic of cells with stem-like properties.

3.4.8 Does the O-GlcNAc EMT Signature Reflect any Role of the O-GlcNAc PTM?

O-GlcNAcylation has previously been found to promote breast cancer progression[9]. OGT silencing and OGA pharmacological inhibition studies have shown that O-GlcNAcylation alters migration and metastasis via downregulation of E-cadherin. Moreover O-GlcNAcylation of β-Catenin and p120, the binding partners of E-cadherin, was thought to

play a role in cell surface localization as well as binding to E-cadherin in adherens junctions. Those studies, however, did not provide sufficient information on the molecular mechanisms behind the changes in migration and metastasis. In the current study, the *in silico* analysis of the potentially O-GlcNAc proteome of the TGF-β1-induced EMT implicates enrichment of EMT and metastasis-associated regulatory network, the core of which features two transcription factors that are regulated by OGT, namely; β-Catenin and Cyclin D1. This network strengthens our hypothesis that there may be cooperation between TGF-β signaling and O-GlcNAcylation in promoting cancer growth, EMT, migration and metastasis. Perhaps the hyperglycaemic conditions associated with SNAIL O-GlcNAcylation in Park *et al*.[10] would enhance such cooperation by elevating the levels of UDP-GlcNAc. In order to test the hypothesis, further studies are necessary to validate identification of some key proteins as well as their O-GlcNAc PTM, and to ensure that they are differentially expressed in the context of TGF-β1-induced EMT.

3.5 CONCLUSIONS

By coupling DBCO-SS-NHS ester to NH_2-terminated beaded resin, a cleavable azide-reactive dibenzocyclooctyne-disulphide resin was developed for the affinity enrichment of O-GlcNAc modified proteins. UV-Vis measurements proved that the new affinity resin had the similar loading capacity as the original resin, and MALDI-TOF measurements showed that the resin is azide-reactive. Successful metabolic labeling of NIH3T3 and NMuMG cells was detected by fluorescence microscopy and SDS-PAGE in combination with in-gel fluorescence scanning. FITC-alkyne, DBCO-fluorescein, DBCO-naphthalimide and 3-azido-7-hydroxycoumarin were used as fluorescent probes. Despite

of the strong signals in fluorescence microscopy, the in-gel fluorescence signals were fairly weak and seemed to be impeded by abundant nonspecific binding proteins. Successful affinity enrichment of GalNAz-labeled proteins from protein extracts provided confidence to apply the affinity enrichment strategy to NMuMG cells undergoing EMT.

Examination of the O-GlcNAc proteome of TGF-β1-induced EMT revealed some insights that underscore findings in other cancer proteomics and O-GlcNAc studies. Representative functional proteins were detected, and among them were enzymes of the glycolysis pathway as well as EMT and metastasis markers such as vimentin. Gene ontology analyses showed that majority of the proteins are nucleocytoplasmic and that, the highly overrepresented pathways included glycolysis and many TGF-β non-canonical pathways. NMuMG cells undergoing EMT resemble tumor progression stage in which carcinoma *in situ* cells acquire mesenchymal characteristics and migrate to invade the surrounding stroma. Upregulation of glycolysis is a characteristic of cancer, which due to "Warburg effect" leads to upregulation of hexose biosynthetic pathway and increase in UDP-GlcNAc, with the result that many nucleocytoplasmic proteins are aberrantly O-GlcNAcylated[11, 20, 58]. The stability and nuclear localization of some transcription EMT inducers such as Snail1 is regulated in this way[10]. Snail and other transcription factors were not obtained in this study. However, *in silico* protein-protein interactions revealed a metastatic regulatory network featuring genes that are regulated by Snail1 such as E-cadherin and MMP-9. Previous Cell biology studies in which GlcNAcylation correlated positively with metastasis and negatively with E-cadherin expression implicated influence of GlcNAcylation on interactions of proteins E-cadherin, β-Catenin and p120

(Catenin delta-1), where E-cadherin level decreased probably due to GlcNAcylation of β-Catenin and p120[9]. These studies did not investigate any cancer-associated signaling processes. Neither did they identify GlcNAc site on adhesion proteins nor its role in modulating E-cadherin. The β-Catenin regulated network generated *in silico* in this study leads us to hypothesize that TGF-β signaling would cooperate with GlcNAcylation during cancer progression to promote metastasis initiated via EMT. Future studies should aim at validating protein identification and mapping the O-GlcNAc sites on identified proteins to establish the role of site-specific GlcNAcylation.

Future research can also be conducted to improve the SPAAC "click chemistry"-based affinity enrichment strategy. Selectivity and specificity of the bead probe could be better ascertained by doing investigations with synthetic GalNAz-labeled proteins, instead of unlabeled proteins. In addition, extensive but focused sample pre-fractionation for enrichment of nuclear fraction would be ideal for identification of O-GlcNAc-modified transcription factors.

REFERENCES

1. E. Foubert, B. De Craene, G. Berx, Key signalling nodes in mammary gland development and cancer. The Snail1-Twist1 conspiracy in malignant breast cancer progression. *Breast Cancer Res.*, **2010,** 12.

2. D. Vergara, P. Simeone, P. del Boccio, C. Toto, D. Pieragostino, A. Tinelli, *et al.*, Comparative proteome profiling of breast tumor cell lines by gel electrophoresis and mass spectrometry reveals an epithelial mesenchymal transition associated protein signature. *Mol. Biosyst.*, **2013,** 9, 1127-1138.

3. J. P. Thiery, J. P. Sleeman, Complex networks orchestrate epithelial-mesenchymal transitions. *Nat. Rev. Mol. Cell Biol.*, **2006,** 7, 131-142.

4. G. J. Inman, F. J. Nicolas, J. F. Callahan, J. D. Harling, L. M. Gaster, A. D. Reith, *et al.*, SB-431542 is a potent and specific inhibitor of transforming growth factor-beta superfamily type I activin receptor-like kinase (ALK) receptors ALK4, ALK5, and ALK7. *Mol. Pharmacol.*, **2002,** 62, 65-74.

5. S. Cha, M. B. Imielinski, T. Rejtar, E. A. Richardson, D. Thakur, D. C. Sgroi, *et al.*, In situ proteomic analysis of human breast cancer epithelial cells using laser capture microdissection: annotation by protein set enrichment analysis and gene ontology. *Mol. Cell. Proteomics,* **2010,** 9, 2529-2544.

6. C. M. Perou, T. Sorlie, M. B. Eisen, M. van de Rijn, S. S. Jeffrey, C. A. Rees, *et al.*, Molecular portraits of human breast tumours. *Nature,* **2000,** 406, 747-752.

7. J. D. Wulfkuhle, K. C. McLean, C. P. Paweletz, D. C. Sgroi, B. J. Trock, P. S. Steeg, *et al.*, New approaches to proteomic analysis of breast cancer. *Proteomics,* **2001,** 1, 1205-1215.

8. J. Biarc, P. Gonzalo, I. Mikaelian, L. Fattet, M. Deygas, G. Gillet, *et al.*, Combination of a discovery LC-MS/MS analysis and a label-free quantification for the characterization of an epithelial-mesenchymal transition signature. *J. Proteomics,* **2014,** 110, 183-194.

9. Y. Gu, W. Mi, Y. Ge, H. Liu, Q. Fan, C. Han, *et al.*, GlcNAcylation plays an essential role in breast cancer metastasis. *Cancer Res.*, **2010,** 70, 6344-6351.

10. S. Y. Park, H. S. Kim, N. H. Kim, S. Ji, S. Y. Cha, J. G. Kang, *et al.*, Snail1 is stabilized by O-GlcNAc modification in hyperglycaemic condition. *EMBO J.*, **2010,** 29, 3787-3796.

11. C. Slawson, R. J. Copeland, G. W. Hart, O-GlcNAc signaling: a metabolic link between diabetes and cancer? *Trends Biochem. Sci.*, **2010,** 35, 547-555.

12. T. Issad, M. Kuo, O-GlcNAc modification of transcription factors, glucose sensing and glucotoxicity. *Trends Endocrinol. Metab.*, **2008,** 19, 380-389.

13. S. Ozcan, S. S. Andrali, J. E. Cantrell, Modulation of transcription factor function by O-GlcNAc modification. *Biochim. Biophys. Acta*, **2010,** 1799, 353-364.

14. K. Kamemura, B. K. Hayes, F. I. Comer, G. W. Hart, Dynamic interplay between O-glycosylation and O-phosphorylation of nucleocytoplasmic proteins: alternative glycosylation/phosphorylation of THR-58, a known mutational hot spot of c-Myc in lymphomas, is regulated by mitogens. *J. Biol. Chem.*, **2002,** 277, 19229-19235.

15. A. Moustakas, C. H. Heldin, Induction of epithelial-mesenchymal transition by transforming growth factor beta. *Semin. Cancer Biol.*, **2012,** 22, 446-454.

16. J. Xue, X. Lin, W. T. Chiu, Y. H. Chen, G. Yu, M. Liu, *et al.*, Sustained activation of SMAD3/SMAD4 by FOXM1 promotes TGF-beta-dependent cancer metastasis. *J. Clin. Invest.*, **2014,** 124, 564-579.

17. S. Thuault, E. J. Tan, H. Peinado, A. Cano, C. H. Heldin, A. Moustakas, HMGA2 and Smads co-regulate SNAIL1 expression during induction of epithelial-to-mesenchymal transition. *J. Biol. Chem.*, **2008,** 283, 33437-33446.

18. T. Vincent, E. P. Neve, J. R. Johnson, A. Kukalev, F. Rojo, J. Albanell, *et al.*, A SNAIL1-SMAD3/4 transcriptional repressor complex promotes TGF-beta mediated epithelial-mesenchymal transition. *Nat. Cell Biol.*, **2009,** 11, 943-950.

19. S. Olivier-Van Stichelen, V. Dehennaut, A. Buzy, J. L. Zachayus, C. Guinez, A. M. Mir, *et al.*, O-GlcNAcylation stabilizes beta-catenin through direct competition with phosphorylation at threonine 41. *FASEB J.*, **2014,** 28, 3325-3338.

20. S. A. Caldwell, S. R. Jackson, K. S. Shahriari, T. P. Lynch, G. Sethi, S. Walker, *et al.*, Nutrient sensor O-GlcNAc transferase regulates breast cancer tumorigenesis through targeting of the oncogenic transcription factor FoxM1. *Oncogene*, **2010,** 29, 2831-2842.

21. L. Wells, K. Vosseller, R. N. Cole, J. M. Cronshaw, M. J. Matunis, G. W. Hart, Mapping sites of O-GlcNAc modification using affinity tags for serine and threonine post-translational modifications. *Mol. Cell. Proteomics*, **2002,** 1, 791-804.

22. K. Vosseller, J. C. Trinidad, R. J. Chalkley, C. G. Specht, A. Thalhammer, A. J. Lynn, *et al.*, O-linked N-acetylglucosamine proteomics of postsynaptic density preparations using lectin weak affinity chromatography and mass spectrometry. *Mol. Cell. Proteomics*, **2006,** 5, 923-934.

23. J. C. Trinidad, D. T. Barkan, B. F. Gulledge, A. Thalhammer, A. Sali, R. Schoepfer, *et al.*, Global identification and characterization of both O-GlcNAcylation and phosphorylation at the murine synapse. *Mol. Cell. Proteomics*, **2012,** 11, 215-229.

24. N. Khidekel, S. B. Ficarro, E. C. Peters, L. C. Hsieh-Wilson, Exploring the O-GlcNAc proteome: direct identification of O-GlcNAc-modified proteins from the brain. *Proc. Natl. Acad. Sci. U. S. A.*, **2004,** 101, 13132-13137.

25. N. Khidekel, S. B. Ficarro, P. M. Clark, M. C. Bryan, D. L. Swaney, J. E. Rexach, *et al.*, Probing the dynamics of O-GlcNAc glycosylation in the brain using quantitative proteomics. *Nat. Chem. Biol.*, **2007,** 3, 339-348.

26. M. A. Nessen, G. Kramer, J. Back, J. M. Baskin, L. E. J. Smeenk, L. J. de Koning, *et al.*, Selective Enrichment of Azide-Containing Peptides from Complex Mixtures. *J. Proteome Res.*, **2009,** 8, 3702-3711.

27. H. Hahne, N. Sobotzki, T. Nyberg, D. Helm, V. S. Borodkin, D. M. van Aalten, *et al.*, Proteome wide purification and identification of O-GlcNAc-modified proteins using click chemistry and mass spectrometry. *J. Proteome Res.*, **2013,** 12, 927-936.

28. A. J. Howden, V. Geoghegan, K. Katsch, G. Efstathiou, B. Bhushan, O. Boutureira, *et al.*, QuaNCAT: quantitating proteome dynamics in primary cells. *Nat. Methods*, **2013,** 10, 343-346.

29. R. P. Temming, M. van Scherpenzeel, E. te Brinke, S. Schoffelen, J. Gloerich, D. J. Lefeber, *et al.*, Protein enrichment by capture-release based on strain-promoted

cycloaddition of azide with bicyclononyne (BCN). *Bioorg. Med. Chem.*, **2012,** 20, 655-661.

30. G. A. Grant, S. L. Frison, J. Yeung, T. Vasanthan, P. Sporns, Comparison of MALDI-TOF mass spectrometric to enzyme colorimetric quantification of glucose from enzyme-hydrolyzed starch. *J. Agric. Food Chem.*, **2003,** 51, 6137-6144.

31. X. Duan, H. Li, H. Chen, Q. Wang, Discrimination of colon cancer stem cells using noncanonical amino acid. *Chem. Commun. (Camb.)*, **2012,** 48, 9035-9037.

32. X. Duan, L. Cai, L. A. Lee, H. Chen, Q. Wang, Incorporation of azide sugar analogue decreases tumorigenic potential of breast cancer cells by reducing cancer stem cell population. *Science China Chemistry*, **2013,** 56, 279-285.

33. K. E. Beatty, J. Szychowski, J. D. Fisk, D. A. Tirrell, A BODIPY-Cyclooctyne for Protein Imaging in Live Cells. *ChemBioChem*, **2011,** 12, 2137-2139.

34. K. Liu, P. Y. Yang, Z. Na, S. Q. Yao, Dynamic monitoring of newly synthesized proteomes: up-regulation of myristoylated protein kinase A during butyric acid induced apoptosis. *Angew. Chem. Int. Ed. Engl.*, **2011,** 50, 6776-6781.

35. S. Lamouille, E. Connolly, J. W. Smyth, R. J. Akhurst, R. Derynck, TGF-beta-induced activation of mTOR complex 2 drives epithelial-mesenchymal transition and cell invasion. *J. Cell Sci.*, **2012,** 125, 1259-1273.

36. B. W. Zaro, Y. Y. Yang, H. C. Hang, M. R. Pratt, Chemical reporters for fluorescent detection and identification of O-GlcNAc-modified proteins reveal glycosylation of the ubiquitin ligase NEDD4-1. *Proc. Natl. Acad. Sci. U. S. A.*, **2011,** 108, 8146-8151.

37. M. Boyce, I. S. Carrico, A. S. Ganguli, S. H. Yu, M. J. Hangauer, S. C. Hubbard, *et al.*, Metabolic cross-talk allows labeling of O-linked beta-N-acetylglucosamine-modified proteins via the N-acetylgalactosamine salvage pathway. *Proc. Natl. Acad. Sci. U. S. A.*, **2011,** 108, 3141-3146.

38. B. W. Zaro, L. A. Bateman, M. R. Pratt, Robust in-gel fluorescence detection of mucin-type O-linked glycosylation. *Bioorg. Med. Chem. Lett.*, **2011,** 21, 5062-5066.

39. Q. Wang, T. R. Chan, R. Hilgraf, V. V. Fokin, K. B. Sharpless, M. G. Finn, Bioconjugation by copper(I)-catalyzed azide-alkyne [3 + 2] cycloaddition. *J. Am. Chem. Soc.,* **2003,** 125, 3192-3193.

40. K. Sivakumar, F. Xie, B. M. Cash, S. Long, H. N. Barnhill, Q. Wang, A fluorogenic 1,3-dipolar cycloaddition reaction of 3-azidocoumarins and acetylenes. *Organic letters,* **2004,** 6, 4603-4606.

41. C. Le Droumaguet, C. Wang, Q. Wang, Fluorogenic click reaction. *Chem. Soc. Rev.,* **2010,** 39, 1233-1239.

42. H. C. Hang, C. Yu, D. L. Kato, C. R. Bertozzi, A metabolic labeling approach toward proteomic analysis of mucin-type O-linked glycosylation. *Proc. Natl. Acad. Sci. U. S. A.,* **2003,** 100, 14846-14851.

43. S. Saha, X. Duan, L. Wu, P. K. Lo, H. Chen, Q. Wang, Electrospun fibrous scaffolds promote breast cancer cell alignment and epithelial-mesenchymal transition. *Langmuir,* **2012,** 28, 2028-2034.

44. S. Ramaswamy, K. N. Ross, E. S. Lander, T. R. Golub, A molecular signature of metastasis in primary solid tumors. *Nat. Genet.,* **2003,** 33, 49-54.

45. M. Sato, T. Matsubara, J. Adachi, Y. Hashimoto, K. Fukamizu, M. Kishida, *et al.,* Differential Proteome Analysis Identifies TGF-beta-Related Pro-Metastatic Proteins in a 4T1 Murine Breast Cancer Model. *PLoS One,* **2015,** 10, e0126483.

46. Z. Wang, N. D. Udeshi, C. Slawson, P. D. Compton, K. Sakabe, W. D. Cheung, *et al.,* Extensive crosstalk between O-GlcNAcylation and phosphorylation regulates cytokinesis. *Science signaling,* **2010,** 3, ra2.

47. Z. Gurel, B. W. Zaro, M. R. Pratt, N. Sheibani, Identification of O-GlcNAc modification targets in mouse retinal pericytes: implication of p53 in pathogenesis of diabetic retinopathy. *PLoS One,* **2014,** 9, e95561.

48. B. De Craene, G. Berx, Regulatory networks defining EMT during cancer initiation and progression. *Nat. Rev. Cancer,* **2013,** 13, 97-110.

49. C. H. Heldin, M. Landstrom, A. Moustakas, Mechanism of TGF-beta signaling to growth arrest, apoptosis, and epithelial-mesenchymal transition. *Curr. Opin. Cell Biol.,* **2009,** 21, 166-176.

50. H. Peinado, D. Olmeda, A. Cano, Snail, Zeb and bHLH factors in tumour progression: an alliance against the epithelial phenotype? *Nat. Rev. Cancer,* **2007,** 7, 415-428.

51. S. B. Jakowlew, Transforming growth factor-beta in cancer and metastasis. *Cancer Metastasis Rev.,* **2006,** 25, 435-457.

52. K. Lee, C. M. Nelson, New insights into the regulation of epithelial-mesenchymal transition and tissue fibrosis. *Int. Rev. Cell Mol. Biol.,* **2012,** 294, 171-221.

53. Z. Sha, L. M. Brill, R. Cabrera, O. Kleifeld, J. S. Scheliga, M. H. Glickman, *et al.*, The eIF3 interactome reveals the translasome, a supercomplex linking protein synthesis and degradation machineries. *Mol. Cell,* **2009,** 36, 141-152.

54. H. H. Milioli, K. Santos Sousa, R. Kaviski, N. C. Dos Santos Oliveira, C. De Andrade Urban, R. S. De Lima, *et al.*, Comparative proteomics of primary breast carcinomas and lymph node metastases outlining markers of tumor invasion. *Cancer Genomics Proteomics,* **2015,** 12, 89-101.

55. J. M. Berg, J. L. Tymoczko, L. Stryer, *Biochemistry, 5th Edition*. W. H. Freeman: New York, 2002.

56. B. T. Hennessy, A. M. Gonzalez-Angulo, K. Stemke-Hale, M. Z. Gilcrease, S. Krishnamurthy, J. S. Lee, *et al.*, Characterization of a naturally occurring breast cancer subset enriched in epithelial-to-mesenchymal transition and stem cell characteristics. *Cancer Res.,* **2009,** 69, 4116-4124.

57. S. A. Mani, W. Guo, M. J. Liao, E. N. Eaton, A. Ayyanan, A. Y. Zhou, *et al.*, The epithelial-mesenchymal transition generates cells with properties of stem cells. *Cell,* **2008,** 133, 704-715.

58. C. Slawson, G. W. Hart, O-GlcNAc signalling: implications for cancer cell biology. *Nat. Rev. Cancer,* **2011,** 11, 678-684.

APPENDIX A

PROTEIN IDENTIFICATION AND LABEL-FREE QUANTIFICATION DATA

Table A.1 SPAAC enriched O-GlcNAc putative IPA-identified proteins

Protein IDs	Gene names	Log2(Int-Ind.)	Log2(Int-Non-ind)	Fold Change
P68134	Acta1	21.51	14.87	81.17
P60710	Actg1	25.00	22.60	5.28
A1BN54	Actn1	22.85	14.87	205.88
P57780	Actn4	20.61	14.87	43.54
P45376	Akr1b1	18.63	14.87	10.99
P10518	Alad	14.87	17.75	-7.32
P84084	Arf5	14.87	17.39	-5.71
Q99PT1	Arhgdia	21.71	14.87	93.24
Q64152-2	Btf3	19.22	14.87	16.61
P14211	Calr	22.48	14.87	159.34
B1ARS0	Cap1	18.52	14.87	10.20
D3YW48	Capns1	14.87	14.87	-1.23
P80314	Cct2	14.87	15.40	-1.44
P80313	Cct7	18.39	14.87	9.32
Q3U8S1	Cd44	21.22	14.87	66.47
P60766	Cdc42	19.24	14.87	16.79
P18760	Cfl1	22.49	21.96	1.45
Q80WV3	Chst2	18.71	14.87	11.64
D3Z036	Cops3	15.16	14.87	-1.01
F6QD74	Cyfip1	14.87	20.13	-38.34
D3Z7N2	Eef1d	18.93	14.87	13.61

Protein IDs	Gene names	Log2(Int-Ind.)	Log2(Int-Non-ind)	Fold Change
Q9D8N0	Eef1g	22.36	14.87	146.58
P58252	Eef2	16.96	14.87	3.45
P17182	Eno1	24.36	24.28	1.05
Q05816	Fabp5	19.05	21.22	0.22
Q920E5	Fdps	17.16	14.87	3.98
B7FAV1	Flna	22.02	14.87	115.29
Q80X90	Flnb	21.91	14.87	106.84
S4R257	Gapdh	22.45	20.02	5.39
E9PZF0	Gm20390	20.75	14.87	47.87
O09131	Gsto1	20.74	14.87	47.44
P19157	Gstp1	19.12	14.87	15.46
P63158	Hmgb1	14.87	21.48	-97.78
O88569-3	Hnrnpa2b1	18.65	14.87	11.16
Q9Z204-4	Hnrnpc	19.38	14.87	18.55
H3BLP7	Hnrnpk	18.38	14.87	9.29
P07901	Hsp90aa1	21.56	14.87	83.87
P11499	Hsp90ab1	23.54	20.29	9.49
Q3U2G2	Hspa4	18.17	14.87	8.01
P20029	Hspa5	23.44	21.58	3.64
P63017	Hspa8	24.59	19.75	28.78
P63038	Hspd1	21.25	14.87	67.88
P70168	Kpnb1	17.31	14.87	4.43
P05784	Krt18	24.90	21.00	14.91
P19001	Krt19	22.11	14.87	122.72

Protein IDs	Gene names	Log2(Int-Ind.)	Log2(Int-Non-ind)	Fold Change
P11679	Krt8	25.34	20.82	22.88
D3Z736	Ldha	21.65	14.87	89.58
P48678-3	Lmna	20.71	14.87	46.72
Q61166	Mapre1	17.35	14.87	4.53
P08249	Mdh2	22.39	14.87	149.53
P26041	Msn	21.59	20.03	2.96
K3W4R2	Myh14	15.52	14.87	1.28
Q60817	Naca	20.35	22.07	-3.30
P09405	Ncl	21.37	19.77	3.03
Q5NC80	Nme1	14.87	14.87	-1.23
Q3TQX1	Orc6	19.25	14.87	16.99
P09103	P4hb	23.11	20.24	7.32
P27773	Pdia3	22.27	14.87	137.20
P70296	Pebp1	14.87	20.20	-40.17
Q11136	Pepd	18.76	14.87	12.02
P62962	Pfn1	22.82	22.17	1.57
Q9DBJ1	Pgam1	22.99	14.87	226.06
P09411	Pgk1	21.33	14.87	71.83
P52480	Pkm	23.25	14.87	271.79
B1AXW5	Prdx1	20.21	21.13	-1.89
D3Z4A4	Prdx2	20.04	19.21	1.79
E9PZ00	Psap	19.65	14.87	22.40
P49722	Psma2	14.87	20.76	-59.02
Q9Z2U0	Psma7	18.95	20.39	-2.71

Protein IDs	Gene names	Log2(Int-Ind.)	Log2(Int-Non-ind)	Fold Change
Q9R1P1	Psmb3	19.51	20.60	-2.13
P99026	Psmb4	19.86	21.27	-2.67
P26516	Psmd7	18.55	14.87	10.46
Q5SW87	Rab1A	17.47	14.87	4.93
P54728	Rad23b	14.87	20.15	-38.90
P14206	Rpsa	20.54	14.87	41.38
P07091	S100a4	14.87	19.31	-21.66
Q62266	Sprr1a	14.87	14.87	-1.23
Q93092	Taldo1	14.87	17.43	-5.89
P26039	Tln1	17.51	14.87	5.07
H7BXC3	Tpi1	20.59	14.87	42.91
E9Q450	Tpm1	20.56	14.87	42.05
D3Z2H9	Tpm3	23.54	20.90	6.28
Q6IRU2	Tpm4	23.18	20.82	5.13
P10639	Txn	14.87	21.86	-127.12
Q64727	Vcl	21.06	14.87	59.35
Q01853	Vcp	19.01	14.87	14.38
P20152	Vim	24.56	20.20	20.53
A2BGG7	Ybx1	14.87	18.84	-15.69
P62259	Ywhae	23.30	14.87	281.49
P61982	Ywhag	18.31	14.87	8.81
F6YY69	Ywhaq	19.80	14.87	24.82

Table A.2 SPAAC enriched O-GlcNAc putative proteins not identified and not used in IPA

Protein IDs	Gene names	Log2(Int-Ind.)	Log2(Int-Non-ind)	Fold Change
A0A087WP98	Ptma	14.87	19.95	-33.66
B1AX58	Pls3	19.72	14.87	23.45
B1AYJ9	Ola1	16.98	14.87	3.52
Q9D312	Krt20	18.15	14.87	7.88
D3Z5N9	Snrpd2	14.87	18.16	-9.79
D6RHT5	Ddx39a	18.68	14.87	11.41
E0CZ27	Hist1h3a	22.26	20.33	3.80
F8WIX8	Hist1h2aa	25.10	23.62	2.78
G3UY49	Calu	16.81	14.87	3.13
Q921D0	Anxa8	19.99	14.87	28.23
P68373	Tuba1c	21.27	14.87	68.82
P08003	Pdia4	18.45	14.87	9.71
P08113	Hsp90b1	20.50	14.87	40.28
Q8CBB6	Hist1h2ba	14.87	15.94	-2.10
Q6ZWY9	Hist1h2bc	15.38	14.87	1.16
Q7TPM0	Cbx1	17.89	14.87	6.60
P24622-2	Cryaa	14.87	16.87	-4.01
P38647	Hspa9	19.51	14.87	20.31
P43275	Hist1h1a	19.65	20.98	-2.50
P43276	Hist1h1b	20.78	22.30	-2.87
P50543	S100a11	17.90	14.87	6.63

Protein IDs	Gene names	Log2(Int-Ind.)	Log2(Int-Non-ind)	Fold Change
P60335	Pcbp1	14.87	14.87	-1.23
P62204	Calm1	21.00	21.69	0.62
P62806	Hist1h4a	24.06	14.87	476.30
Q14AA6	Ran	18.50	14.87	10.07
P63028	Tpt1	19.09	14.87	15.18
P99024	Tubb5	20.58	14.87	42.59
Q3TML0	Pdia6	14.87	16.96	-4.26
Q3U1J4	Ddb1	14.87	14.87	-1.23
Q8C9B9	Dido1	14.87	14.87	-1.23
Q9CPU0	Glo1	18.70	20.27	-2.99
Q9CQI6	Cotl1	18.37	19.76	-2.62
Q9D305	Thap2	20.40	14.87	37.62
Q9JMG7	Hdgfrp3	17.11	14.87	3.84

Table A.3 Biological functions overrepresented in high confidence in O-GlcNAc proteins

Categories	Biofunctions	p-value	Molecules
Cancer, organismal injury and abnormalities	Metastasis	7.09E-03	PRDX2, PSAP, S100A4, TLN1
Carbohydrate metabolism, drug metabolism, small molecule biochemistry	Catabolism of hyaluronic acid	9.30E-03	CD44
Carbohydrate metabolism, drug metabolism, small molecule biochemistry	Internalization of hyaluronic acid	9.30E-03	CD44
Embryonic development, tissue development	Branching morphogenesis of mammary organoid	1.85E-02	HSP90AB1
Cellular development, cellular growth and proliferation	Proliferation of melanoma cell lines	1.85E-02	PRDX2
Cancer, organismal injury and abnormalities	Metastatic potential of breast cancer cell lines	2.76E-02	PSAP